BTeV-doc-2497
Beams-doc-1001

Design of an Interaction Region at C0 in the Tevatron

Contacts
Michael D. Church, Level 2 Manager
Peter H. Garbincius, Editor

December 3, 2004

Table of Contents

1 Introduction

The C0 Interaction Region (IR) project provides a solution for creating high luminosity proton-antiproton collisions at the C0 region of the Tevatron for the BTeV experiment. The two largest technical components are modified LHC-style quadrupoles and newly designed corrector magnet packages (spools). This project takes full advantage of the Tevatron luminosity upgrades of the Run II Collider Program to obtain the highest luminosity possible for BTeV. It is designed to allow continued operation of the CDF and D0 experiments with the BTeV experiment installed – collider stores can be alternately dedicated to BTeV and CDF/D0, but not both simultaneously. It makes use of proven existing Tevatron infrastructure to the fullest extent possible without compromising design goals. Modifications to the Tevatron are almost entirely restricted to the region from B43 to C17 (445 meters) and the 3 associated service buildings above ground.

The lattice design is robust. It utilizes anti-symmetric quadrupole triplets on either side of the IR to produce a 35 cm β^* at C0 − the same design β^* as at B0 and D0. Additional quadrupoles, some new and some reused from the Tevatron Low Beta Project, match to the Run II lattice at all energies and at all steps of the transition from injection to the low beta lattice. The C0 insertion itself introduces exactly one unit of tune to both horizontal and vertical planes, so that the Tevatron fractional tunes remain unchanged. This design minimizes the impact on Tevatron operation. Corrector magnet packages are designed to give excellent orbit control and coupling correction to provide added insurance against magnet misalignments and imperfections. The power supply configuration is versatile enough to tune out any foreseeable magnet errors. This lattice design is optimized for 36 x 36 bunch operation but does not preclude 132 nsec operation.

The LHC IR quadrupole produced by the Fermilab Technical Division is a well tested and proven magnet. A modification of this design provides a cost-effective and timely solution for the C0 IR project. The modifications are restricted to the iron yoke, cryostat, and end enclosures of the magnet − the collared coil assembly remains the same as the original LHC design.

The unique demands of the C0 IR and the antiquity of the original Tevatron spools preclude the use of these spools in this project. New spools will be designed and fabricated. The baseline design uses a standard nested $\cos(n\theta)$ coil package to produce dipole, quadrupole, and sextupole fields. In addition, these spools contain the high current leads for the low beta quadrupoles. Limitations in the helium liquifying capacity of the Tevatron cryogenic system necessitate the use of high temperature superconductor for these leads.

The scope of this project also encompasses the construction and installation of new power supplies, new cryogenic elements in the Tevatron tunnel, modifications to low conductivity water systems, vacuum systems, beam collimation systems, controls infrastructure, software, instrumentation, and operational procedures − all the things necessary to make a high energy accelerator function.

2 Accelerator Physics

2.1 Lattice

Every facet of successful Tevatron collider operations is tied intimately to specific details of the optical lattice functions in the ring. As examples, the locations of beam collimators, separators for helix generation, and the feed-down circuits are all determined largely by the distribution of betatron phase advance. So as not to disrupt these nominal Run II operating parameters it is essential that a new C0 Interaction Region (IR) insertion meld seamlessly with this existing Tevatron lattice. This implies the need to create an entirely localized insertion – one which is transparent to the rest of the machine. This constraint has important design implications, the most notable of which are pointed out below:

- An IR design similar to that employed at CDF & D0 is unacceptable as a C0 candidate. The addition of such a (single) low-β region to the machine would raise the tune by a half-integer in each plane, moving them far from the standard operating point and smack onto the 21.0 integer resonance. The nominal (fractional) tunes can most elegantly be retained by adding 2 low-β's locally in each plane, thereby boosting the machine tunes by a full integer.
- The B0 & D0 IR's are not optically-isolated entities. Progression through the B0/D0 low-β squeeze involves adjusting, not only the main IR quadrupoles, but also the tune quad strings distributed around the ring. The result is that lattice functions at any point in the ring, and the phase advances across any section of the ring, are not fixed quantities, but vary through the squeeze sequence. For the operational mode of B0/D0-only collisions, the C0 insertion must be sufficiently flexible to track these changing matching conditions.
- With collisions only at B0 & D0 the unit of tune added by the C0 insert ensures that the incoming & outgoing helices are automatically matched into the Run II values. To maintain this match with collisions at all 3 IP's, however, would require additional separators in the short B0 $\rightarrow$ C0 & C0 $\rightarrow$ D0 arcs. There is no space available for more separators, so high luminosity collisions can only be created at B0 & D0, or just C0, but not all three simultaneously. Furthermore, without new arc separators the 2 IP collision options – B0 & C0 or D0 & C0 – are also excluded.

Both the series & independent IR quad circuits are illustrated in Figure 2-1. The specialized IR magnets required fall into 3 gradient ranges. First, there are LHC-like magnets operating at or below 170 T/m. This is substantially less than the basic >220 T/m LHC design, but the gradients are limited here by the Tevatron 4.5 ^{o}K cryogenics. Second, there are high-field 140 T/m Q1 quadrupoles previously installed for Tevatron collider operation. And third, there are strong (25 T·m/m) quad correction spools for the final optical match into the arcs.

Composition of the quadrupole circuits is described below, with the indicated lengths being magnetic lengths.

- The triplets:

Q1	: 94.5"	170 T/m
Q2	: 169.875"	170 T/m
Q3	: 94.5"	170 T/m

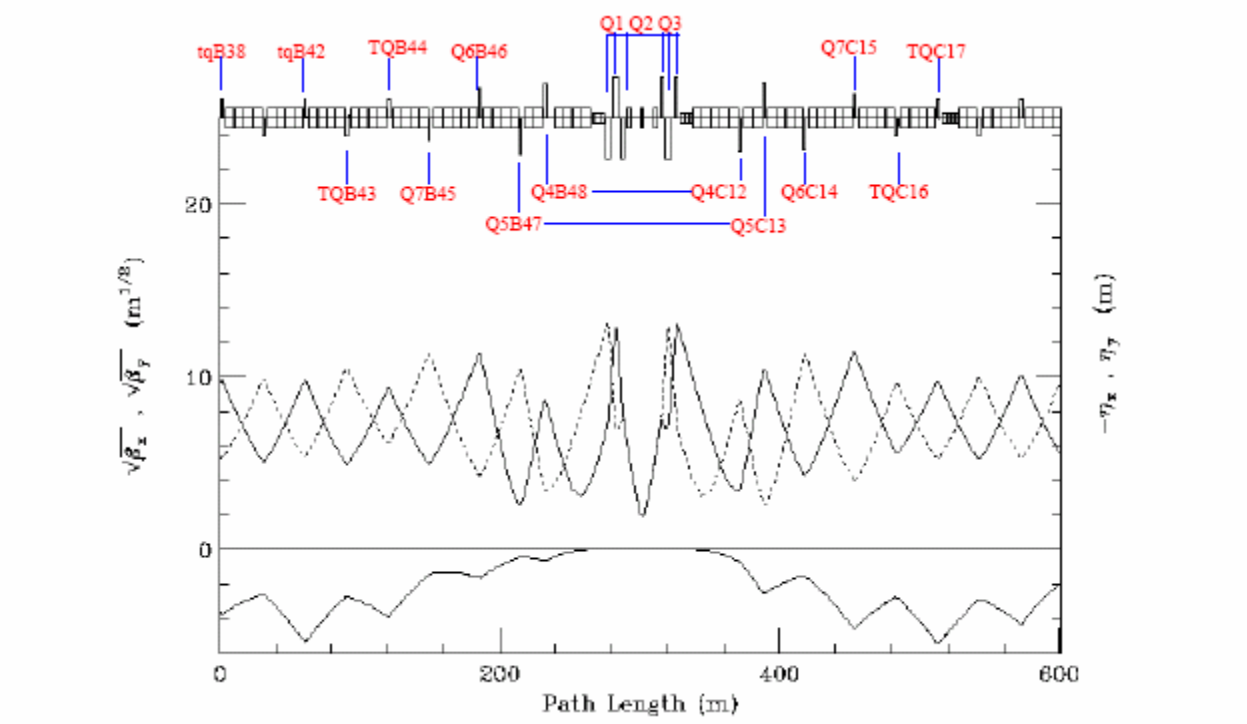

Figure 2-1: Power circuits of the IR quadrupoles.

Schematic layout of an IR triplet is given in Figure 2-2, showing the slot lengths (the length between interfaces between adjacent components) and magnetic lengths of the elements, and spaces allocated for flanges, cryo, coil supports, etc. A special correction package is installed between the Q2 & Q3 magnets. This contains both vertical & horizontal BPMs, dipole correctors in each plane, plus a trim skew quad. The dipole correctors are well situated for beam control at the IP: $\beta_X = \beta_Y > 60\% \beta_{max}$, and the betatron phase advance to the IP is almost exactly 90^o in both planes. Because of the almost zero degrees of phase advance across the triplet magnets, the trim skew quad is perfectly located to compensate locally for triplet roll mis-alignments. The final focus triplets are powered in series, with a small (<200 A) shunt added across each of the Q1/Q3 pairs for independent gradient variations to complete the match to the appropriate IP optics.

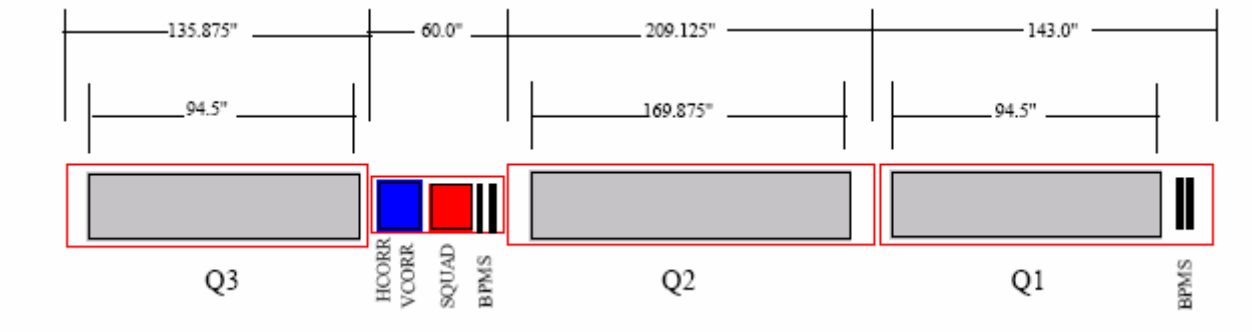

Figure 2-2: Details of the IR triplet.

- B48/C12 & B47/C13:

Q4 : 79" 170 T/m

Q5 : 59" 170 T/m

Apart from their magnetic lengths the Q4 & Q5 magnets are the same design as the triplet quadrupoles, having adequate space at each end of the cryostat to accommodate the necessary ancillary hardware (see Figure 2-2). These quadrupoles are accompanied by new, short (60.00") spools, containing BPM's and dipole correctors in each plane. These spools also serve as the magnet power feeds & transport the main bus.

- B46 → B45 & C14 → C15:

Q6 : 55.19" 140 T/m

Q7 : 55.19" 140 T/m

The four Q6 & Q7 magnets are independently powered. The regular 66.1" arc quads and their spools at the B46, B45, C14 & C15 locations are replaced with relocated high–field Q1 low-beta quads (unused in Run II) from CDF & D0, along with their accompanying TSP-spools. The P-spools have BPM's and dipole correctors in each plane, plus a skew quad. These spools also serve as the magnet power feeds & transport the main bus.

- B43 → B44 & C16 → C17:

The normal 72" Tevatron arc spools at these 4 locations are replaced by 72" spools containing high-field (25 T·m/m) trim quads plus standard strength horizontal or vertical dipoles and chromaticity sextupoles.

- B38 → B42:

The trim quads (7.5 T·m/m) at B38 & B42 are removed from the tune quad circuits and are independently powered for final optical matching to the arc.

The design uses non-standard separations between some of the insertion's inner arc quadrupoles. Between the B48 & B47 [C12 & C13] quadrupoles, for example, space is reduced by 2 dipoles,

whereas between B46 & B45 [C14 & C15] separation increases by 1 dipole slot length. Extensive simulations have shown this configuration contributes markedly to the robustness of the IR's tuning range.

Trim quads are allocated in a lop-sided configuration, with 2 more installed in the upstream end of the insert. In B-sector it is possible to extend insert elements a good distance back into the arc before interfering with Run II operations. This is not so in C-sector. The 4 vertical separators at C17 are integral components of Run II operation and, therefore define the downstream insert boundary.

There are 15 optical constraints the insertion satisfies. The 6 incoming Twiss parameters are matched at the IP to $\beta_x^* = \beta_y^* = \beta^*$, $\alpha_x^* = \alpha_y^* = 0$, $\eta^* = 0$, $\eta'^* = 0$, and then matched back into the nominal arc values at the downstream end of the insert (at C17). The fractional Run II phase shifts, $\Delta\mu_x$ and $\Delta\mu_y$, are preserved across the insert. The final constraint imposed in the design is that $\beta_{x,max} = \beta_{y,max}$ in the triplets each side of the IP. While this last restriction isn't really crucial, it is the best choice, minimizing the consumption of aperture in the low-β quads.

Every stage of the C0 low beta squeeze from $\beta^* = 3.50 \rightarrow 0.35$ m can match exactly to any step in the B0/D0 low beta squeeze. Subsequent sections illustrate these lattice parameters corresponding to the specific operational conditions:

(1) Injection : $\beta^* = 3.50$ m @ C0 : $(\beta_x^*, \beta_y^*) = (1.61, 1.74)$ m @ B0/D0

(2) C0 Collisions : $\beta^* = 0.35$ m @ C0 : $(\beta_x^*, \beta_y^*) = (1.61, 1.74)$ m @ B0/D0

(3) B0/D0 Collisions : $\beta^* = 3.50$ m @ C0 : $\beta^* = 0.35$ m @ B0 & D0

All gradient entries in the accompanying tables reflect 1 TeV/c operations. Highlighted entries indicate those magnets that must change polarity at some point during the transition between the various operating modes.

2.1.1 Injection

In the injection lattice, shown in Figure 2-3, $\beta^* = 3.50$ m results in a β_{max} of 169 m in the triplets. This is appreciably less than the >240 m of the B0 & D0 injection lattices and so is not anticipated to pose any aperture problems for Tevatron operations. The corresponding quadrupole gradients are listed in Table 2-1 (at 1 TeV/c).

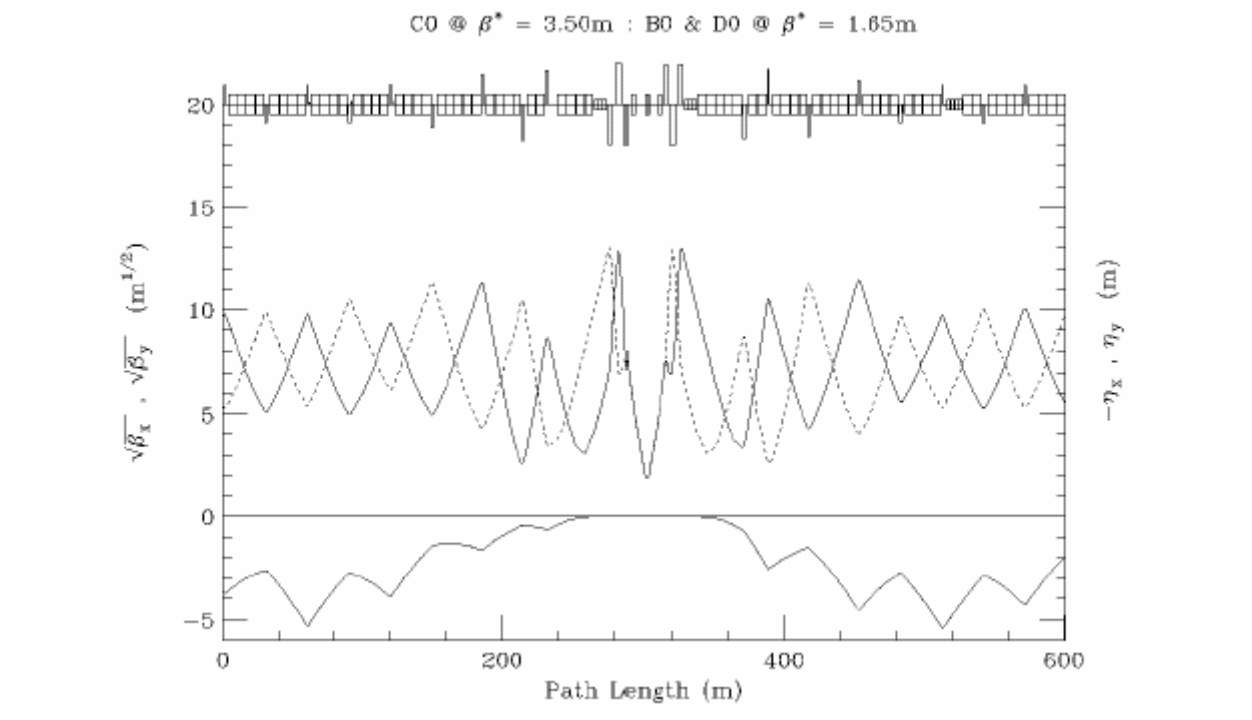

Figure 2-3: C0 injection optics.

2.1.2 C0 Collisions

For collisions at C0 the B0 & D0 optics remain in their injection configuration, while at C0 β* is squeezed from 3.50 m at injection to 0.35 m. See Figure 2-4 and Table 2.2. Current Tevatron Collider understanding and experience suggests that at B0 & D0 the smallest realistic β* attainable is limited largely by the adverse impact on the beam by high-order multipoles in the low-β quadrupoles and, therefore, βmax in the low−β triplets. This is not expected to be the limiting factor for C0 collisions, however. With just one interaction point instead of two, and the somewhat higher quality LHC quadrupoles, tracking studies indicate that at β* = 35 cm the dynamic aperture of the machine with C0 collisions is nearly twice that of Run II (Section 2.5).

For C0 collisions β* at the IP is squeezed to 35 cm – the same value as for B0/D0 collisions. The luminosity at C0 will therefore be identical to that of B0/D0 at the end of Run II. Anticipated Collider parameters at the end of Run II are summarized in Table 2-3.

Table 2-1: C0 IR gradients for 1 TeV/c injection optics.

INJECTION OPTICS : C0 @ β* = 3.50m : B0/D0 @ β* = 1.65m (1 TeV/c)					
	Gradient (T/m)	Current (A)		Gradient (T/m)	Current (A)
Q1D	-167.398	9414	Q1F	167.398	9414
Q2F	170.013	9561	Q2D	-170.013	9561
Q3D	-167.398	9414	Q3F	167.398	9414
QB48	140.058	7876	QC12	-140.058	7876
QB47	-148.554	8354	QC13	148.554	8354
QB46	123.312	4261	QC14	-132.453	4577
QB45	-92.287	3189	QC15	96.108	3321
TB44	12.077		TC16	-32.384	
TB43	12.240		**TC17**	-4.888	
TB42	9.606				
TB39	0				
TB38	1.594				

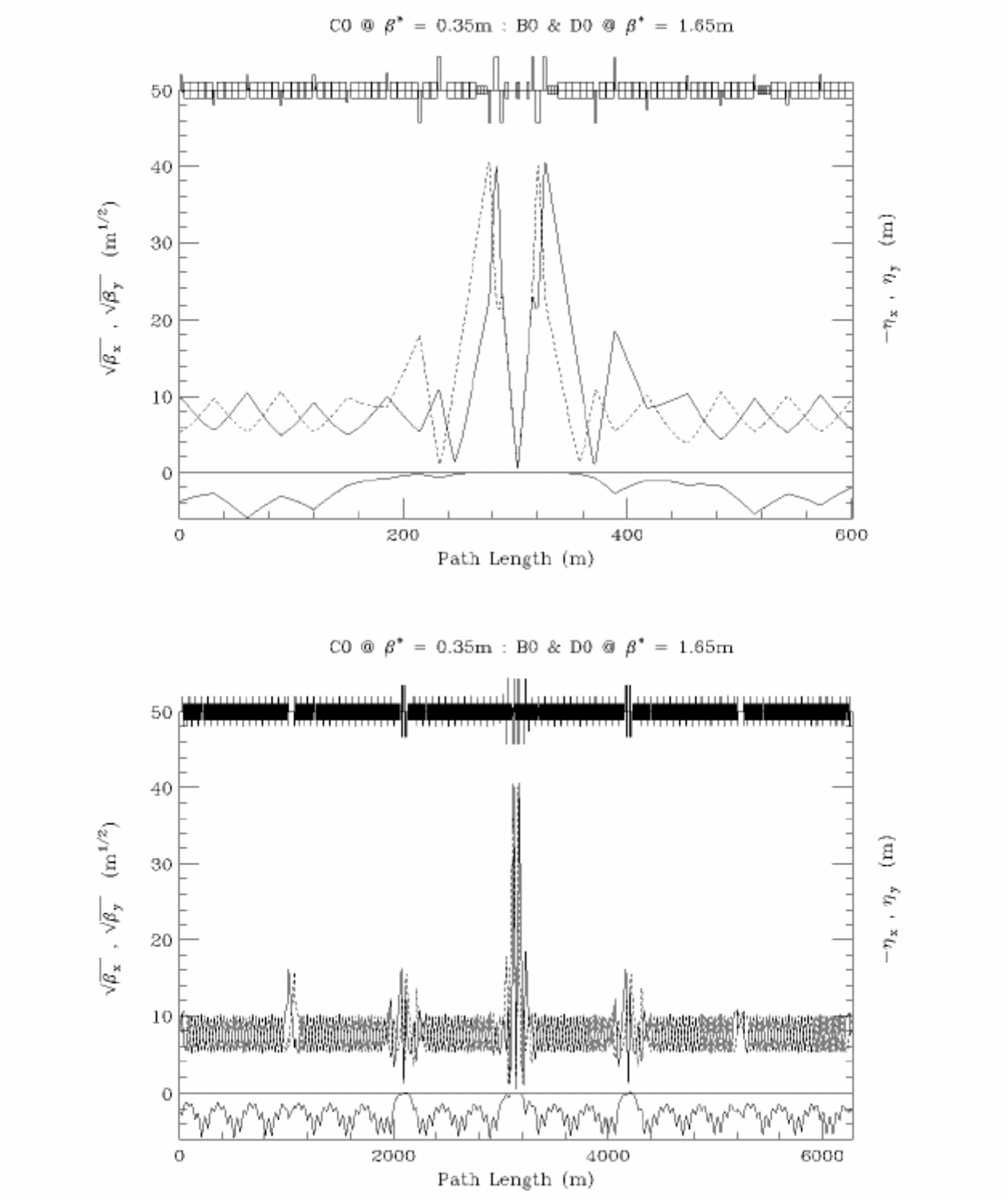

z

Figure 2.4: C0 collision optics – B38 → C19 (top), and ring-wide (bottom).

Table 2-2: IR gradients for C0 collisions at β* = 35 cm.

C0 COLLISIONS @ β* = 0.35 m : B0/D0 @ β* = 1.65 m (1 TeV/c)					
	Gradient (T/m)	Current (A)		Gradient (T/m)	Current (A)
Q1D	-168.470	9474	Q1F	168.470	9474
Q2F	168.882	9497	Q2D	-168.882	9497
Q3D	-168.470	9474	Q3F	168.470	9474
QB48	170.081	9565	QC12	-170.081	9565
QB47	-168.342	9467	QC13	168.342	9467
QB46	89.205	3082	QC14	-103.355	3571
QB45	-60.233	2081	QC15	71.741	2479
TB44	14.168		TC16	-38.525	
TB43	-7.607		**TC17**	25.049	
TB42	7.218				
TB39	0				
TB38	-6.759				

Table 2-3: Tevatron Collider design parameters projected for the end of Run II. (DOE mini-review of Run II, September 2004)

Run II COLLISION PARAMETERS		
protons/bunch	270	x 10^9
pbars/bunch	131	x 10^9
proton emittance	25	π μm
pbar emittance	15	π μm
β^* at C0 IP	0.35	m
Bunches	36	
Bunch length (rms)	0.5	m
Hour-Glass Form Factor	0.70	
Proton tune shift	0.008	
Pbar tune shift	0.018	
Initial Luminosity	284	x 10^{30} $cm^{-2}s^{-1}$

2.1.3 B0/D0 Collisions

For collisions at just B0 & D0 the C0 β^* is fixed at its injection value of 3.50 m while at B0 & D0 β^* is squeezed from ~1.65 m at injection to 0.35 m (see Figure 2-5). A comparison of C0 IR gradients listed in Table 2-4 with the injection values of Table 2-1 demonstrates the small tuning changes required at C0 to fix β^* = 3.50 m while maintaining the ideal optical match to the nominal Run II squeeze lattice.

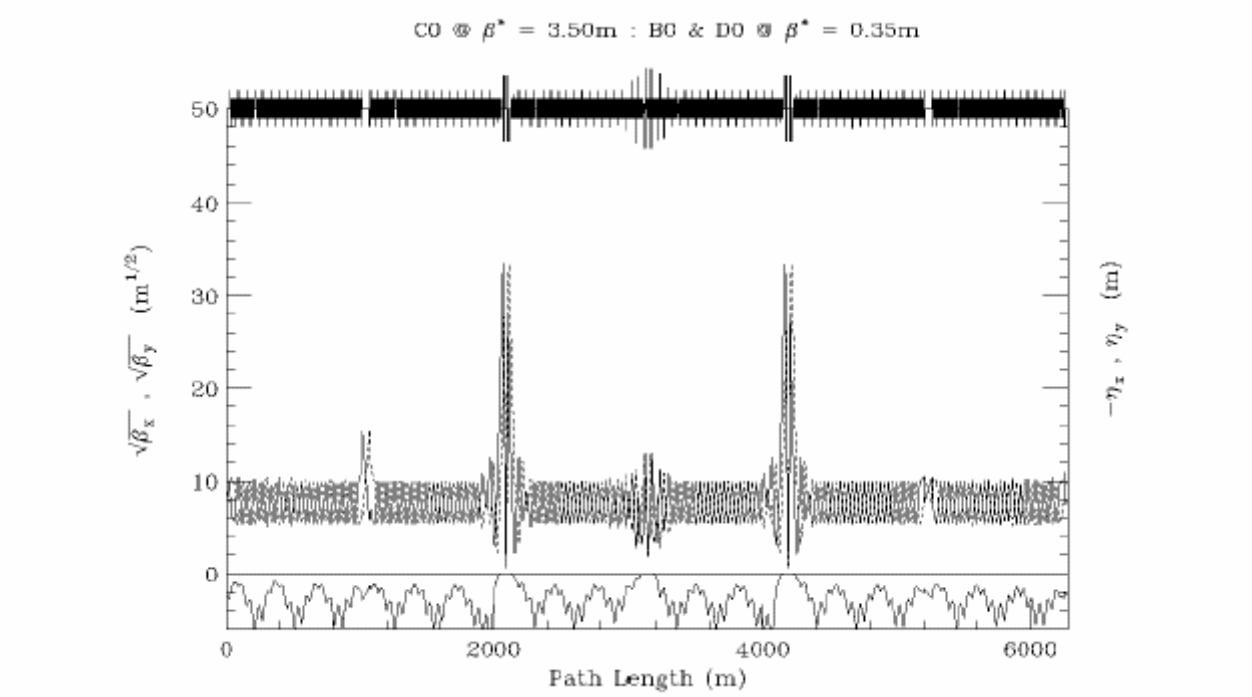

Figure 2-5: B0/D0 collision optics.

2.2 Helix

With 36x36 bunch operation in the Tevatron there are 72 potential collision points between each proton and pbar bunch. In Run II there are currently 6 sets of electrostatic separator modules available in both horizontal and vertical planes to keep the proton and pbar orbits separated everywhere in the ring except at the B0 & D0 IP's during collisions. One part of the Run II upgrade project is to increase by as many as 5 the number of separator modules in the ring. The optimum sites for these new separators is still being studied. Another part of the plan is to enhance the performance of the existing units. The present separators are run with gradients as high as ~40 kV/cm (~10.3 μrad kick at 1 TeV/c) before sparking becomes a problem. This is believed to be a conservative estimate of the maximum attainable gradient, and that, with conditioning, as much as a 30% increase should be possible. The outcome of these separator upgrades will be a better controlled, smoother helix at injection, where apertures are problematic, and increased beam separation at collision where the helix is limited by the available gradients. In view of the uncertainties still associated with implementing the Run II separator upgrade, however, in the discussions to follow only the currently installed ring separator configuration is considered, and the modules are assumed to have the conservative maximum electric field gradient of 40 kV/cm.

In the BTeV era it is expected that the Tevatron will continue with 36x36 bunch operations. Additional separator modules will then need to be added to create collisions at the C0 IP. Like the other 2 IR's these will be installed immediately outboard of the C0 IR triplets. At B49 there will be a set of 2 horizontal modules and 1 vertical module, with the reverse configuration installed at C11.

Table 2-4: C0 IR gradients for B0/D0 collisions and β* fixed at 3.50 m at C0.

B0/D0 COLLISIONS @ β* = 0.35 m : C0 @ β* = 3.50 m (1 TeV/c)					
	Gradient (T/m)	Current (A)		Gradient (T/m)	Current (A)
Q1D	-168.651	9484	Q1F	168.651	9484
Q2F	170.094	9565	Q2D	-170.094	9565
Q3D	-168.651	9484	Q3F	168.651	9484
QB48	136.692	7687	QC12	-136.692	7687
QB47	-147.184	8277	QC13	147.184	8277
QB46	119.811	4140	QC14	-127.377	4402
QB45	-91.586	3165	QC15	92.396	3193
TB44	14.397		TC16	-23.177	
TB43	4.954		**TC17**	-3.542	
TB42	9.855				
TB39	0				
TB38	4.079				

2.2.1 Injection Helix

At the injection energy of 150 GeV, separation of the p-pbar orbits is controlled using a small sub-set of the 12 separators available in the machine. Separator strength is not an issue at 150 GeV, but the large beam sizes lead to aperture problems. The horizontal orbits are largely determined by the B17 separators, and the vertical by the C17 separators. The horizontal B17 gradients in particular are constrained by the aperture restrictions at the F0 injection Lambertson.

One separator solution from Run II is listed in Table 2-5. Here, only 4 sets of separators are used to create the helix, and the new B49/C11 separators are not used at all. The resulting beam separation around the ring is shown in Figure 2-6. Outside of the B38 → C17 C0 insert the helix

is unchanged from the Run II value, and through the C0 IR region it can be seen that beam separation is at least as good as throughout the rest of the ring. The average separation is ~8σ.

Table 2-5: Injection Separator gradients at 150 GeV/c.

INJECTION HELIX : C0 @ β* = 3.50m : B0/D0 @ β* = 3.50m (150 GeV/c)					
	Horizontal			Vertical	
	#	kV/cm		#	kV/cm
A49	1	0.0	A49	2	0.0
B11	2	-14.800	B11	1	-9.050
B17	4	25.740			
B49	2	0.0	B49	1	0.0
C11	1	0.0	C11	2	0.0
			C17	4	-26.150
C49	1	0.0	C49	2	0.0
D11	2	0.0	D11	1	0.0
D48	1	0.0			
			A17	1	0.0

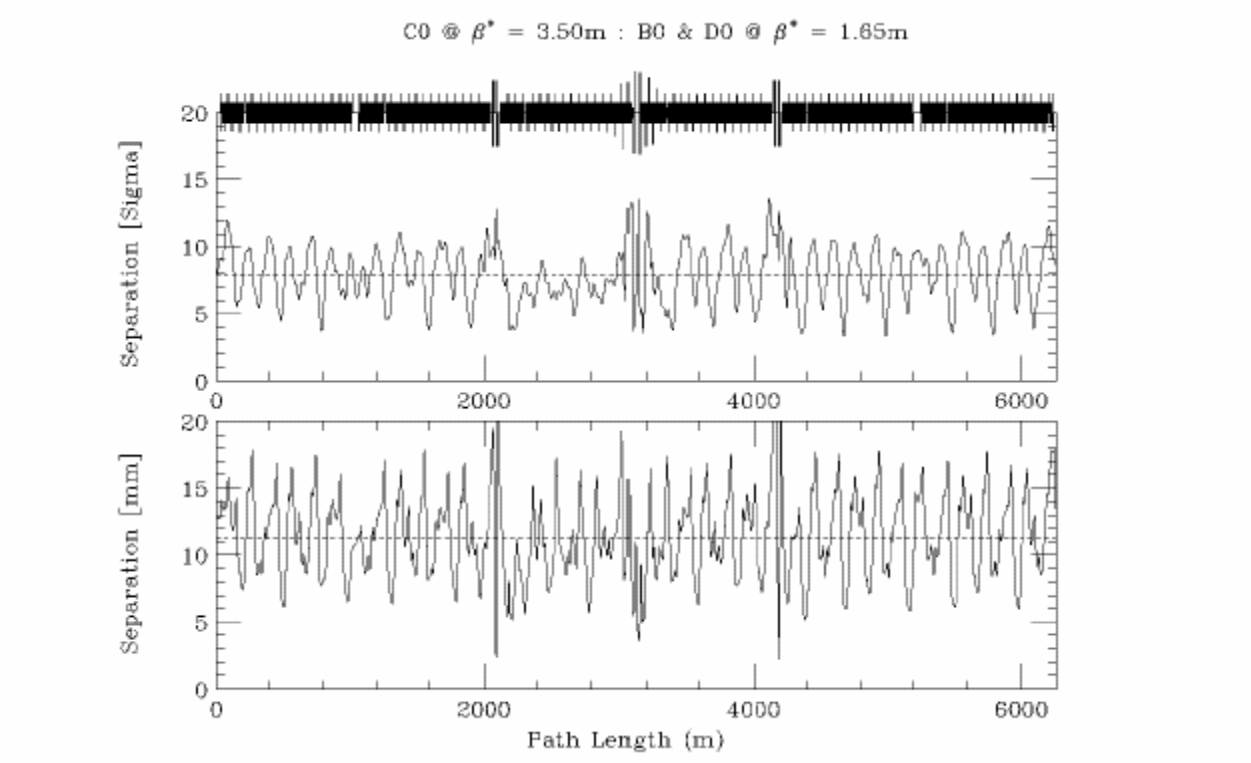

Figure 2-6: Injection helix at 150 GeV/c. $\varepsilon_N = 20\pi$ μm & $\sigma_p/p = 6.E\text{-}4$.

2.2.2 C0 Collision Helix

For collisions at C0 the optics at B0 & D0 remain in their Injection configuration. In this case, all the separators in the ring become available for bringing beams together at the C0 IP, while keeping them separated everywhere else. One possible separator solution is given in Table 2.6 below. The selection of separators has not been optimized particularly, other than to ensure adequate beam separation around the ring. Many more combinations still need to be explored.

Figures 2-7 and 2-8 illustrate the beam separation across the insert from B38 → C21, and also the separation around the ring. With this separator solution the closest approach of proton and pbar bunches through the insert is at the 1st parasitic crossing, where separation is about 6.5 σ. Elsewhere in the ring, separation drops close to 6σ, but the average separation is ~9 σ. Oscillations in the helix could probably be smoothed further using a larger subset of separators.

Table 2-6: C0 collision separator gradients at 1 TeV/c.

C0 COLLISIONS @ β* = 0.35 m : B0/D0 @ β* = 1.65 m (1 TeV/c)					
Horizontal			Vertical		
	#	kV/cm		#	kV/cm
A49	1	-21.543	A49	2	26.487
B11	2	21.543	B11	1	-26.487
B17	4	15.659			
B49	2	-40.000	B49	1	-40.000
C11	1	40.000	C11	2	40.000
			C17	4	-22.438
C49	1	0.0	C49	2	0.0
D11	2	0.0	D11	1	0.0
D48	1	40.000			
			A17	1	0.0

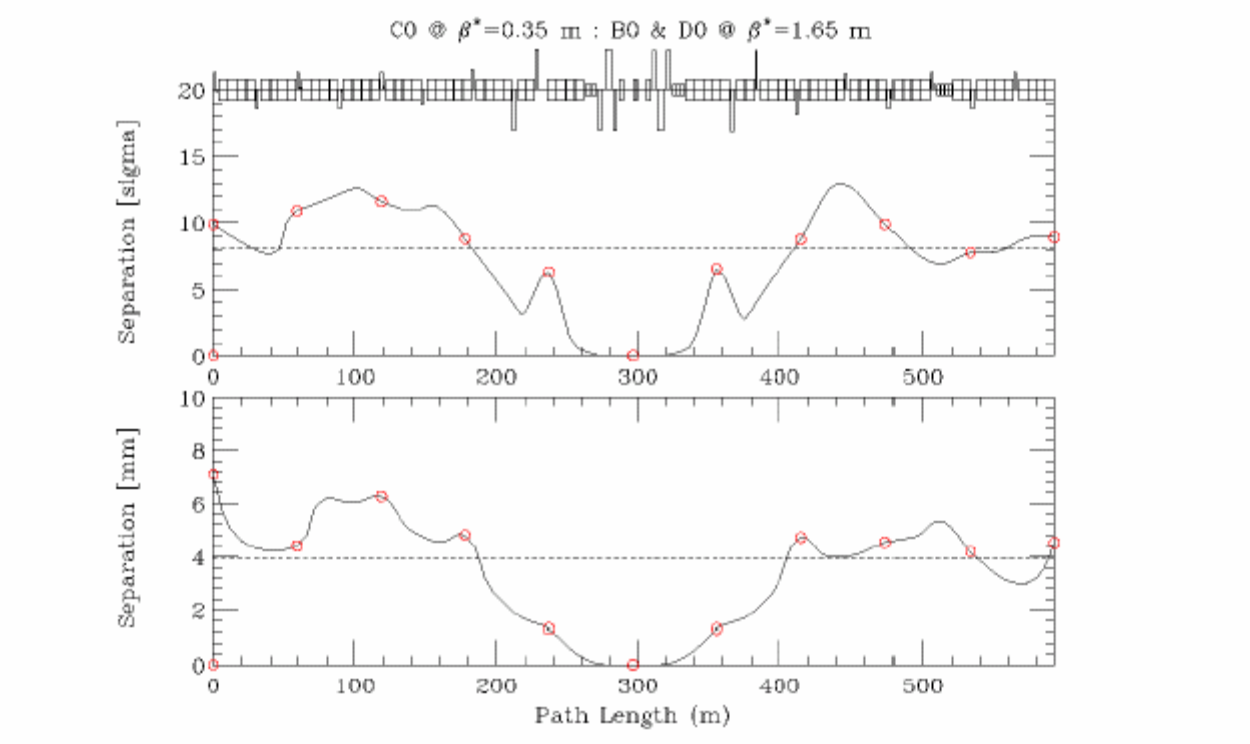

Figure 2-7: C0 IR beam separation during C0 collisions. $\varepsilon_N = 20\pi$ μm & $\sigma_p/p = 1.47E\text{-}4$.

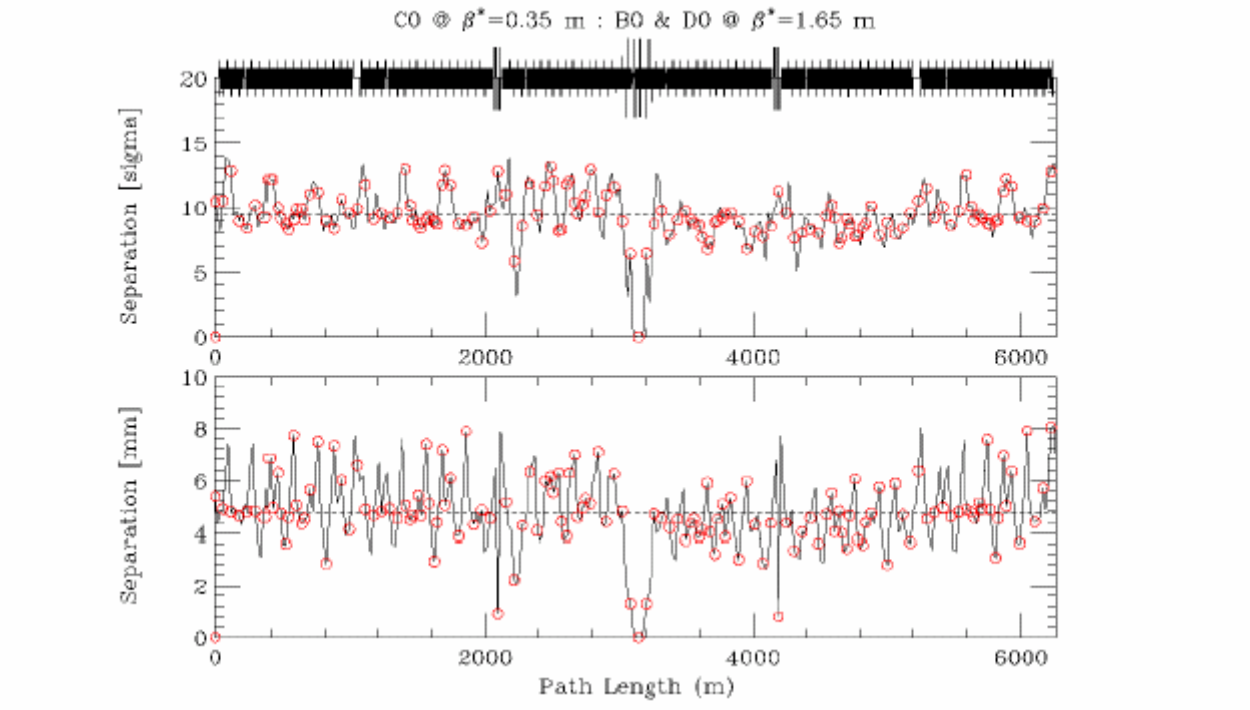

Figure 2-8: Ring-wide beam separation during C0-only collisions. $\varepsilon_N = 20\pi$ μm & $\sigma_p/p = 1.47E\text{-}4$.

2.2.3 B0/D0 Collision Helix

With collisions at just B0 & D0, the optics at C0 remain at the injection value of β* = 3.50 m, and the B49 & C11 separators voltages are turned up to create horizontal & vertical separation bumps at the C0 IP. Because the phase advance across the C0 separators is nearly 180^{o} in each plane, to a very good approximation the C0 bumps cancel away from the IR region. The settings of the rest of the ring separators remain essentially unchanged from their nominal Run II B0/D0 collision helix values (see Table 2-7). The resulting beam separation around the machine is shown in Figure 2-9 below. Away from the B0 & D0 IP's beam separation is >5 σ everywhere, with an average separation of ~8.5 σ.

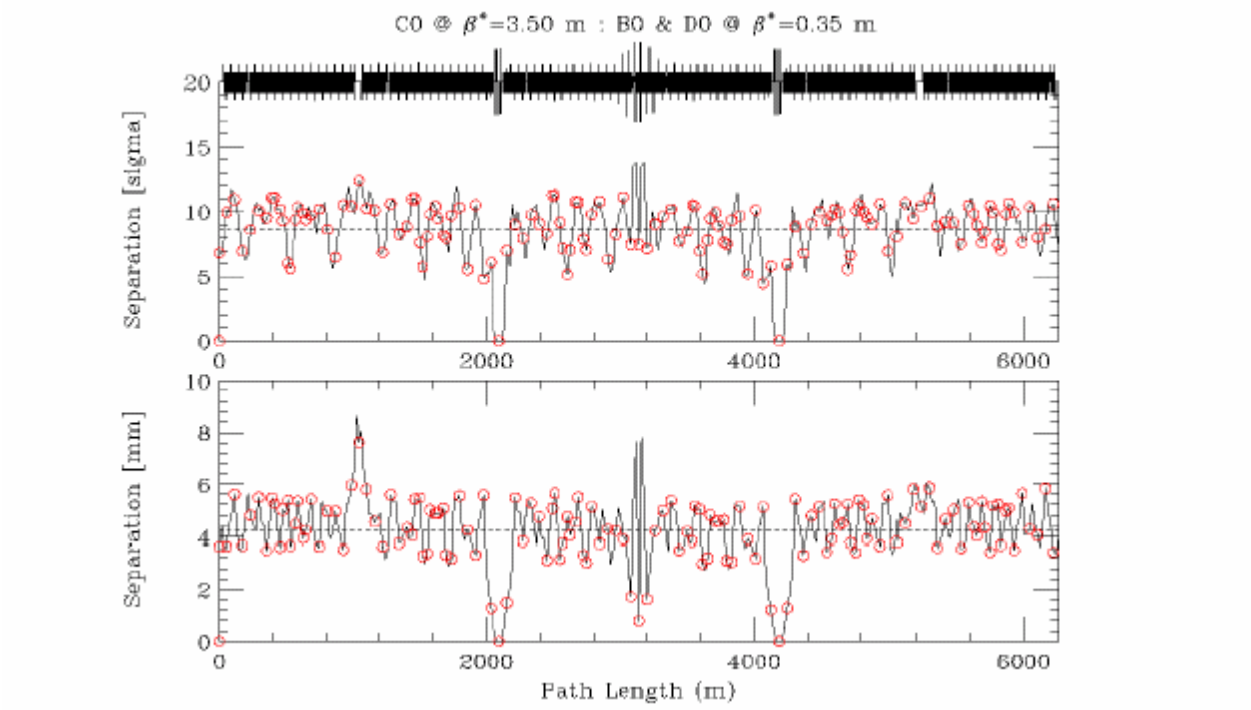

Figure 2-9: Separation during B0/D0 collisions. ε_N = 20π μm & σ_p/p = 1.47E-4.

Table 2-7: Separator gradients for B0/D0 collisions at 1 TeV/c.

B0/D0 COLLISIONS @ β* = 0.35 m : C0 @ β* = 3.50 m (1 TeV/c)					
	Horizontal			Vertical	
	#	kV/cm		#	kV/cm
A49	1	40.000	A49	2	-33.278
B11	2	40.000	B11	1	40.000
B17	4	-20.348			
B49	2	40.000	B49	1	40.000
C11	1	40.000	C11	2	40.000
			C17	4	-20.520
C49	1	37.119	C49	2	32.583
D11	2	-34.492	D11	1	40.000
D48	1	-5.089			
			A17	1	1.644

2.3 Orbit Correction and Physical Aperture

2.3.1 Beam Manipulation at the IP

From Table 2-8, dipole corrector bumps can be calculated for controlling position and angle at the IP. Tables 2-9 and 2-10 give the correct kick ratios for 2 efficient position bumps and 2 angle bumps in each plane. Other choices of magnet combinations are possible. The dipole correctors have integrated fields of 0.48 T·m. At 1 TeV/c this translates into a maximum kick angle of 144 μrad. Solutions (a) & (c) use the triplet spool package correctors, while solutions (b) & (d) use only arc correctors.

Table 2-8: C0 IR correctors and lattice functions ($\mu_x = \mu_y = 0$ at F0).

C0 IR CORRECTION SPOOL PACKAGES							
Site	Spool Type	Elements	βx (m)	μx (2π)	ηx (m)	βy (m)	μy (2π)
B38	TSE	HD, QTF, SxF	90.4	9.402	3.66	29.6	9.342
B39	TSB	VD, QTD, SxD	32.8	9.502	2.98	87.6	9.434
B42	TSC	HD, QTF, SxF	102.4	9.581	5.81	30.1	9.540
B43	X1	VD, QT, SxD	25.4	9.691	3.22	102.7	9.623
B44	X1	HD, QT, SxF	77.9	9.796	4.61	30.2	9.722
B45	TSP	H&VD, SQ, H&VBPM	25.1	9.913	1.69	94.5	9.808
B46	TSP	H&VD, SQ, H&VBPM	93.5	10.037	0.77	81.1	9.880
B47	X2	H&VD, H&VBPM	34.6	10.136	0.28	266.0	9.908
B48	X2	H&VD, H&VBPM	90.8	10.177	0.59	2.44	10.259
C0 U	X3	H&VD, SQ, H&VBPM	1021.	10.646	0.00	1021.	10.376
C0*			0.35	10.893	0.00	0.35	10.625
C0 D	X3	H&VD, SQ, H&VBPM	1021.	11.142	0.00	1021.	10.872
C12	X2	H&VD, H&VBPM	10.6	11.573	0.94	105.9	11.347
C13	X2	H&VD, H&VBPM	326.6	11.613	2.66	30.9	11.400
C14	TSP	H&VD, SQ, H&VBPM	72.1	11.645	1.03	96.3	11.483
C15	TSP	H&VD, SQ, H&VBPM	99.7	11.711	1.68	16.1	11.678
C16	X1	VD, QT, SxD	20.3	11.845	2.06	103.3	11.800
C17	X1	HD, QT, SxF	88.3	11.956	5.27	30.3	11.898

HBPM & VBPM	- position monitors	
HD & VD	- trim dipoles	0.48 T·m
QTF & QTD	- tune quads	7.5 T·m/m
SxF & SxD	- chromaticity sextupoles	450 T·m/m^2
QT	- strong trim quads	25 T·m/m
SQ	- skew quadrupole	7.5 T·m/m

Table 2-9: Relative dipole kick strengths to vary the beam positions (x*, y*) at the IP while fixing the angles (x'*, y'*) = 0. Positions (x*, y*) are in mm and θ is corrector kick angle in mrad of the strongest corrector.

	X^* POSITION BUMP COEFFICIENTS		Y^* POSITION BUMP COEFFICIENTS	
	(a)	(b)	(a)	(b)
B45			-0.0831	+0.4497
B46	-0.0966	+0.3358		
B47				+0.5247
B48		+1.0 θ		
C0U	+1.0 θ		+0.9988	
C0	X* = 19.3 θ	-7.0 θ	Y* = 19.3 θ	-7.3 θ
C0D	+0.9997		+1.0 θ	
C12				+1.0 θ
C13		+0.4679		
C14			-0.0937	+0.2931
C15	-0.0801	+0.3904		

For position control at the IP the solutions (a), using the triplet correctors, are most effective. With β_{corr} > 1000 m for β* = 0.35 m, and with almost exactly 90° of phase between the correctors and the IP, the beam position can be adjusted by as much as ±2.75 mm. This is nearly 3 times the control possible at the B0/D0 IR's. Furthermore, because there is nearly 180° of phase separating the upstream & downstream packages the cancellation between the triplet corrector kicks is excellent, with very little orbit distortion leaking into the arcs for final elimination. The position bumps (b) use only arc spool packages. These would be useful either to supplement the triplet corrector solution or to provide the IP position control in the event that the triplet dipoles are being used primarily to compensate for triplet quad mis-alignments. In any case, with the much smaller β-functions in the arc, solutions (b) are comparable to the orbit control at B0 & D0. At full corrector field the beam positions at the IP can be shifted by ±1.0 mm with solutions (b).

Table 2-10: Relative dipole kick strengths to vary the angles (x'*, y'*) at the IP while fixing the beam positions (x*, y*) = 0. Angles (x'*, y'*) are in μrad and θ is corrector kick angle in μrad of the strongest corrector.

	X'* ANGLE BUMP COEFFICIENTS		Y'* ANGLE BUMP COEFFICIENTS	
	(c)	(d)	(c)	(d)
B45			+1.0 θ	+1.0 θ
B46	-0.6824	-0.7655		
B47				-0.5589
B48		+0.6247		
C0U	-0.1624		+0.2786	
C0	X'*= -7.1 θ	-9.8 θ	Y'*= +6.8 θ	+9.9 θ
C0D	+0.2851		-0.1523	
C12				+0.5817
C13		-0.5142		
C14			-0.6382	-0.7728
C15	+1.0 θ	+1.0 θ		

For angle control at the IP there is no overpowering reason to prefer one of solutions (c) or (d) over the other. In either case the IP angle must be generated out in the arcs and the level of angle control possible at the IP is limited by the aperture in the low-β triplet quadrupoles rather than the available field strengths of the correction dipoles. For a 20π μm beam at 1 TeV, and β_{max} = 1630 m in the triplets, the 1 sigma beam width is ~2.3 mm. The quadrupole physical aperture has a radius of only 31.5 mm. In an extremely optimistic scenario which imagines the beam orbit can be displaced by as much as 25 mm in the triplet quadrupoles, the corresponding angle control at the IP is ±1.04 mrad.

2.3.2 C0 Straight Section Apertures

Unlike the solenoid spectrometers at CDF & D0, the BTeV experiment uses a dipole analysis magnet (SM3) plus 2 compensating 10' B2's to displace the beams vertically by 7.6 mm at the IP.

Current plans call for the beam pipe to be aligned to this vertical trajectory, and for the vertical 3-bump to be ramped from injection to flattop. These magnets are contained inboard of the IR triplets and, therefore, do not impact the final focus optics. A small vertical dispersion of η_y = 7.6 mm does get introduced locally at the IP purely from geometric considerations, but this has a negligible impact on the beam size. For example, with β^* = 35 cm, and 20π (95%) emittance beams at 1 TeV, the unperturbed beam size is σ_y = 33.09 μm. The 7.6 mm of vertical dispersion, coupled with a momentum spread of $\delta p/p$ (95%) = 3.4E-4, inflates this value insignificantly to 33.11 μm.

The rolled B2's have inside dimensions of 1.902"(H) x 3.902"(V), placing an additional horizontal aperture constraint in the IR region where there are also reduced diameter beam pipes. On each side of the C0 IP the beam pipe is 1" i.d. between 0.75 and 3.82 meters, then 1.92" i.d. from 3.82 meters to the ends of the B2's at ~7.6 m. The pixel detector is not an aperture concern, as is clearly illustrated by the detector cross-section shown in Figure 2-10. With the detector retracted it can be seen that, for beams within a few mm's of the center of the pixel opening, the horizontal aperture is ~50 mm (full-width) and the vertical aperture is infinite for all practical purposes.

Two operational modes have been studied in which any potential aperture problems in the detector region would become apparent: at 150 GeV injection, when the beams are large, and during stores of B0/D0 collisions, where β^* = 3.50 m at the C0 IP and the beams are off-center on separated orbits. The beam envelopes and apertures at injection are shown in Figures 2-11 and 2-12, and Figures 2-13 and 2-14 give the corresponding results during B0/D0 collisions.

Magnet apertures are displayed in two sets of units: as measured in terms of the transverse beam σ, and in absolute values (mm). In units of σ the tightest apertures are not in the detector at all, but at the B49 vertical & C11 horizontal separators during injection, where the aperture is ~15σ. In absolute terms the nearest approach to the aperture occurs both at injection and during B0/D0 collisions in the vicinity of the 1" pipe, where the "orbit + 1 cm" envelope narrowly clears the beam pipe wall. In either parameterization of the apertures, though, there is still ample room for maneuvering beam positions both at injection and at top energy.

During C0 collisions at β^* = 35 cm aperture is not a concern through the detector region – the beams are smaller than at the injection energy of 150 GeV and are not offset from the central trajectory as they were in the preceding discussion. However, with β_{max} = 1630 m in the IR triplets, aperture constraints in these magnets need to be examined. The beam envelopes and apertures during C0 collisions are shown in Figures 2-15 and 2-16. For 20p μm beams the maximum transverse beam σ in the triplets is ~2.25 mm, which gives ~14σ separation between the beam centroids and the 63 mm i.d. IR beam pipe. Although this C0 aperture is less than the ~18 σ clearance in the B0/D0 triplets (70 mm i.d.) during B0/D0 collisions, this is not an issue: first, because this is still about twice the machine physical aperture imposed by collimators, and; second, the limiting aperture in the C0 straight section is, again, created by the B49 & C11 electrostatic separators.

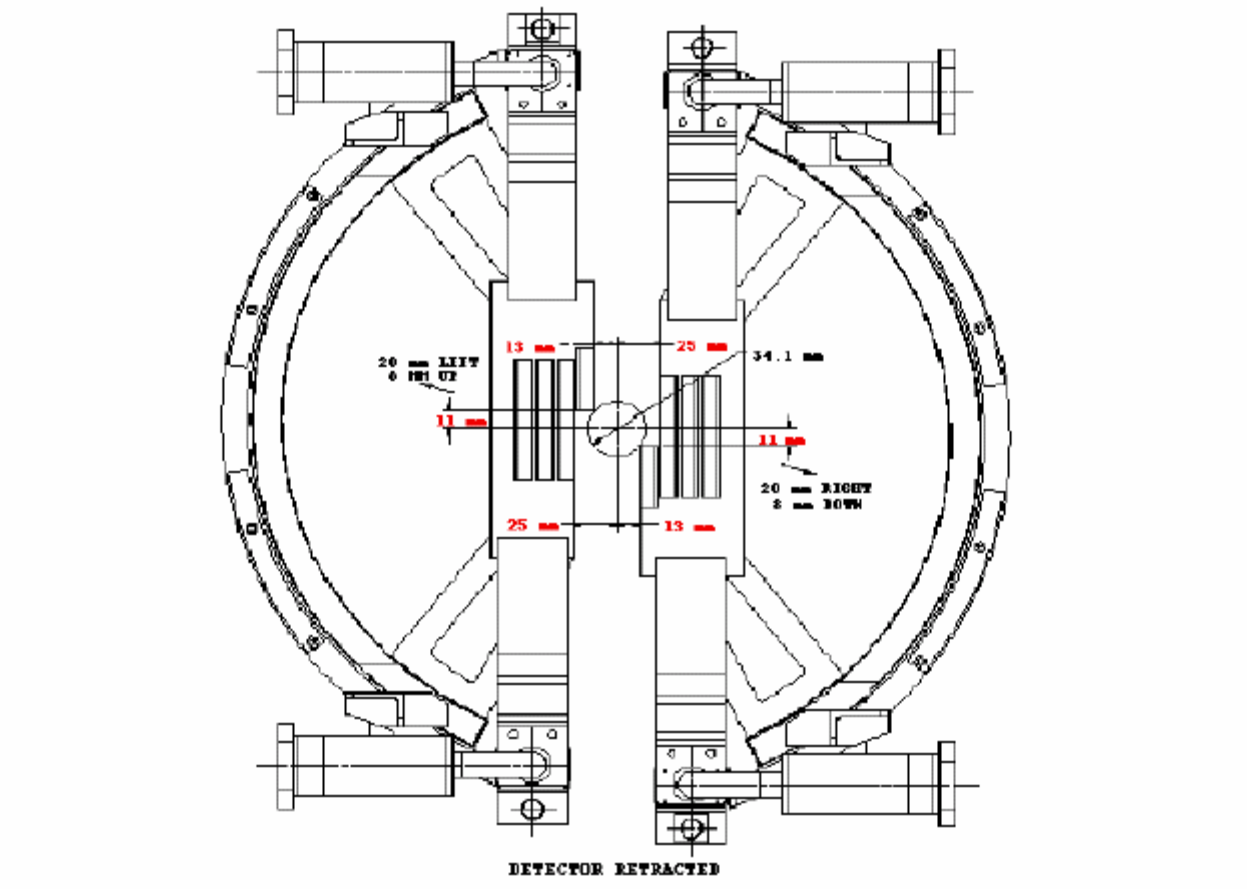

Figure 2-10: Horizontal & vertical apertures in the pixel detector with the detector retracted.

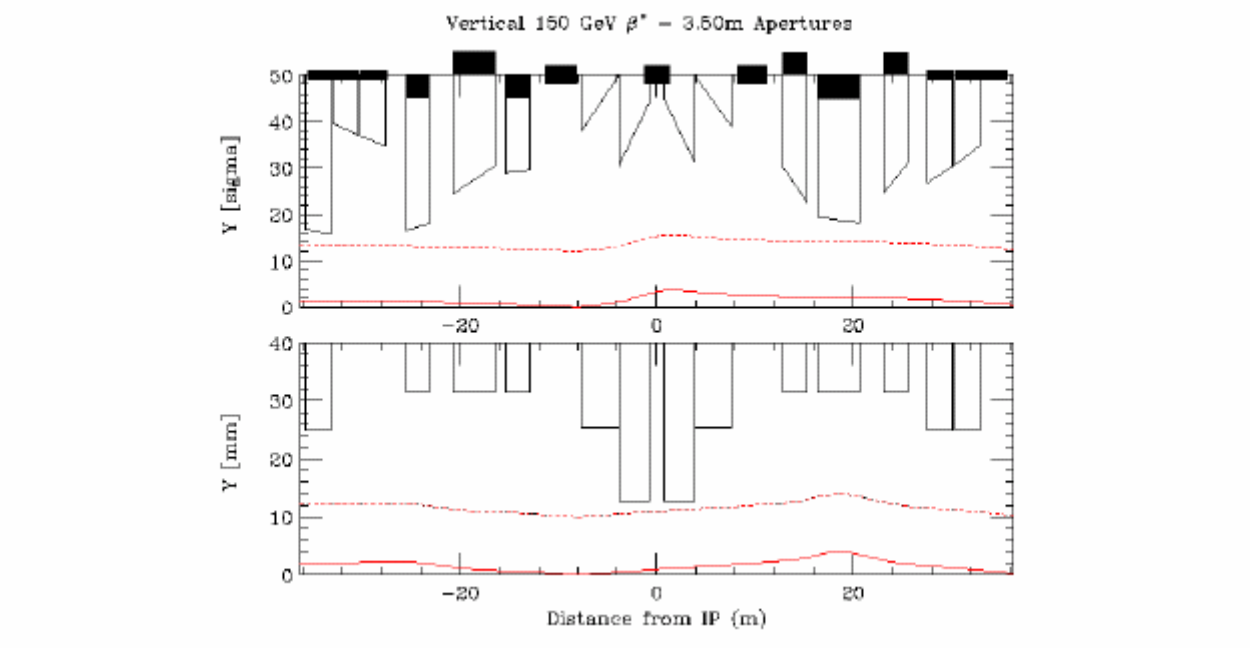

Figure 2-11: Vertical beam envelope & apertures at injection from the B49 through C11 separators. Quantities in the top diagram are measured in terms of the beam σ (_____ central orbit; ------- orbit + 12σ). In the bottom plot the measurements are in mm's (_____ central orbit; ------- orbit + 1 cm).

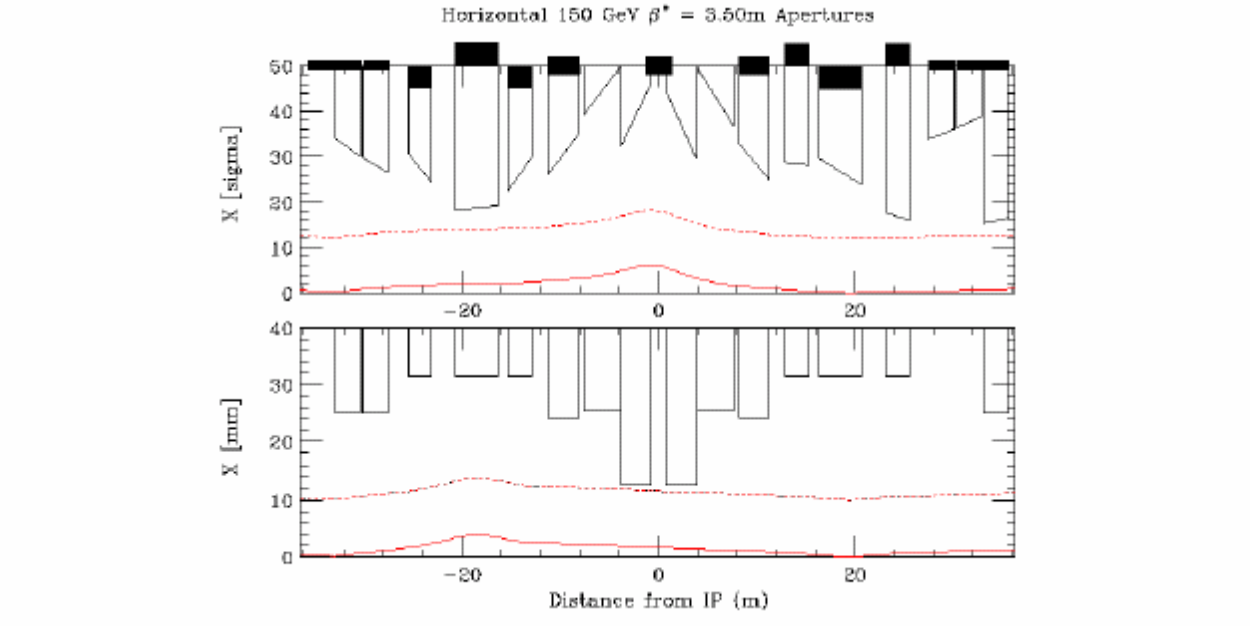

Figure 2-12: Horizontal beam envelope & apertures at injection. (Same legend as for Figure 2-11).

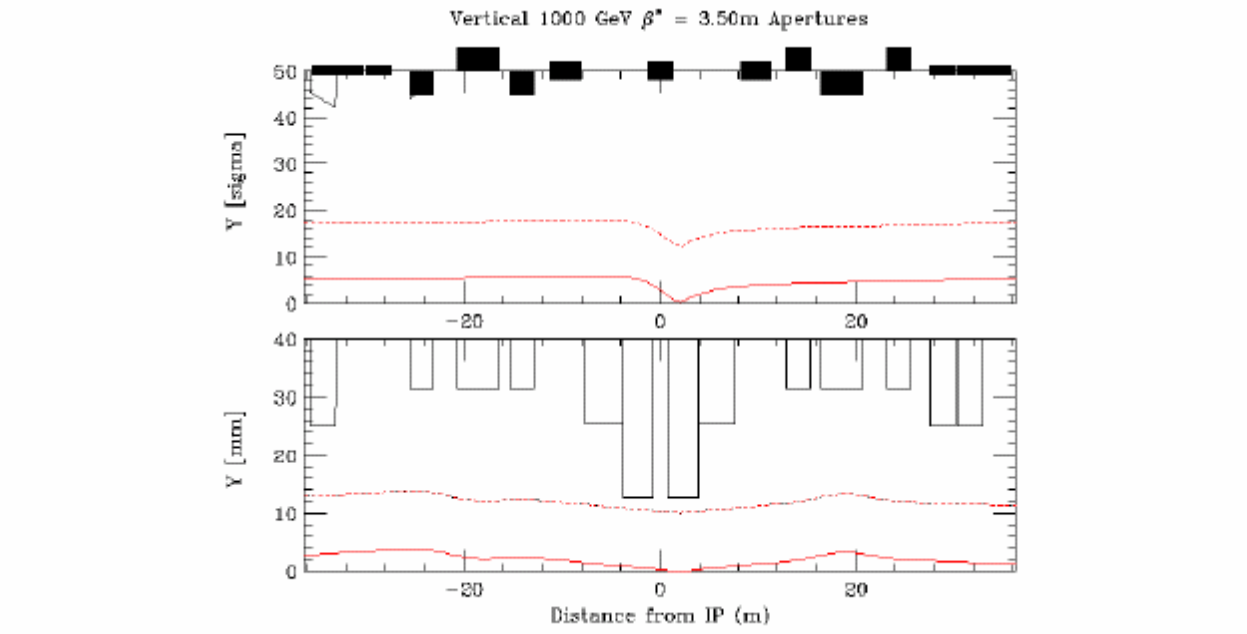

Figure 2-13: Vertical beam envelope & apertures at 1 TeV during B0/D0 collisions. (Same legend as for Figure 2-11).

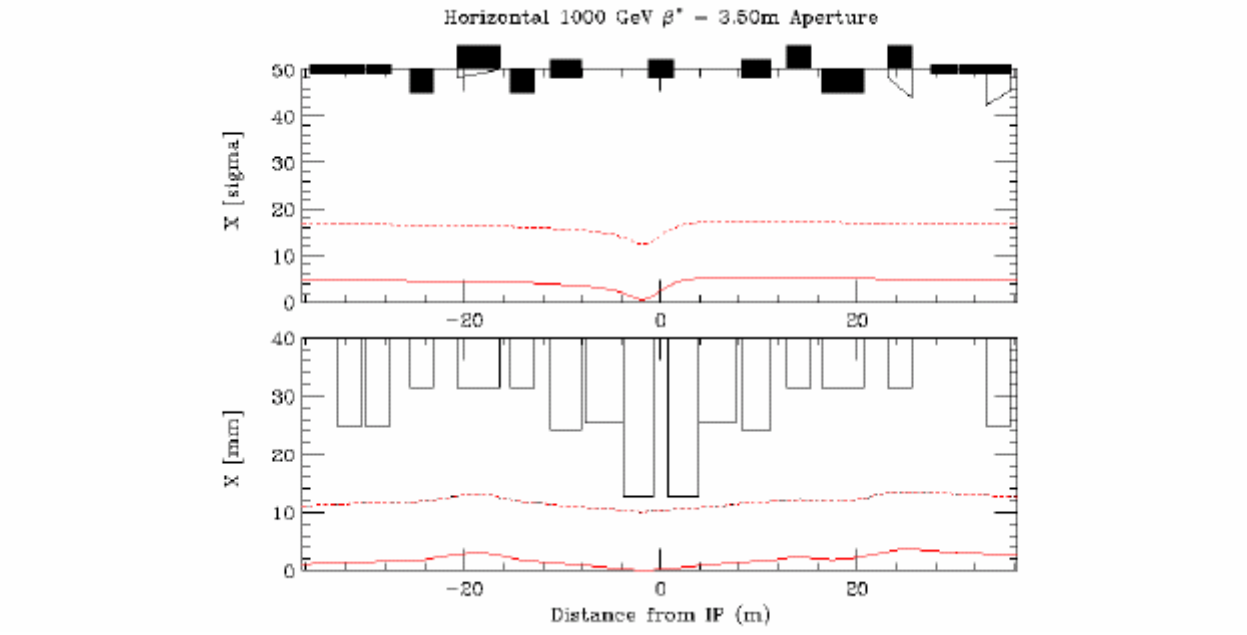

Figure 2-14: Horizontal beam envelope & apertures at 1 TeV during B0/D0 collisions. (Same legend as for Figure 2-11).

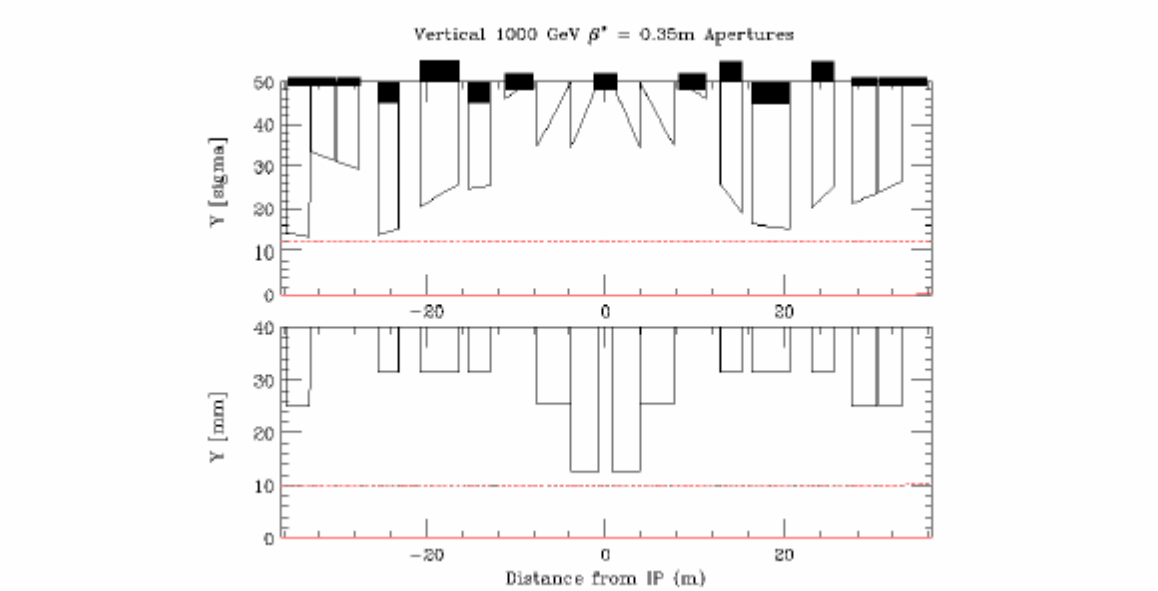

Figure 2-15: Vertical beam envelope & apertures at 1 TeV during C0 collisions. (Same legend as for Figure 2-11).

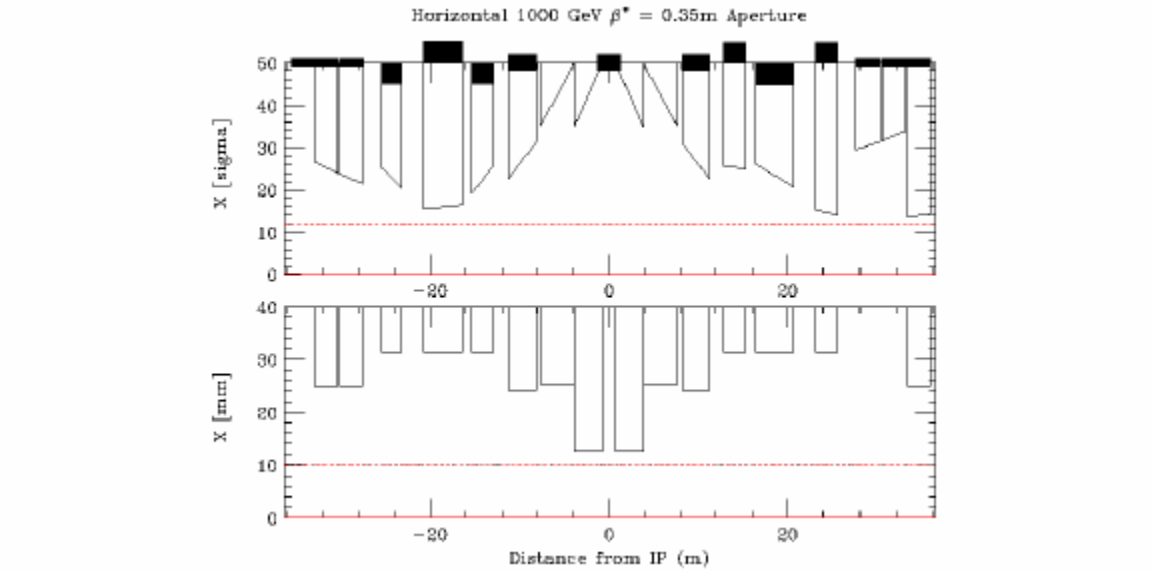

Figure 2-16: Horizontal beam envelope & apertures at 1 TeV during C0 collisions. (Same legend as for Figure 2-11).

2.4 Higher Order Correction

2.4.1 Quadrupole Misalignments

The effects of misaligned quadrupoles other than the triplet quadrupoles are straightforward to correct using the arc correction spools between B38 and C17 listed in Table 2-8. The following discussion therefore is limited to the triplets. Two types of misalignment are particularly harmful – transverse misalignments, which deliver kicks to the beam, and roll of the quadrupoles about the longitudinal axis, leading to coupling of the transverse planes. The beam optics are not as sensitive to other misalignments, such as translation of the magnets along their longitudinal axis.

Transverse displacements of the triplet quadrupoles produce dipole kicks which translate principally into beam offsets at the IP. These orbit distortions can be corrected using the position and angle bumps described previously in Section 2.3.1, and it is not difficult to estimate the range of misalignments that can be tolerated. In general the IR quads will suffer both systematic and random displacements. Using Table 2-11, and the known quadrupole magnetic lengths and gradients, the offset at the IP resulting from a systematic transverse error of Δ_S mm is estimated to be $1.44\Delta_S$ mm. In the absence of random transverse errors, the 0.48 T·m triplet spool dipoles can therefore compensate for systematic errors Δ_S as large as ±1.9 mm. Similarly, for transverse errors distributed randomly over the range $-\Delta_r \rightarrow +\Delta_r$ mm the average (r.m.s.) offset at the IP is calculated to be $3.23\Delta_r$ mm, and the largest error range that can be corrected is $\Delta_r = 0.83$ mm.

Roll of the triplet quadrupoles introduces coupling that degrades luminosity. Although this coupling can be corrected globally with distributed skew quadrupole circuits, reduction in luminosity is unavoidable unless there are skew correction elements situated physically at the location of the triplets. Table 2-11 lists the locations of skew quadrupoles, and their contributions to the real and imaginary components of the coupling coefficient. Since there is essentially zero phase advance across the triplets it can be seen that the triplet skew quad elements at C0U and C0D are ideally situated to correct for roll errors in the triplets.

The efficiency of the C0U and C0D skew quads at compensating coupling can be estimated by considering a hypothetical case in which the triplet magnets all undergo roll misalignments somewhere in the range of ±Φ mrad. A systematic roll of the 3 quadrupoles has an almost insignificant impact on coupling because of the large cancellation between opposite polarity magnets. Using Table 2-11, and the known quadrupole magnetic lengths and gradients, the approximate systematic real and imaginary coupling contributions in this case are just 4Φ and 14Φ T·m, respectively. In the worst misalignment case the 3 coupling terms add. With all quads rolled through Φ mrad, but with Q1 & Q3 rolled in the opposite direction to Q2, the total coupling terms become 156Φ and 1250Φ T·m. The maximum integrated field of the C0U & C0D skew quadrupoles is 7.5 T·m/m, so that even in this worst case scenario the triplet correctors are capable of compensating locally for roll angles Φ as large as ±6.0 mrad on each of the individual magnets. Such large errors are more than would be expected in practice. In a more realistic error estimate the roll errors would be randomly distributed over the range $-\Phi \rightarrow +\Phi$ mrad. For a

uniform error distribution the average (r.m.s.) cosine and sine coupling terms are a factor of ~2.8 smaller than in the worst case, giving 56Φ and 448Φ T·m, respectively. If desired, the B45, B46, and C14, C15 correctors are also available to fine tune cancellation of the real coupling component.

Table 2-11: Locations of spool packages that contain both skew quadrupoles & dipole correctors in both planes, and useful optics parameters for evaluating the impact of triplet misalignments. Also shown are lattice functions for the Q1, Q2, and Q3 IR quads, averaged over the lengths of the magnets [$\mu_X = \mu_Y = 0$ at F0 & $\Delta\mu = 2\pi(\mu_x - \mu_y)$].

Spool	βx (m)	μx (2π)	βy (m)	μy (2π)	$\sqrt{\beta x \beta y} \cdot \cos(\Delta\mu)$ (m)	$\sqrt{\beta x \beta y} \cdot \sin(\Delta\mu)$ (m)
PACKB45	25.1	9.913	94.5	9.808	38.48	29.85
PACKB46	93.5	10.037	81.1	9.880	48.04	72.63
Q3D	588	10.646	1556	10.376	-119.88	948.96
PACKC0U	1021	10.646	1021	10.376	-127.97	1012.95
Q2F	1478	10.647	510	10.377	-108.82	861.42
Q1D	625	10.647	518	10.379	-66.05	565.66
C0*	0.35	10.893	0.35	10.625		
Q1F	518	11.140	625	10.871	-66.05	565.66
Q2D	510	11.141	1478	10.871	-108.82	861.42
PACKC0D	1021	11.142	1021	10.872	-127.97	1012.95
Q3F	1556	11.142	588	10.872	-119.88	948.96
PACKC14	72.1	11.645	96.3	11.483	43.76	70.91
PACKC15	99.7	11.711	16.1	11.678	39.21	8.25

2.4.2 Feed-down Circuits

Separating the proton and pbar beams onto helical orbits causes the beams to travel off-axis through the Tevatron's chromatic sextupoles. If left uncorrected, the feed-down from these non-linear fields into normal and skew quadrupole components would split the proton and pbar tunes

oppositely away from the nominal central orbit values, and also result in coupling between the transverse planes. To compensate for these undesirable effects, additional circuits of feed-down sextupoles and skew sextupoles distributed around the ring are used to adjust the tunes and coupling of the protons and pbars independently during collider operations. The impact of a single feed-down element on the closed orbit optics depends on the orientation of the helix at that location, the polarity and roll angle of the magnet, and on the horizontal and vertical betatron phases.

A thin sextupole, of integrated field $K_{2L} = B''L/B_o\rho$, will generate feed-down normal and skew quadrupole fields, respectively, of strengths:

$$K_1L_{NQ} = K_2L\cdot[x_o\cdot\cos 3\psi - y_o\cdot\sin 3\psi] \;\; ; \quad K_1L_{SQ} = K_2L\cdot[x_o\cdot\sin 3\psi + y_o\cdot\cos 3\psi]$$

where (x_o, y_o) is the center of the helical orbit, and ψ is the roll angle of the magnet with respect to the central trajectory (zero for a normal sextupole, and $\pm 30^o$ for skew sextupoles). The first order change in differential tunes due to a family of such feed-down elements is found to be:

$$\Delta\nu_x = \frac{1}{4\pi}\cdot\sum\beta_{x,i}\cdot K_1L_{NQ,i} \quad \text{, and;} \quad \Delta\nu_y = -\frac{1}{4\pi}\cdot\sum\beta_{y,i}\cdot K_1L_{NQ,i}\,.$$

Here, the tune shifts are defined for a beam with respect to the central orbit, or half the values produced between the proton and pbar trajectories. Compensation of the differential couplings depends on the feed-down into skew quadrupole fields and can be decomposed (ideally) into orthogonal cosine and sine contributions as:

$$\Delta C_{SQ} = \frac{1}{2\pi}\cdot\sum\sqrt{\beta_{x,i}\cdot\beta_{y,i}}\cdot K_1L_{SQ,i}\cdot\cos(\mu_{y,i} - \mu_{x,i})$$

$$\Delta S_{SQ} = \frac{1}{2\pi}\cdot\sum\sqrt{\beta_{x,i}\cdot\beta_{y,i}}\cdot K_1L_{SQ,i}\cdot\sin(\mu_{y,i} - \mu_{x,i})$$

with the betatron phases $\mu_{x,i}$ and $\mu_{y,i}$ measured from any convenient starting point in the ring. Unfortunately, it is not possible in the Tevatron to construct ΔC_{SQ} and ΔS_{SQ} correction circuits which are even approximately orthogonal. With $\mu_y - \mu_x$ never exceeding $\sim 30^o$ at spool locations in the arcs, the ΔS_{SQ} term is unalterably small for any reasonable values of corrector currents.

Currently there are a total of 49 normal and skew sextupole feed-down elements in the Tevatron, organized into 8 correction families. Typically, about half the families are used for differential tune and coupling correction on the injection helix, while another subset of 4 families are used for the collision helix. Circuits S6 and S7 were added at the beginning of Run II specifically to try to provide additional ΔS_{SQ} correction ability, and the lone Accumulator sextupole magnet S8 was installed for the same reason in the A0 straight section during the 2003 shutdown.

A complete listing of feed-down elements along with their corresponding circuits is provided in Table 2-12, while Table 2-13 lists the primary functions of the 8 families during Run II collider operations.

Table 2-12: Locations, magnetic elements, and polarities of members of the 8 Run II feed-down families. Tevatron spool types TS:C and TS:D contain skew sextupoles – all others contain normal sextupoles. The skew sextupoles at B43 and B47 will be removed when transforming from the Run II lattice to the C0 IR configuration.

Circuit Name	Polarity	Magnet location	Spool type	Circuit Name	Polarity	Magnet location	Spool type
C:S1B1A	-	B19	E	C:S3A2A	+	A17	C
C:S1B3A	+	B38	E		-	A24	C
C:S1C2A	+	C24	E	C:S3D2A	-	D19	C
	-	C32	G		+	D26	C
C:S1E2A	+	E24	E	C:S3D4A	+	D38	C
	-	E28	E		-	D46	C
C:S1F2A	+	F19	E	C:S3E1A	-	E17	C
	-	F26	G		+	E22	C
C:S1F3A	+	F34	E	C:S3E3A	-	E32	C
	-	F38	E		+	E36	C
C:S2A1A	-	A14	D	C:S4C2A	+	C19	E
C:S2A3A	+	A33	D		-	C26	G
C:S2B4A	-	B43	D	C:S4C2B	+	C22	G
	+	B47	D		-	C28	E
C:S2C3A	+	C27	D	C:S4F2A	+	F24	E
	-	C33	D		-	F28	E
C:S2D2A	-	D23	D	C:S5A2A	+	A18	D
	+	D27	D	C:S5A3A	-	A37	D
C:S2F1A	+	F12	D	C:S5D3A	-	D33	D
	-	F16	D		+	D37	D
C:S2F2A	+	F23	D	C:S5F1A	-	F14	D
C:S2F4A	-	F43	D	C:S5F3A	+	F33	D
				C:S6A4A	+	A46	T:SF
				C:S6C4A	-	C46	T:SF
				C:S7B1A	+	B14	T:SD
				C:S7D1A	+	D14	T:SD
				C:S8A0A	+	A0	PBAR

Installation of new magnets in the C0 interaction region from B43–C17 will eliminate the 2 skew sextupoles at B43 and B47 from the S2 feed-down family. But, because the C0 IR insertion is designed to be transparent to the rest of the machine through the extra integer of tune inserted from B38–C17, it is guaranteed that the helix outside the IR region is unaltered from its configuration in the Run II lattice for any given setting of the ring electrostatic separators. It is sufficient (and complete), therefore, to focus only on the disrupted S2 family when considering feed-down modifications that might be required.

Table 2-13: Feed-down circuits and their functionality for the injection helix described in Sect. 2.2.1 and the Run II B0/D0 collision helix: $\Delta\nu_x$, $\Delta\nu_y$ are the differential tunes, and; ΔC_{sq}, ΔS_{sq} are the cosine and sine components of differential coupling.

Circuit	Injection Helix	Collision Helix
S1	$\Delta\nu_x$	ΔC_{sq}
S2	$\Delta\nu_y$	
S3	ΔC_{sq}	
S4		$\Delta\nu_x$
S5		$\Delta\nu_y$
S6		
S7	ΔS_{sq}	ΔS_{sq}
S8	ΔS_{sq}	

During Run II the S2 circuit is used only on the injection helix, and mainly for adjusting the differential vertical tune. To preserve this functionality in the BTeV era two options have been considered. First, the functionality of the B43 and B47 elements could be transferred to alternate sites in the ring having the appropriate helix orientation and lattice functions. Parameters of one such viable pair of locations are compared with those at B43 and B47 in Table 2-14. Here, the existing, unused skew sextupoles in the E27 and E33 spools would replace the B43 and B47 elements in the S2 circuit. Another possible option is to simply omit the B43 and B47 magnets from the circuit, since the loss of 2 elements from the 12-member S2 family is likely to be an acceptable perturbation.

Table 2-14: Comparison of injection helix parameters between the B43 and B47 spools and their possible replacements at E27 and E33.

Site	Spool	βx (m)	βy (m)	μx − μy (deg ^{o})	Xo (mm)	Yo (mm)
B43	TS:D	32.7	95.4	26.6	-0.50	-5.20
B47	TS:D	30.5	89.8	28.1	+3.62	+4.02
E33	TS:F	33.2	93.9	29.2	-0.67	-5.86
E27	TS:FR	30.7	93.2	28.1	+3.73	+6.39

The implications of the 2 options for compensating the loss of B43 and B47 in the S2 circuit are illustrated by Table 2-15. Shown there is the matrix correspondence between currents in the S_i circuits and desired changes in the differential tunes and coupling for 3 cases: (i) the Run II feed-down configuration with B43 and B47 intact; (ii) the B43 and B47 functions are replaced by E27 and E33 spools, and; (iii) the B43 and B47 skew sextupoles are eliminated entirely.

Although, by any practical standard, the solution in which B43 and B47 are relocated to E27 and E33 is equivalent to the existing Run II feed-down configuration, it should be apparent that there is no clear advantage to pursuing this option. The alternative, of reducing the S2 circuit to 10 magnets by dropping the B43 and B47 contribution entirely, is nearly identical, apart from a modest ~17% increase in the S2 currents.

Table 2-15: Run II 150 GeV injection helix of Sect. 2.2.1 – Currents in the S_j feed-down circuits (Amps) as functions of changes in the differential tunes and coupling (units of 0.001). Results shown correspond to: (i) Run II configuration for S2; (ii) replacement of B43 and B47 with E27 and E33, and (iii) elimination of B43 and B47 feed-down skew sextupoles in S2.

(i) Run II complement of S2 magnets:

$$\begin{pmatrix} S_1 \\ S_2 \\ S_3 \\ S_{7+8} \end{pmatrix} = \begin{pmatrix} -.1207 & -.0406 & -.0173 & -.0765 \\ .0466 & .1361 & .0044 & .0104 \\ .0109 & .0176 & .0956 & -.0109 \\ -.0078 & -.0085 & -.3176 & -.7624 \end{pmatrix} \bullet \begin{pmatrix} \Delta\nu_x \\ \Delta\nu_y \\ \Delta C_{sq} \\ \Delta S_{sq} \end{pmatrix}$$

(ii) E27 and E33 replace B43 and B47:

$$\begin{pmatrix} S_1 \\ S_2 \\ S_3 \\ S_{7+8} \end{pmatrix} = \begin{pmatrix} -.1206 & -.0403 & -.0173 & -.0765 \\ .0442 & .1289 & .0042 & .0098 \\ .0107 & .0172 & .0956 & -.0109 \\ -.0076 & -.0077 & -.3176 & -.7623 \end{pmatrix} \bullet \begin{pmatrix} \Delta\nu_x \\ \Delta\nu_y \\ \Delta C_{sq} \\ \Delta S_{sq} \end{pmatrix}$$

(iii) S2 reduced to 10 elements:

$$\begin{pmatrix} S_1 \\ S_2 \\ S_3 \\ S_{7+8} \end{pmatrix} = \begin{pmatrix} -.1213 & -.0426 & -.0173 & -.0767 \\ .0547 & .1598 & .0052 & .0122 \\ .0088 & .0114 & .0954 & -.0114 \\ -.0107 & -.0171 & -.3179 & -.7631 \end{pmatrix} \bullet \begin{pmatrix} \Delta\nu_x \\ \Delta\nu_y \\ \Delta C_{sq} \\ \Delta S_{sq} \end{pmatrix}$$

2.5 Single Beam Dynamics

Realistic tune footprint & dynamic aperture calculations require the inclusion of lattice nonlinearities. The studies described below include the B0/D0 IR triplet quadrupole multipoles,

chromatic sextupoles, and the multipoles of the C0 LHC triplet magnets. The LHC multipoles are listed in Table 2-16. All calculations correspond to the top energy of 980 GeV for C0 collisions at $\beta^* = 35$ cm on the collision helix.

Table 2-16: LHC quadrupole magnetic nonlinearities included in beam dynamics studies.

LHC HARMONICS @ 11922 A					
	Average	Sigma		Average	Sigma
b3	0.31	0.47	a3	-0.57	0.65
b4	0.02	0.48	a4	0.30	0.39
b5	-0.03	0.13	a5	-0.38	0.18
b6	-0.02	0.45	a6	-0.04	0.11
b7	-0.01	0.03	a7	0.01	0.03
b8	0.00	0.02	a8	0.01	0.03
b9	0.03	0.01	a9	-0.02	0.03
b10	0.00	0.02	a10	-0.03	0.02

- LHC harmonics reported in "units" at a reference radius of 17 mm.

- Harmonics are a weighted average over body + end fields for 6 magnets.

- All data taken at 215 T/m.

2.5.1 Tune Spread

The single beam tune footprint can be a good measure of the impact of the machine nonlinearities on the beam. Figure 2-17 shows the tune footprint extending to amplitudes of 6σ in each plane. Without the C0 triplet magnet errors the tune spread generated by the arc magnets and B0/D0 IR's is approximately $(\Delta\nu_x, \Delta\nu_y) = (3E\text{-}4, 3E\text{-}4)$. The inclusion of C0 IR errors more than doubles this spread to $(\Delta\nu_x, \Delta\nu_y) = (8E\text{-}4, 8E\text{-}4)$. Figure 2-18 compares the footprint from only the octupoles with that generated by all errors, indicating that the source of the tune spread is nearly entirely the octupole component of the IR quadrupoles. The corresponding tune footprint in the current Run II Tevatron lattice with B0/D0 collisions is shown in Figure 2-19. The single beam tune spread in the C0 lattice and in Run II are comparable. Discussions presented in subsequent sections will demonstrate that beam-beam effects swamp these single-beam results by much more than an order of magnitude.

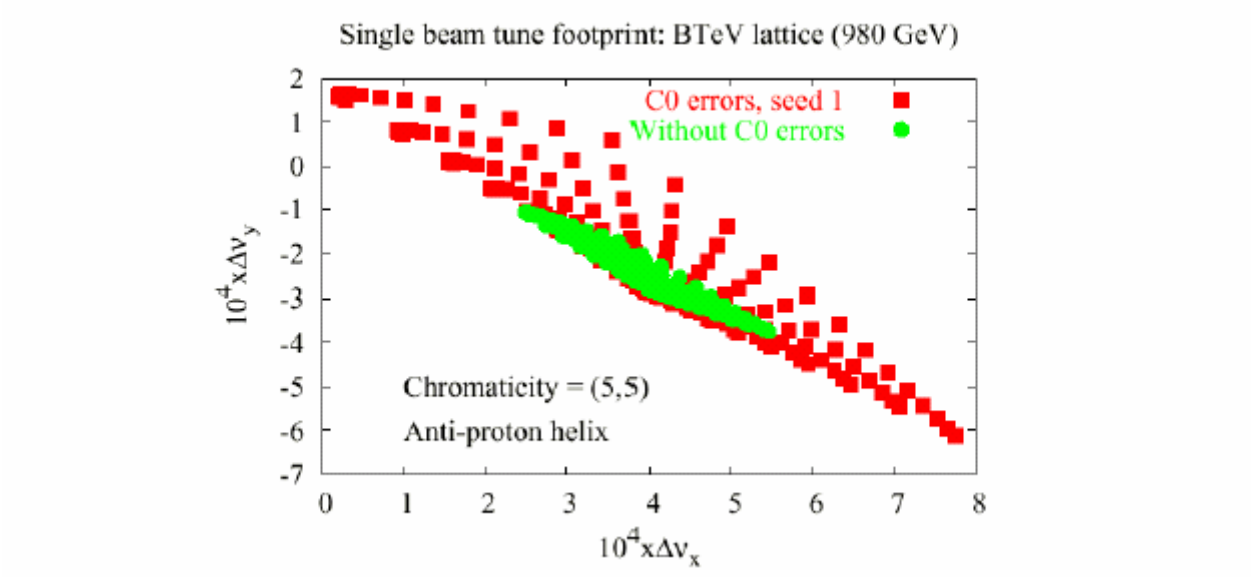

Figure 2-17: Single beam tune footprint in the C0 lattice showing the tune spread in the absence of IR quadrupole errors and the contribution from the C0 multipole errors of Table 2-16.

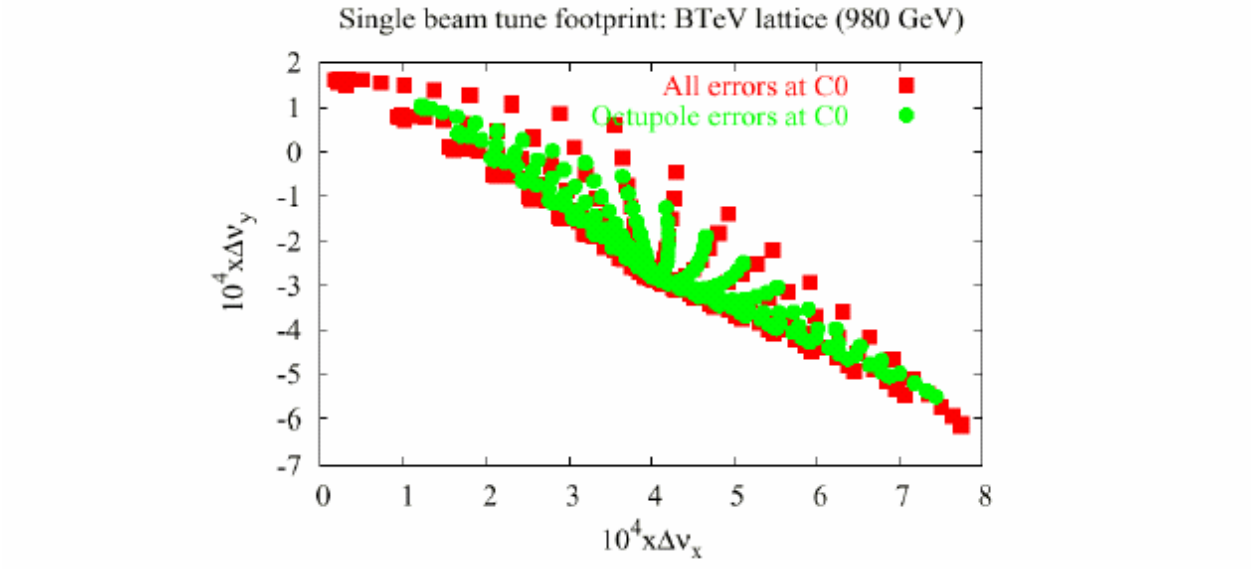

Figure 2-18: Single beam tune footprint due to just the octupole moment of the IR quadrupoles compared with the total contribution from all C0 IR errors.

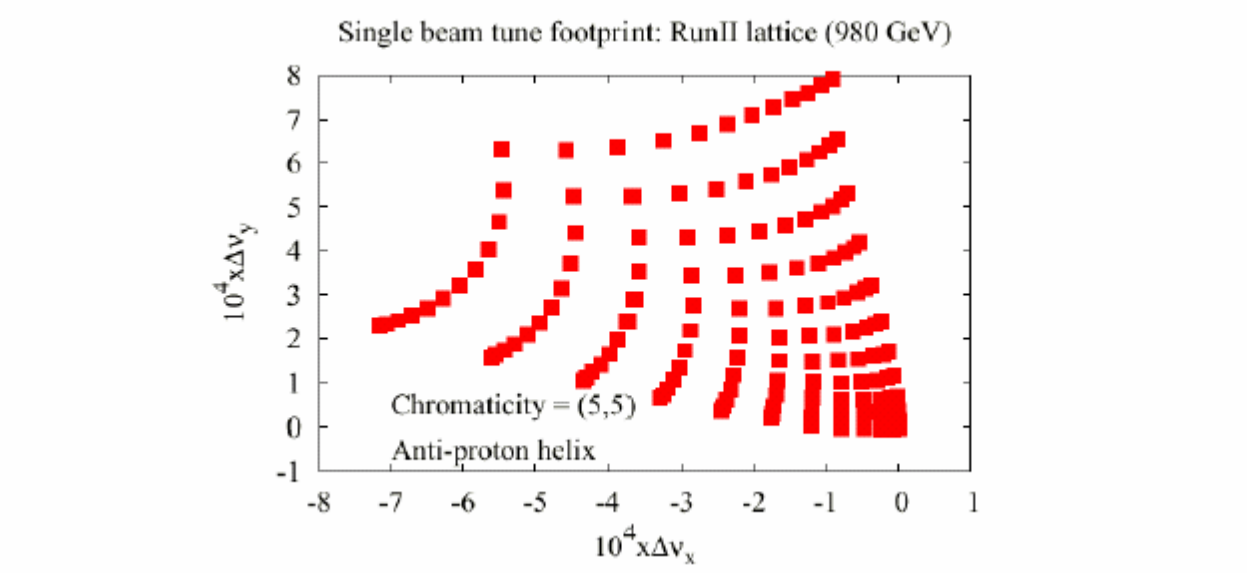

Figure 2-19: Tune footprint of a single beam in the current Run II lattice, with collisions at B0 & D0.

2.5.2 Dynamic Aperture

The dynamic aperture calculation involves launching particles at several angles in x – y space. In the following calculations 13 launch points were taken, spaced apart by 7.5^o from 0^o (horizontal) to 90^o (vertical). The radial dynamic aperture at each angle is then calculated to be the largest stable amplitude below which all amplitudes are stable. A comparison of the single beam dynamic aperture with the dynamic aperture including beam-beam forces indicates the relative importance of beam-beam effects.

Figure 2-20 shows the calculated single beam dynamic aperture for C0 collisions averaged over 5 seeds for the magnetic multipoles. The maximum separation launched was 30 σ. The average BTeV dynamic aperture is 24 σ, which is well beyond the physical aperture of the low–β quads. It can also be seen that the average DA of this C0 collision lattice is nearly twice as large as the single beam dynamic aperture calculated for Run II B0/D0 collisions. In the latter case, also calculated for $\Delta p/p$ = 3E-4, the average dynamic aperture is just 12.9 σ.

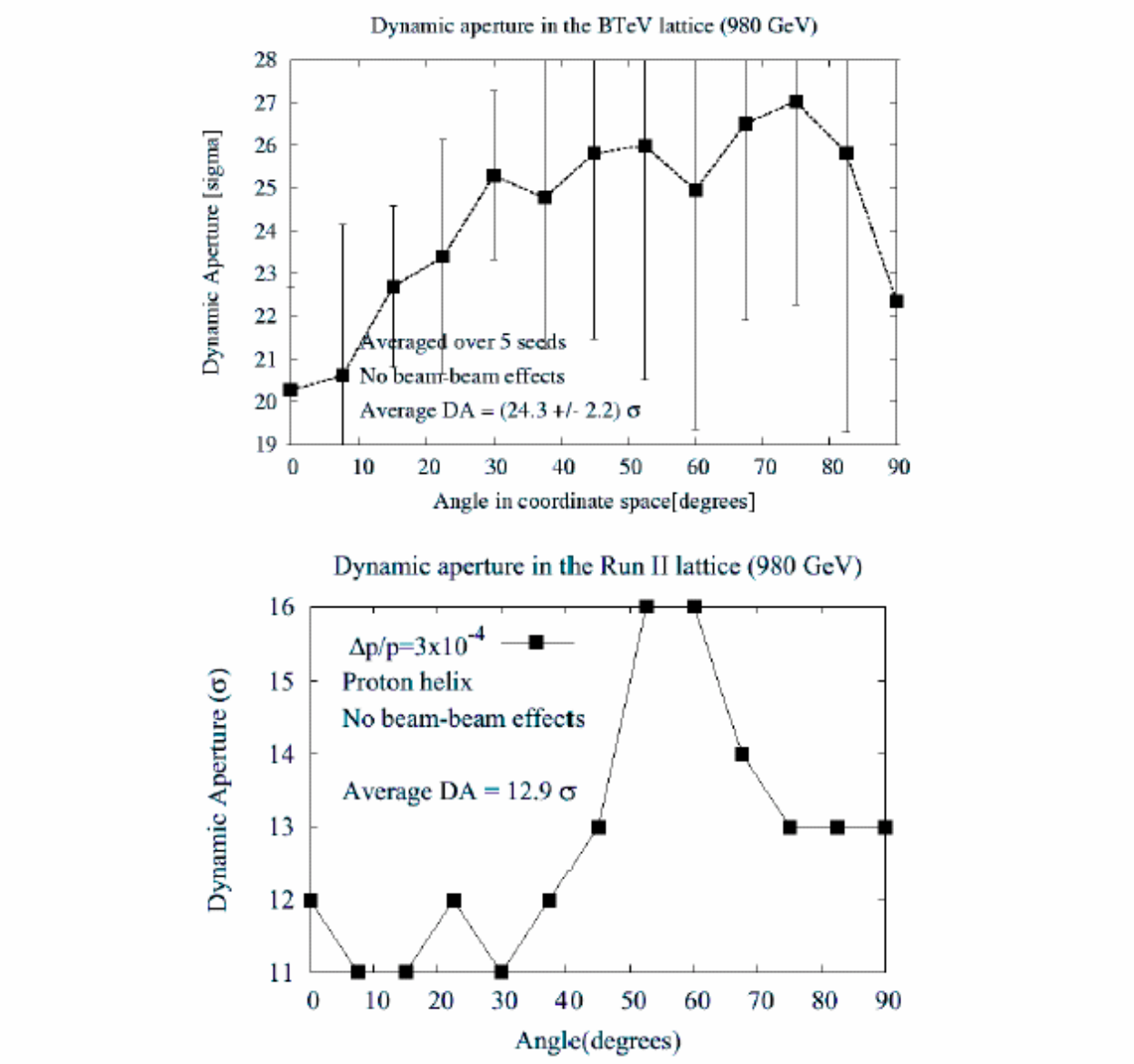

Figure 2-20: Single beam dynamic aperture on the proton helix for C0 collisions (top), and the current Run II lattice (bottom): $\varepsilon_N = 20\pi$ μm & $\Delta p/p = 3E\text{-}4$.

2.5.3 Intra-Beam Scattering

Emittance growth due to intra-beam scattering depends on the beam brightness (in six-dimensional phase space) and on the optics in the ring. Optics of the BTeV lattice are quite different from Run II B0 & D0 collision optics, and during collisions at C0 the B0/D0 insertions remain tuned to injection optics parameters. There is no obvious reason then to expect that IBS growth rates during BTeV collisions will be the same as during Run II.

The beam size growth times in the longitudinal & transverse planes are defined as:

$$\frac{1}{T_p} = \frac{1}{\sigma_p}\frac{d\sigma_p}{dt} \qquad \frac{1}{T_x} = \frac{1}{\sigma_x}\frac{d\sigma_x}{dt} \qquad \frac{1}{T_y} = \frac{1}{\sigma_y}\frac{d\sigma_y}{dt}$$

Growth rates for the BTeV and Run II lattices have been calculated using the Bjorken-Mtingwa formalism implemented in MAD. (It should be mentioned that the MAD calculation does not include coupling between planes). Beam parameters are assumed to be the same for both lattices, and are summarized in Table 2-17.

Table 2-17: Beam parameters assumed for BTeV & Run II IBS calculations.

Energy	980	GeV
Proton bunch intensity	270×10^{9}	
Hor. emittance (95%)	20	π μm
Ver. emittance (95%)	20	π μm
RMS bunch length	0.6	m
RMS momentum spread	1.4×10^{-4}	

Momentum spread and dispersion are key parameters in determining growth rates. When the transverse momenta change due to scattering, betatron oscillations are excited and the transverse emittance grows for non-zero dispersion. Therefore, calculated horizontal emittance growth due to IBS is much faster than vertical growth in the absence of coupling. Realistically, coupling tends to equalize the growth rates in the transverse planes.

Table 2-18 shows the beam size growth times for protons on the proton helix obtained using MAD. The calculations show that in the BTeV lattice longitudinal growth will be slightly faster than in Run II but transverse growth is somewhat slower. The negative table entries for vertical growth times reflect the absence of coupling in the calculations and the resulting depletion of vertical emittance to feed growth in both the horizontal and vertical planes. Run II observations confirm the earlier statement that, in reality, the transverse growth times are approximately equal. The differences between the lattices are small though – less than 10%. It is not expected, therefore, that the BTeV optics will create any major changes in the beam emittance growth.

Table 2-18: IBS beam size growth times for BTeV & Run II at 980 GeV. (Negative vertical values are discussed in the text.)

Growth Time (hrs)	BTeV	Run II
T_p	25.4	26.4
T_x	25.4	23.6
T_y	< 0	< 0

2.6 Beam-Beam Effects

With the 36x36 operations planned for BTeV collisions each bunch experiences 71 long-range interactions between the separated proton and pbar beams in addition to the head-on collision at the C0 IP. There are a total of 138 such locations around the ring where pbar–p interactions occur. The sequence & locations of the 72 interaction points seen by each bunch is different and so bunch-by-bunch effects also differ. The long-range interactions are more complex than the head-on collisions. In addition to changing the tunes, these parasitic interactions also change the orbits, coupling, and chromaticity.

2.6.1 Tune Shift and Spread

The tune footprints for representative pbar bunch #6 are compared in Figure 2-21 for the C0 and Run II collision lattices, including beam-beam forces in addition to the magnetic nonlinearities discussed earlier. The tune spreads have grown by more than an order of magnitude over the results from the single beam analyses. Nonetheless, the C0 spreads of $\Delta\nu_x = \Delta\nu_y = 0.011$ are a factor of 2 less than in the corresponding Run II footprint. In both lattices the contribution to tune shift comes mostly from the head-on collisions and 1st parasitic crossings each side of the IP. Beam separation at the first parasitics is comparable in the two collision lattices, but the much smaller C0 tune spread is largely the result of there being only one IP and two nearest miss points, as compared to the two IP's and four nearest misses of Run II.

The tune spread is a significant indicator of the extent to which the working point can be manipulated within the space between strong resonance lines. The much smaller extent of the BTeV footprint indicates that this is not an issue.

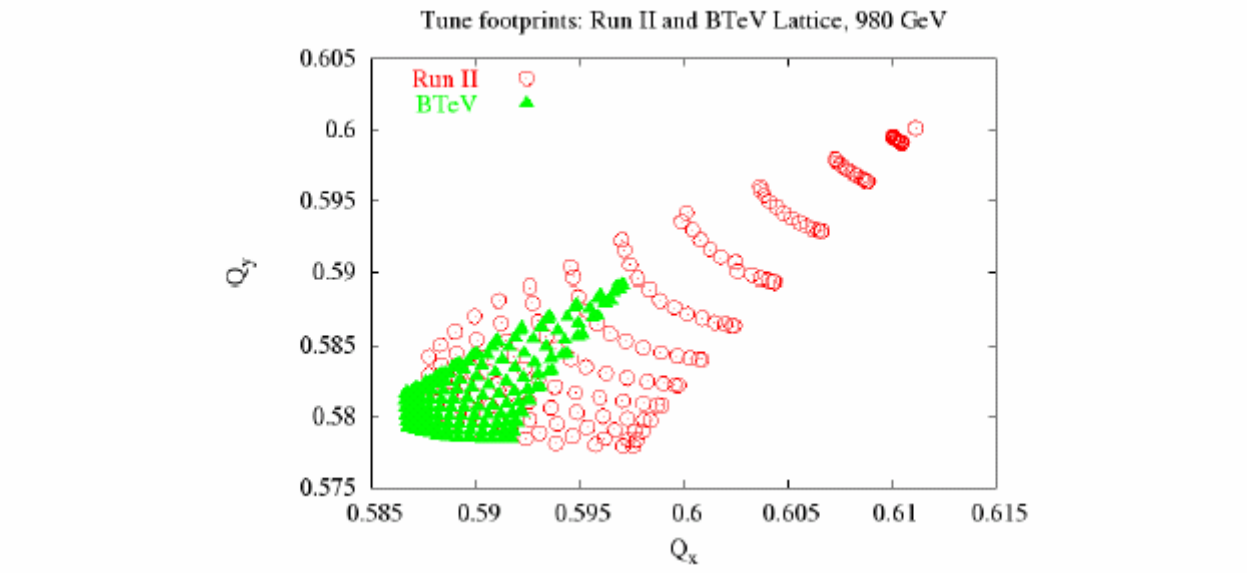

Figure 2-21: Beam-beam tune footprints extending from 0 to 6 σ of pbar bunch #6 in the BTeV and Run II collision lattices. The (0,0) particles are in the upper right of the plots & (6,6) are at bottom left. IR errors plus machine errors are included in the calculations.

The relative importance of the 1st parasitic crossings & head-on collisions is illustrated by Figure 2-22, which shows the small amplitude contribution from each of the 72 interaction points to the tune shifts of pbar bunch #6 during C0 collisions. Refinements to the collision helix should reduce the impact from the handful of other significant long-range interactions apparent in the plot.

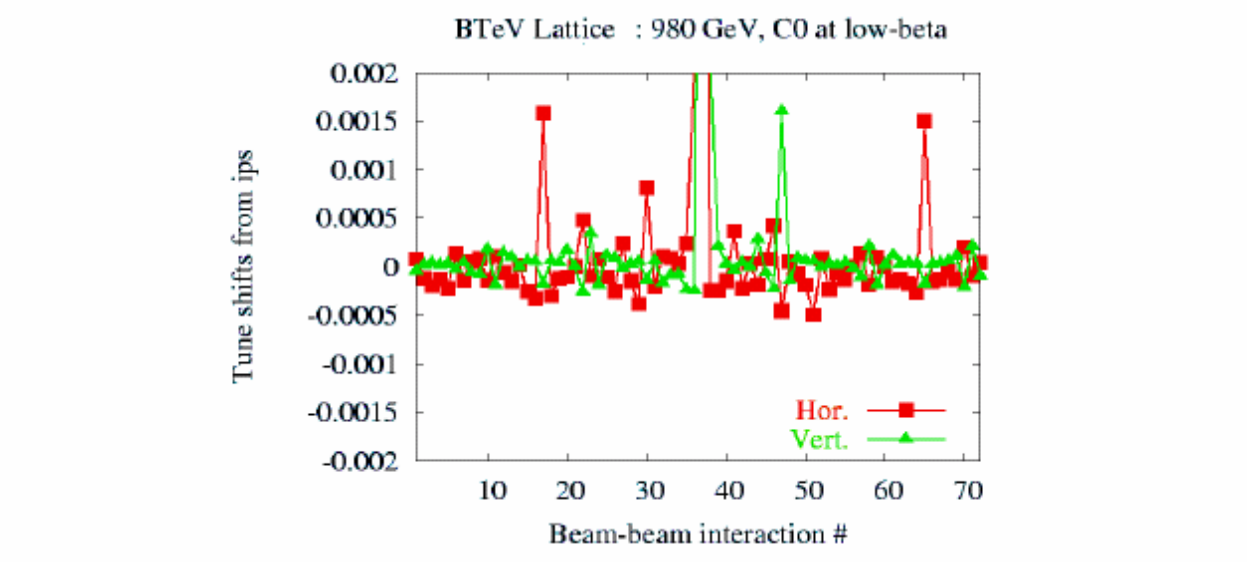

Figure 2-22: Zero amplitude contributions to the tune shifts from the 72 beam-beam interactions of pbar bunch #6 in the BTeV lattice. Contributions from the 1st parasitic crossings (at IP #36 & #38) are dominant among the long-range interactions (the C0 IP is off scale).

Bunch-by-bunch variation of the small amplitude tune shifts for C0 collisions and in Run II are shown in Figure 2-23 for all 12 pbar bunches in a train. Both the maximum tune shift and the bunch-by-bunch variation are significantly smaller in the BTeV lattice. The C0 vertical tune shifts are generally larger than the horizontal because vertical beta functions are larger at most of the parasitic crossings. In the C0 lattice the bunch #1 horizontal tune and the bunch #12 vertical tune are noticeably smaller than the tune shift of most bunches in the middle of the train. This is because the first & last bunches experience long-range interactions at only one of the two nearest miss points from the IP. Deviation of the 1st and 12th bunch tunes in Run II are much more pronounced since these bunches see only 2 out of the 4 total nearest miss locations.

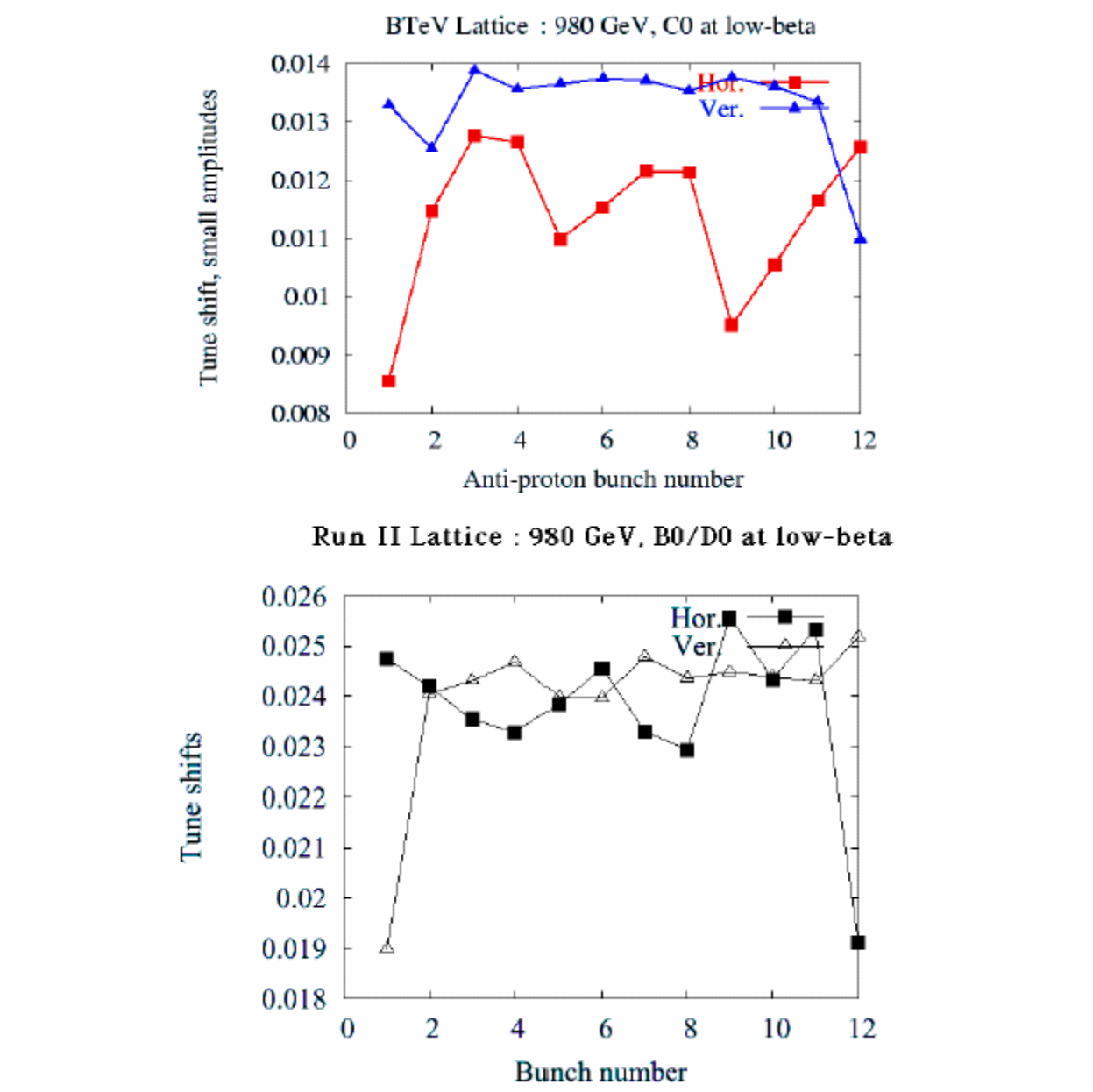

Figure 2-23: Bunch-by-bunch zero amplitude tune shifts of the 12 pbar bunches in a train for C0 collisions (top), and in the Run II lattice (bottom).

2.6.2 Dynamic Aperture

Figure 2-24 shows the dynamic aperture including beam-beam effects for C0 and Run II B0/D0 collisions. In each case beam-beam interactions reduce the average dynamic aperture by ~3 σ per IP relative to the single beam results. This analysis indicates that the average DA of the C0 lattice is more than twice as large as the 8 σ average DA calculated for Run II B0/D0 collisions. The simulations also predict that the C0 minimum dynamic aperture of 16 σ will significantly exceed the physical aperture set by the primary collimators, which are typically placed at ~8 σ.

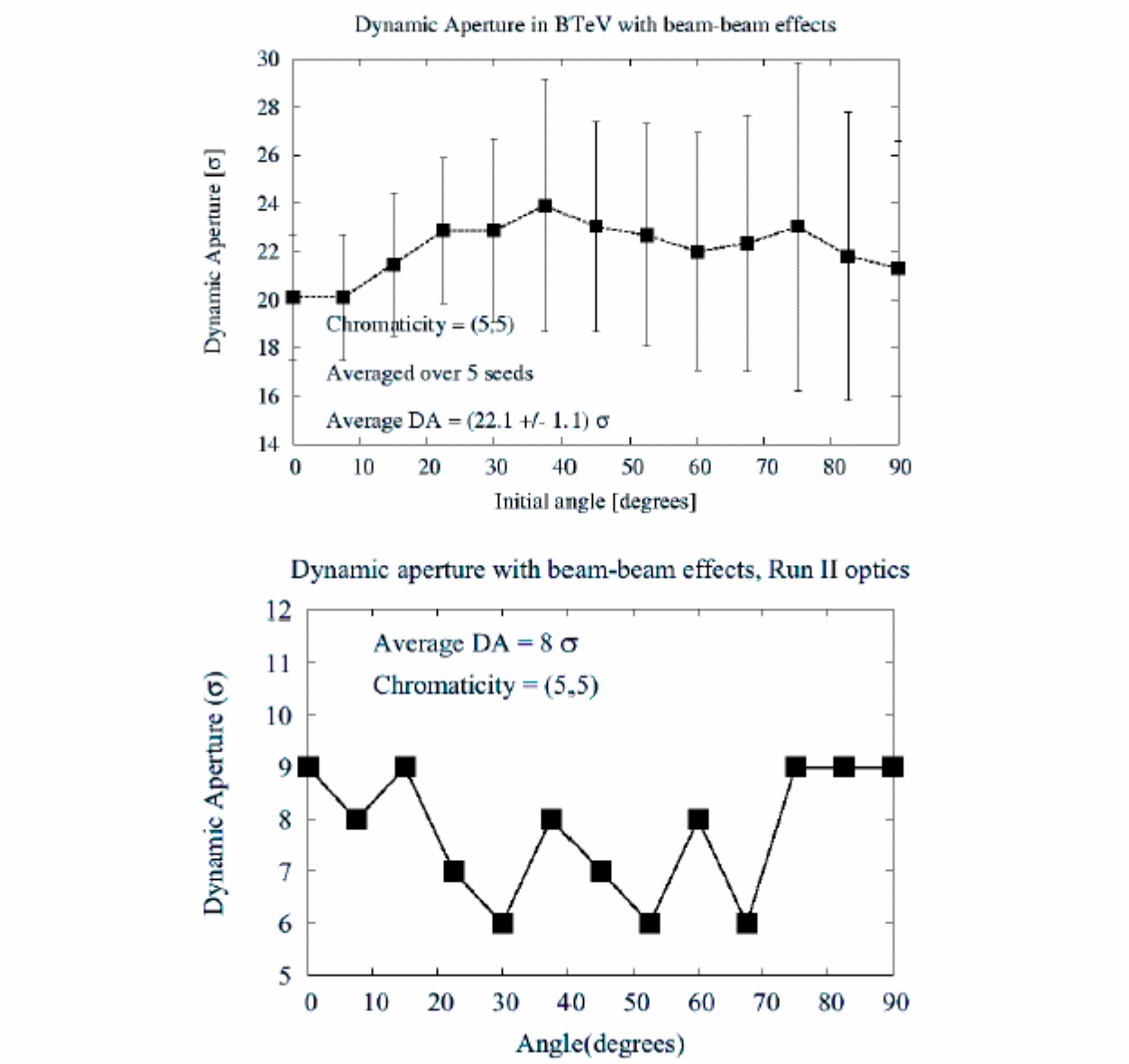

Figure 2-24: Dynamic aperture of pbar bunch #6 including beam-beam effects: C0 collision lattice (top), and Run II (bottom). $\varepsilon_N = 20\pi$ μm & $\Delta p/p = 3E\text{-}4$.

2.6.3 Minimum Tune Split

Long range interactions contain a skew quadrupole component in addition to other higher order multipoles that couple motion in the transverse planes. The degree of coupling can be characterized by the minimum tune split introduced between horizontal & vertical planes. This parameter can be significant because it is a measure of how closely the tune working point can approach the main diagonal in tune space, which is the largest region free of resonances.

Figure 2-25 compares the small amplitude bunch-by bunch minimum tune splits for the BTeV and Run II collision lattices. In general, the C0 bunch-by-bunch tune splits are a factor of ~5 larger than they are currently in Run II. The maximum values of ~0.003 are comparable to the coupling introduced by machine nonlinearities, and are larger than desirable. It is believed that it will be possible to greatly reduce the C0 tune splits through refinements to the collision helix. In addition, the coupling can be compensated globally using the Tevatron sextupole feed-down circuits discussed in sub-section 2.4.2. In Run II these circuits reduce coupling typically to about 0.003.

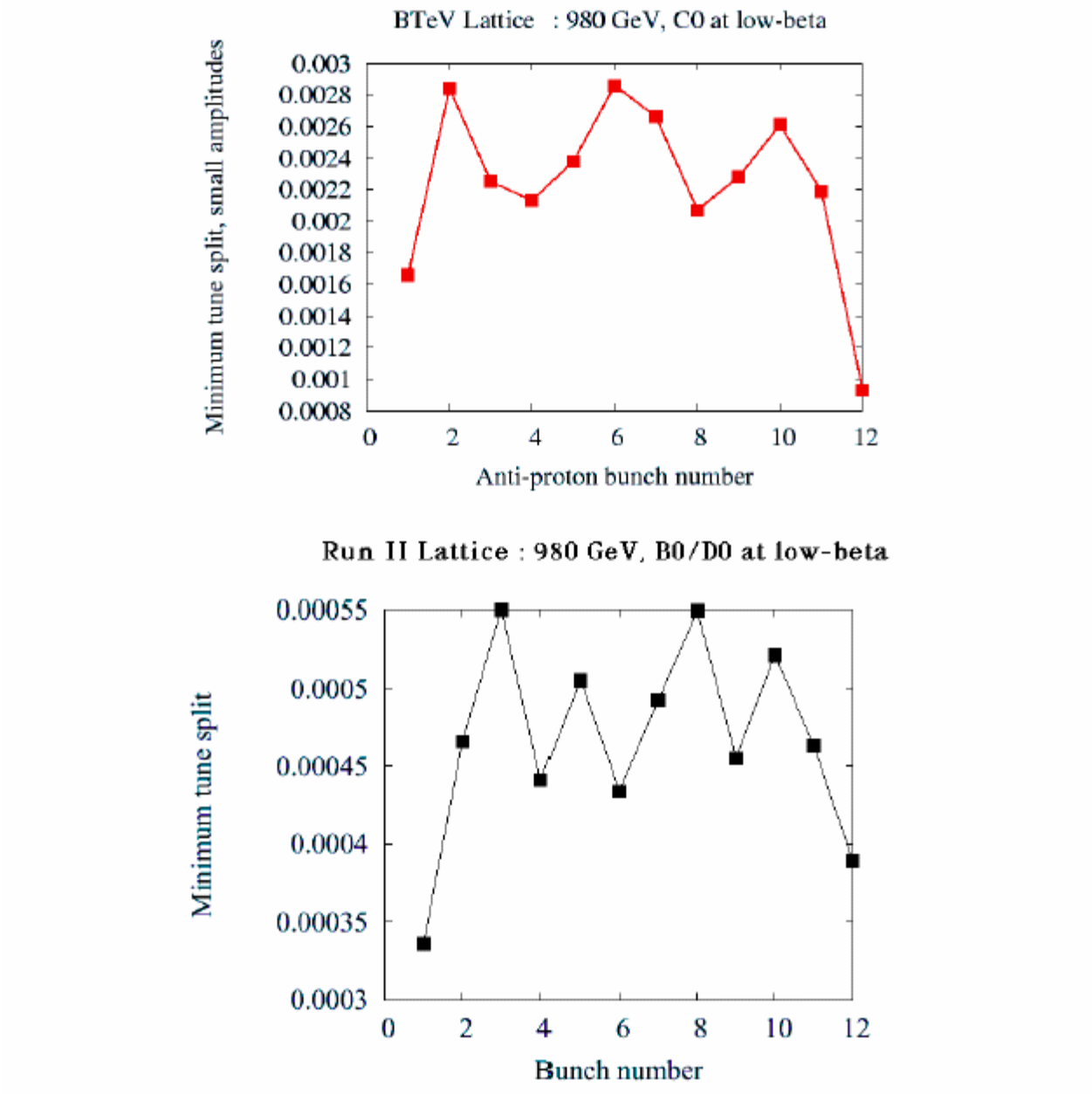

Figure 2-25: Small amplitude pbar bunch-by-bunch coupling tune shifts from long range interactions: C0 collision lattice (top), and Run II (bottom).

2.6.4 Linear Chromaticity

Long range interactions that occur in regions of dispersion change the machine chromaticity. Figure 2-26 compares pbar chromaticities during C0 & Run II collisions. Vertical chromaticity is comparable in the two lattices and small because vertical dispersion is only generated by the electrostatic separators. Horizontal chromaticity is generally much larger due to the large dispersion in the arcs. Maximum chromaticity in the BTeV lattice is less than half that in Run II, and the variation bunch-to-bunch is also half of the spread in Run II. The smaller BTeV values suggest these bunches will have better lifetimes. At collision the machine chromaticity is typically set to ~20 units in both planes, which is sufficient to keep all bunch chromaticities positive.

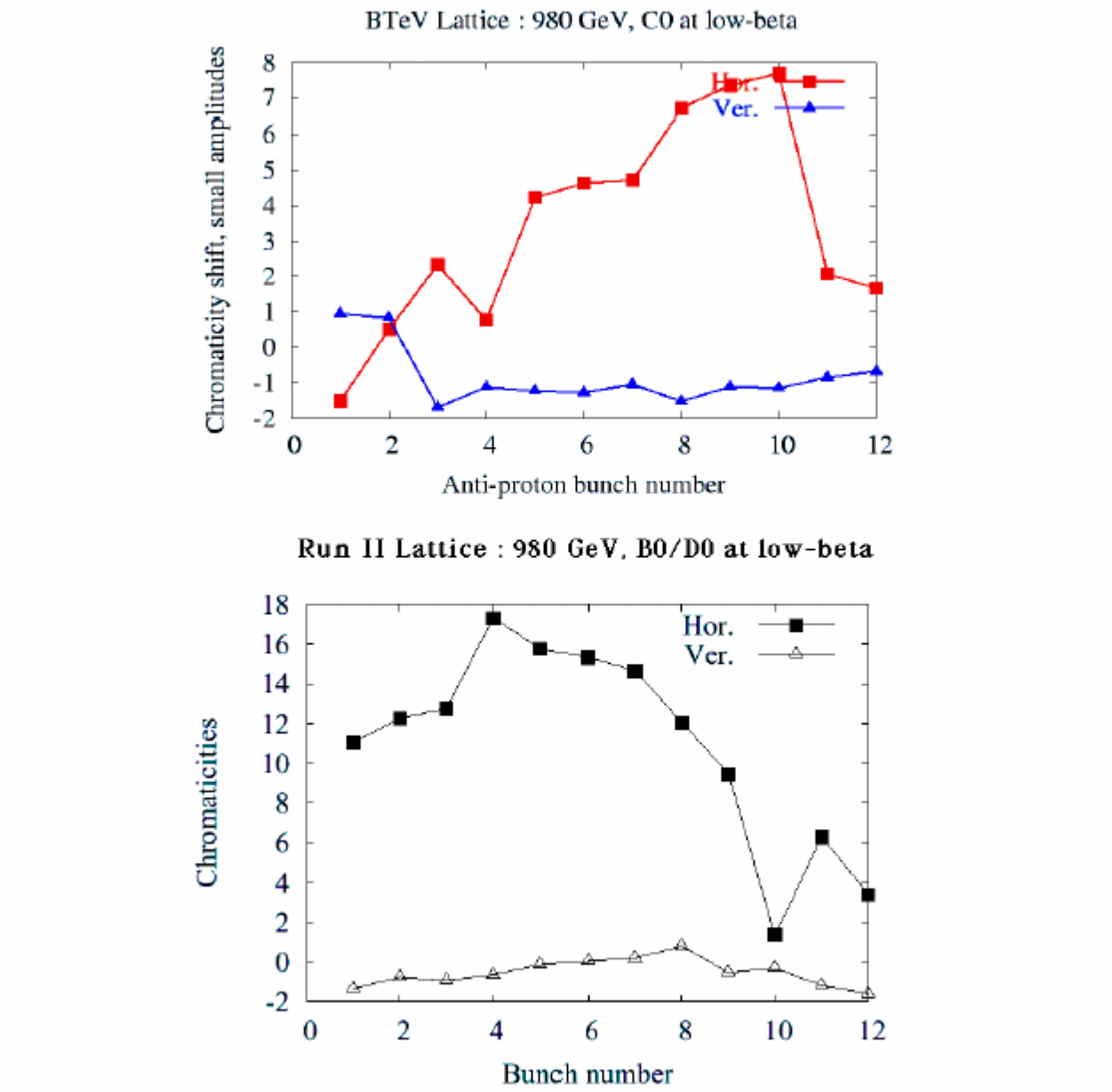

Figure 2-26: Bunch-by-bunch small amplitude beam-beam chromaticities of pbars for C0 collisions (top) and in the Run II lattice (bottom).

2.6.5 Beam-Beam Resonances

The head-on collision creates the strongest nonlinear fields but drives only even order resonances, and the 12^{th} order in particular. Due to the large proton bunch lengths, and the rapidly changing betatron phase at the IP, the impact of this resonance is greatly weakened by phase averaging. The 12^{th} order resonance effects are insignifcant in Run II and, with only 1 IP instead of 2 during C0 collisions, it is not expected to pose any problem during BTeV operations either.

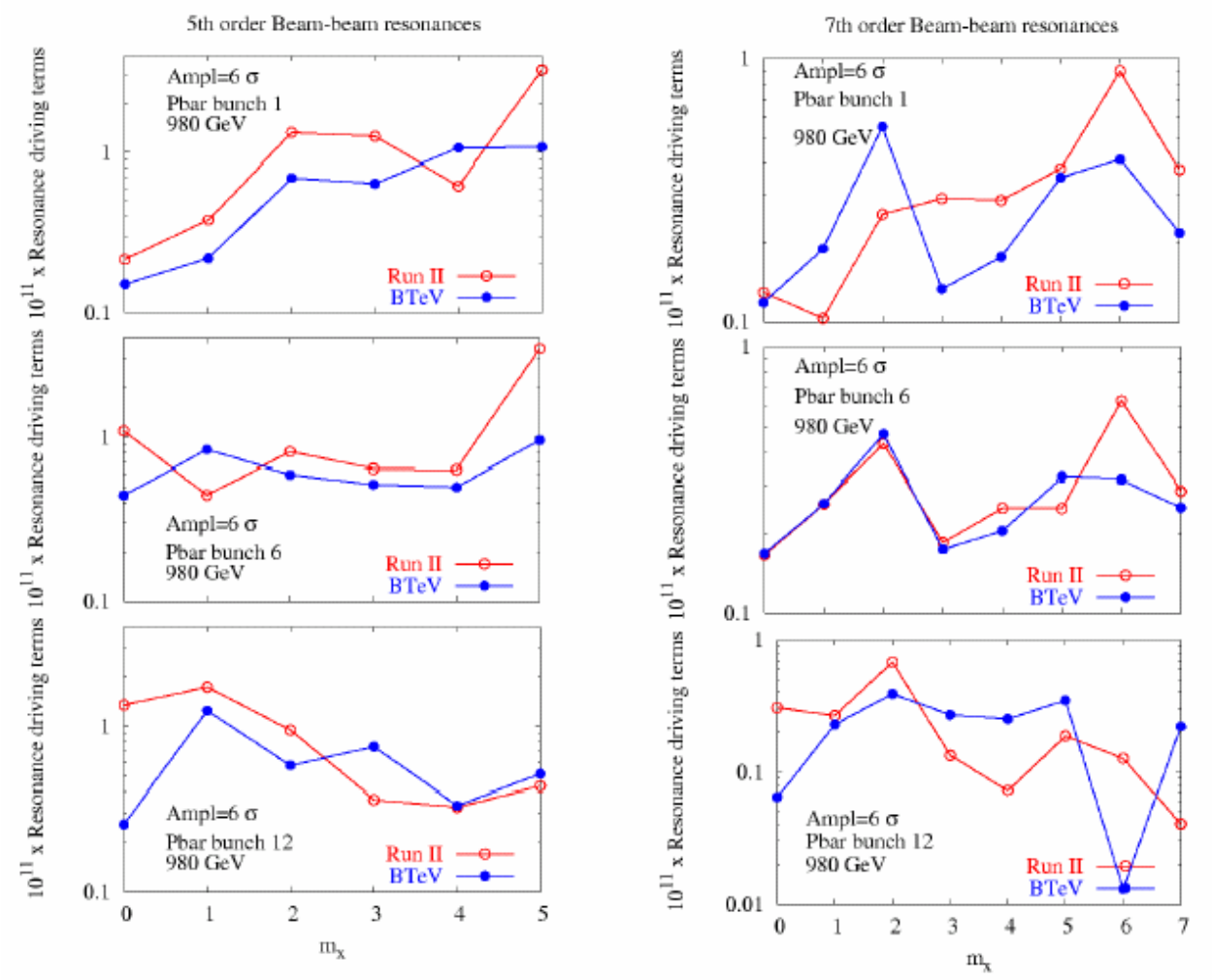

Figure 2-27: Resonance driving terms for bunches 1, 6, & 12 in the BTeV and Run II lattices: 5^{th} order resonance (left), and 7^{th} order (right). The horizontal axis labels the resonance $m_x\nu_x+(n-m_x)\nu_y$, where n = 5 or 7.

The long-range interactions drive the odd 5^{th} and 7^{th} order resonances. Figures 2-27 compares these resonance driving terms in BTeV with those of Run II for pbar bunches at the ends of the train and for a representative bunch in the middle. Resonances are evaluated at an amplitude of 6σ. In the cases studied the maximum resonance driving strength is always smaller in the BTeV lattice than in Run II. In addition, the average resonance driving terms for BTeV are also smaller. For 5^{th} order resonances the average strengths in BTeV are reduced by ~45% for pbar bunches 1 and 6, and by ~30% for bunch 12 relative to the Run II results. The improvements are not quite as dramatic for the 7^{th} order terms. For pbar bunches 1 and 6 the average resonance strength is ~20% weaker in the C0 collision lattice. For bunch 12 the average strengths are roughly the same in the two lattices, but the maximum strength is nearly a factor of 2 weaker in the BTeV lattice. Again, the improvements seen in the BTeV lattice can be attributed largely to the fact there are only two nearest miss interaction points, as compared to the four nearest misses in Run II.

2.6.6 Diffusion Coefficient and Emittance Growth

Analytical calculations of resonance driving terms and dynamic aperture simulations have predicted that beam-beam effects will not be as strong in the BTeV lattice. The weaker nonlinearities should have a direct impact on observable quantities such as diffusion, emittance growth and beam lifetimes. Multi-particle simulations have been used to calculate these quantities using the code BBSIM developed at FNAL. The simulation model includes the head-on and long-range beam-beam interactions with linear transport between the interactions. Effects due to machine nonlinearities are not included.

The horizontal diffusion coefficient, for example, is calculated at an amplitude A after N turns as follows:

$$DJ_x(A) = \frac{1}{N} \cdot \left\langle\left\langle \Delta \left| Var J_x(A) \right| \right\rangle\right\rangle$$

where $\Delta|Var\mathrm{J_X(A)}|$ is the change in the variance of the horizontal action. The double average << >> signifies two averages: the action at each turn is first averaged over 100 particles placed at each amplitude and then a second average is taken every 1000 turns (about 2 synchrotron periods) to eliminate short term amplitude beating from phase space distortions. The variance of this averaged action is calculated. The diffusion coefficient at each amplitude thus calculated typically converges after about a million turns.

Figure 2-28 shows the horizontal and vertical diffusion coefficients for the two lattices at several amplitudes. At amplitudes between 3-5 σ, the coefficients in BTeV are smaller by an order of magnitude or more. This implies that the transverse beam tails will grow more slowly in the BTeV lattice.

Emittance growth in both lattices has also been calculated by tracking $2 \cdot 10^4$ particles for 10^6 turns. Figure 2-29 shows the statistical emittances within a 3 σ envelope for the BTeV and Run II lattices. Again, emittance growth in BTeV is about an order of magnitude less and is at the level of statistical noise in these simulations. It is not possible from these simulations to estimate meaningfully the pbar lifetime due to beam-beam interactions in the BTeV lattice. With the machine aperture set at 8 σ in the tracking, none of the twenty thousand particles were lost in 1 million turns.

The results of the diffusion and emittance growth simulations are therefore consistent with the expectation that nonlinear effects due to beam-beam effects will be weaker in the BTeV lattice than in the Run II lattice.

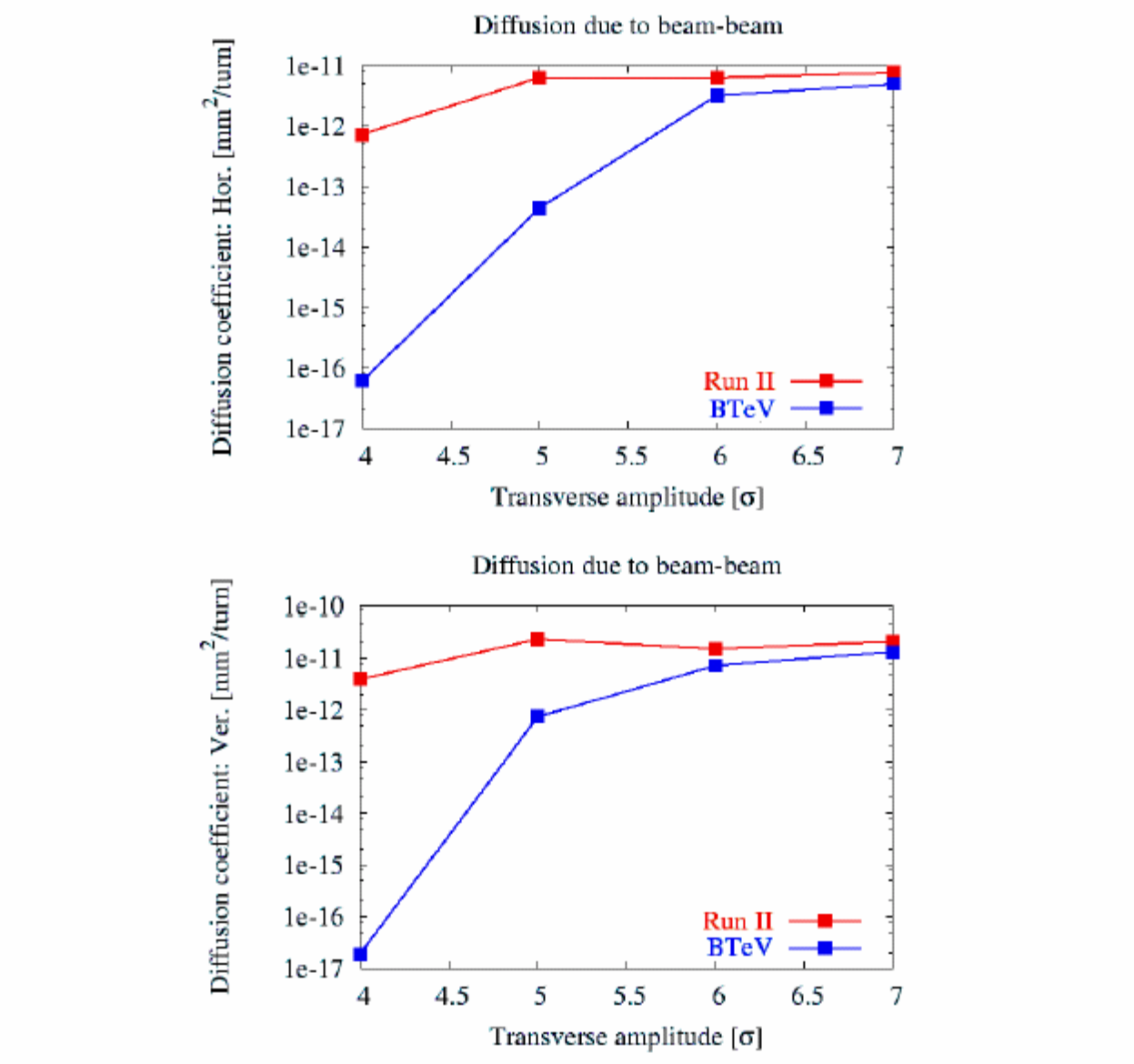

Figure 2-28: Diffusion at several amplitudes due to beam-beam interactions in the BTeV and Run II lattices.

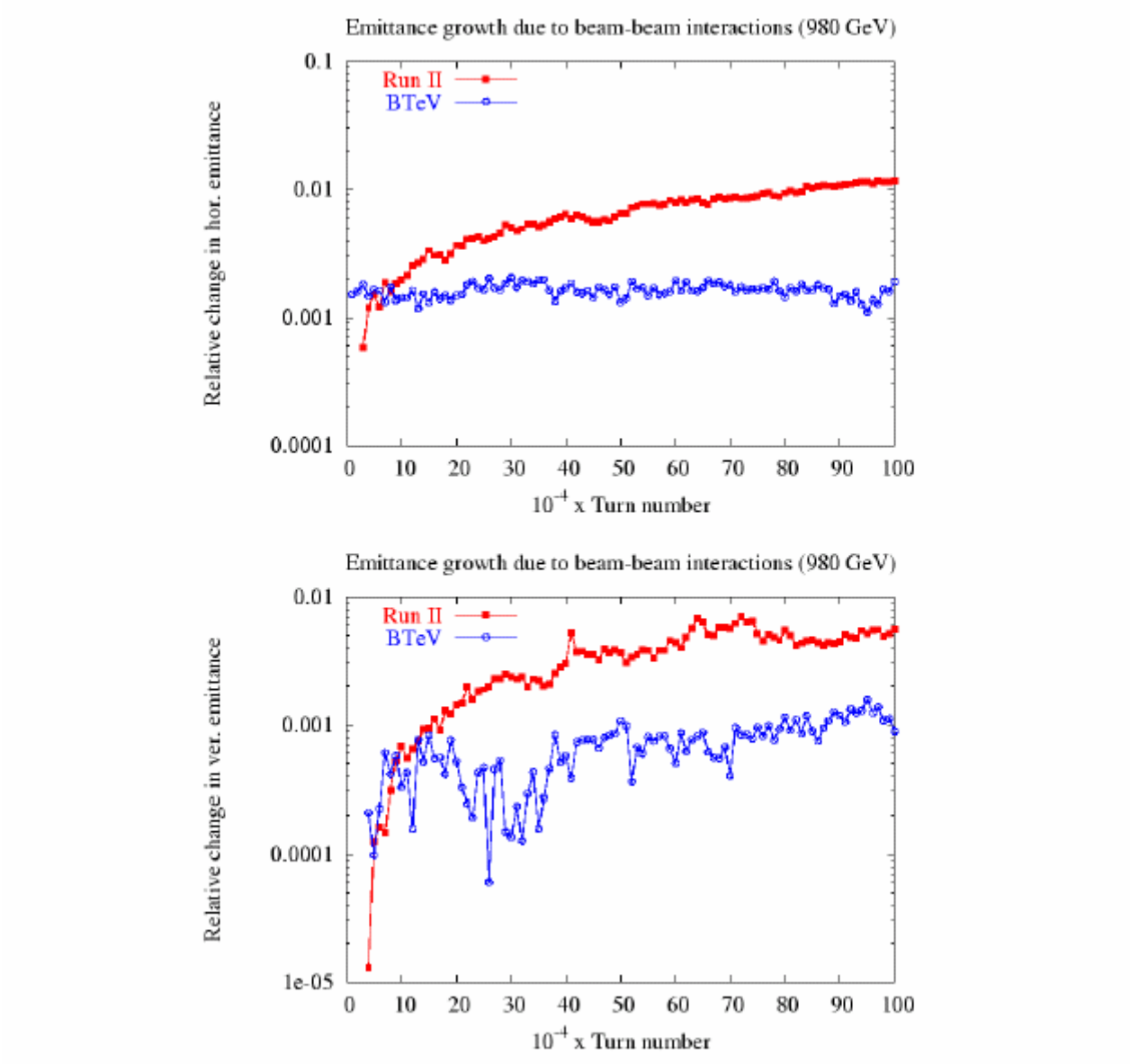

Figure 2-29: Relative changes in the horizontal emittance (top) and vertical emittance (bottom) due to beam-beam interactions in the BTeV and Run II lattices.

2.7 Beam Halo Calculations and Collimators

Note: This section describes a study of beam halo and collimation based on an earlier version of the low-β optics. In particular, on the higher intensity incident proton side of the I.P., the positions of the Q4 quadrupole magnet and the proposed collimator have since been interchanged. Similarly the positions of some components have been re-arranged on the much lower intensity incident anti-proton side of the I.P. It is anticipated that these slight changes in

component positions and optics will not substantially affect the design and effectiveness of the proton collimation system considered here. However, it is understood that the actual collimation system remains to be optimized for the final beam design.

2.7.1 Modeling with STRUCT and MARS14

A fraction of the Tevatron beam leaves the beam core producing a beam halo. This happens because of beam-gas interactions, intra-beam scattering, proton-antiproton collisions in the IPs, and particle diffusion due to RF noise, ground motion, and resonances excited by the accelerator magnet nonlinearities and power supplies ripple [1]. As a result of halo interactions with limiting apertures, hadronic and electromagnetic showers are induced in accelerator and detector components causing excessive backgrounds in the CDF, D0 and BTeV detectors. A two-stage collimation system has been developed for the Tevatron Run II [2] to reduce uncontrolled beam losses in the machine to an allowable level. About 0.1% of primary particles hitting the collimators are scattered back into the beam pipe leading to collimation system inefficiency. These particles are lost mostly in the high-β regions upstream of the experimental halls, producing background rates in the detector on the level of a few percent of those due to proton-antiproton collisions.

To evaluate these rates for the BTeV detector, multi-turn proton beam tracking through the Tevatron lattice with elastic beam scattering on the residual gas and halo interactions with the collimators was conducted with the STRUCT code [3]. All accelerator components with their real strengths and aperture restrictions were taken into account. Using the beam loss distributions calculated this way in the vicinity of C0 for protons above 0.7 TeV, detailed hadronic and electromagnetic shower simulations with the MARS14 code [4] were performed in the machine, detector and tunnel components with a cutoff energy for hadrons, leptons, and protons of 0.1 MeV. Two protective measures – a short steel collimator/mask at the B48 location and a concrete shielding wall at the tunnel/collision hall interface on the proton side – were considered as ways to reduce the machine related backgrounds in the BTeV detector. Files of background particles entering the collision hall were collected in each run for further tracking through the detector components.

The Tevatron lattice designed for BTeV operation (collisions at C0 only with $\beta^* = 35$cm) was used for the calculations. The BTeV pixel aperture radius is 2.75mm, the LHC-type quadrupole aperture radius is 31.5mm, and all other machine components with their apertures were implemented in the model. The luminosity at C0 is assumed to be $2x20^{32}$ $cm^{-2}s^{-1}$. The collimator parameters and residual gas pressure distribution (Figure 2-30) of Run II [1,2] were assumed in the modeling. Detailed 3D geometry, magnetic field and materials description in a 70m region upstream of the C0 IP were implemented in the MARS14 model for all lattice and tunnel components along with a few meters of the dirt surrounding the tunnel.

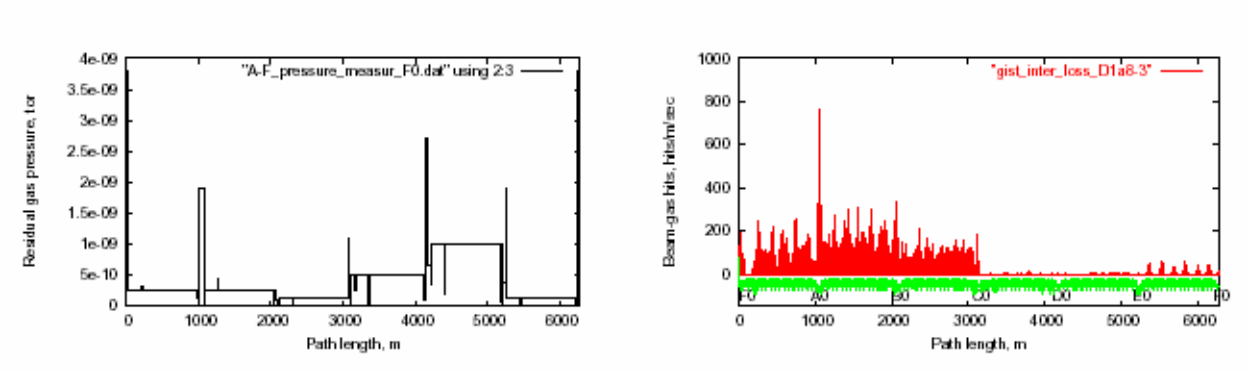

Figure 2-30: Measured residual gas pressure in the Tevatron Run II (left) and beam-gas hit distribution for protons lost at C0 (right).

Table 2-19: Beam loss rates ($10^4 s^{-1}$) in the 70m regions upstream of D0 and B0 (now) and C0 (2009) with run II vacuum parameters.

Source	D0	B0	C0
Nuclear elastic beam-gas	8.8	8.0	9.4
Large angle Coulomb beam-gas	0.12	0.06	0.1
Tails from collimators	2.4	3.5	0.99
Elastic p-pbar at two IP's	0.144	0.105	-

2.7.2 Results

Calculations and measurements show that the Tevatron Run II collimation system does its job nicely, drastically reducing slow beam loss rates in the IPs. For the current vacuum conditions, the nuclear elastic beam-gas interactions is a dominant source of beam loss on the electrostatic separators and low-β quadrupoles as shown in Table 2-19. Calculated beam loss distributions in the C0 region due to elastic beam-gas interactions are shown in Figure 2-31 for the baseline layout and the case with a 1m long stainless mask/collimator at the B48 warm region. The mask jaws are at 12 beam σ's from the beam axis. Beam loss rates are noticeably reduced on the electrostatic separators and in the triplet quads with the B48 collimator.

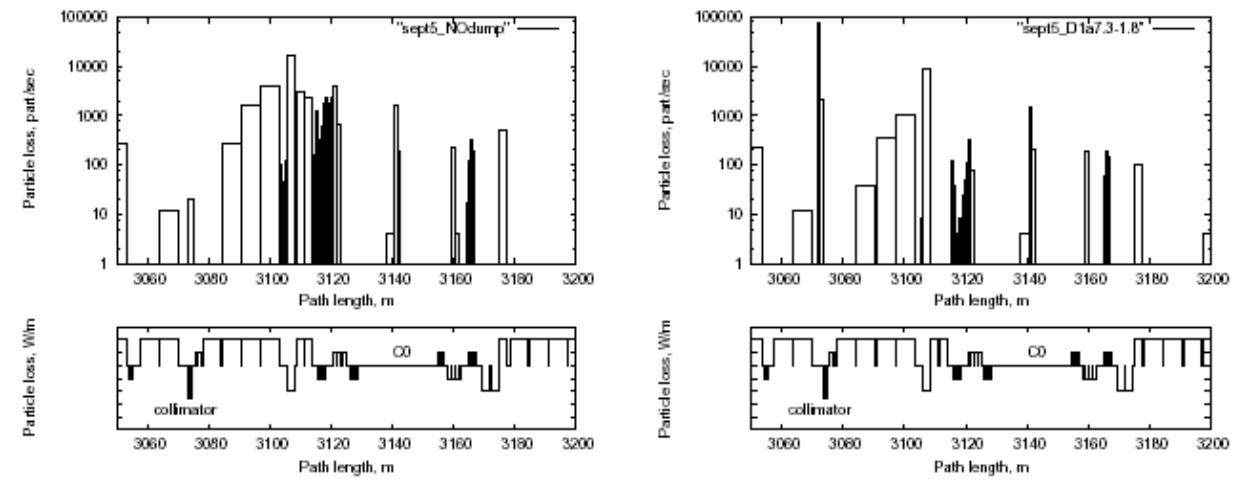

Figure 2-31: Beam-gas induced beam loss distributions in the C0 region: baseline (left) and with the B48 collimator (right).

Particle flux isocontours (threshold energy = 0.1 MeV) in the orbit plane in the 60m long region preceding the BTeV collision hall are presented in Figure 2-32. Shown are neutrons in the baseline configuration and charged hadrons for the case with the B48 collimator and 2m concrete wall. Figure 2-33 shows hadron flux XY-isocontours at the entrance to the collision hall for the case with the B48 collimator and shielding wall. Total background rates are summarized in Table 2-20. The dominant component is photons: $\sim 10^8$ soft photons per second (baseline) entering the collision hall around the beam line. Electrons and neutrons account for the second and third largest fluxes, respectively. There is no wall effect at R < 0.25m. The B48 collimator alone reduces the backgrounds by a factor of two compared to the baseline configuration. Installation of the shielding wall results in a combined reduction effect of a factor of ten. The numbers in Table 2-20 should be increased by ~10% to account for tails from the Tevatron main collimators.

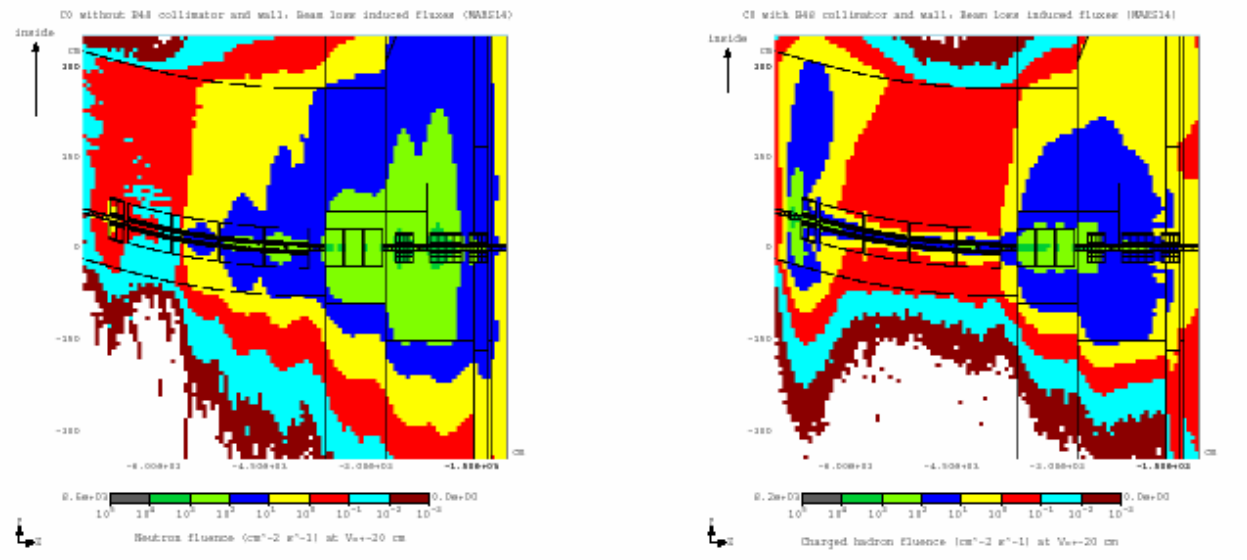

Figure 2-32: Particle isofluxes in the C0 region: neutrons, baseline (left) and charged hadrons with B48 collimator and 2m concrete wall (right).

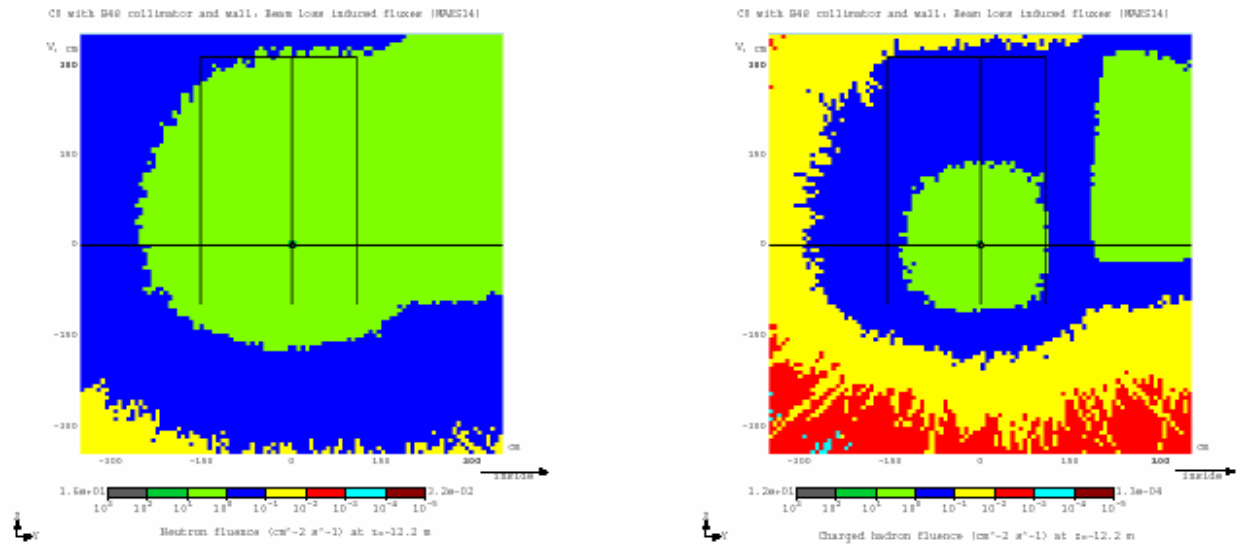

Figure 2-33: Neutron (left) and charged hadron (right) isofluxes at the entrance to the C0 hall, with B48 collimator and 2m concrete wall.

Table 2-20: Number of particles above 0.1 MeV entering the BTeV hall at z = -12.192m and R < 3.5m ($10^5 s^{-1}$).

Scenario	n	$h^{\pm}$	$e^{\pm}$	γ	$\mu^{\pm}$
No B48, no wall	24.2	14.5	58.9	1147	2.80
B48, no wall	11.0	9.29	42.4	730	1.81
B48, 2m wall	6.29	2.48	7.55	132	1.00

2.7.3 Conclusions

A STRUCT model of the Tevatron and MARS14 model of the C0 IR has been built. Beam loss distributions – induced by beam-gas (dominant) and collimator tails – have been calculated and corresponding showers in the C0 IR have been modeled, providing files of particle fluxes at the entrance to the BTeV collision hall. About $3x10^6$ hadrons and 10^8 photons enter the BTeV collision hall per second. A 1m long stainless steel collimator in the B48 warm region reduces these numbers by a factor of two and protects the low-β quads against quenches at normal operation. Preliminary calculations show that this collimator in a combination with the existing A11 and A48 collimators protects the BTeV pixel detectors and the low-β quads during an abort kicker pre-fire. A 2m concrete shielding wall at 12.7m – 14.7m upstream of the IP further reduces the particle flow into the BTeV collision hall, with a combined effect of a factor of ten. With a 5 GeV cutoff, this puts the machine-related backgrounds in the BTeV pixel detectors at a percent level of those from proton-antiproton collisions.

References

[1] A.I. Drozhdin, V.A. Lebedev, N.V. Mokhov, et al., "Beam Loss and Backgrounds in the CDF and D0 Detectors due to Nuclear Elastic Beam-Gas Scattering", Fermilab-FN-734 (2003); *Proc. 2003 Particle Accelerator Conf.,* Portland, OR, May 12-16 (2003); Fermilab-Conf-03/088 (2003)

[2] M.D. Church, A.I. Drozhdin, A. Legan, N.V. Mokhov, R.E. Reilly, "Tevatron Run II Beam Collimation System", *Proc. 1999 Particle Accelerator Conf.,* pp. 56-58, New York, March 29-April 2, 1999; Fermilab-Conf-99/059 (1999)

[3] I.S. Baishev, A.I. Drozhdin, N.V. Mokhov, "STRUCT Program User's Reference Manual," SSCL-MAN-0034 (1994); http://www-ap.fnal.gov/~drozhdin/

[4] N.V. Mokhov, "The MARS Code System User's Guide," Fermilab-FN-628 (1995); NV Mokhov, O.E. Krivosheev, "MARS Code Status," *Proc. Monte Carlo 2000 Conf.,* pp. 943-948, Lisbon, Oct. 23-26, 2000; Fermilab-Conf-00/181 (2000); N.V. Mokhov, "Status of MARS Code," Fermilab-Conf-03/053 (2003); http://www-ap.fnal.gov/MARS/

3 LHC Style Quadrupoles

3.1 Overview and Conceptual Design

The C0 IR described in section 2.0 requires quadrupoles of a new design for the Q1 through Q5 magnets. Table 3-1 shows the locations, gradient, magnetic length and mechanical slot length requirements of these elements. The nominal operating temperature is 4.5 ^{o}K.

Table 3-1: Q1 – Q5 Parameters

Magnet	Nominal Gradient	Magnetic Length	Magnetic Center	Mechanical Slot Length
	(T/m)	(m)	(m from IP)	(m)
Q1	168.7	2.40	14.119	3.213
Q2	170.0	4.31	18.502	5.312
Q3	168.7	2.40	24.355	3.451
Q4	170.0	2.01	69.798	2.979
Q5	170.0	1.50	86.848	2.471

To meet these requirements, we propose a design based on the collared coil assembly of the well proven LHC IR quadrupole currently in production, with the magnet length, iron yoke, cryostat, cryogenic system, and interconnects re-optimized for the C0 IR. Figure 3-1 shows a cross-section of the collared coil of such a magnet.

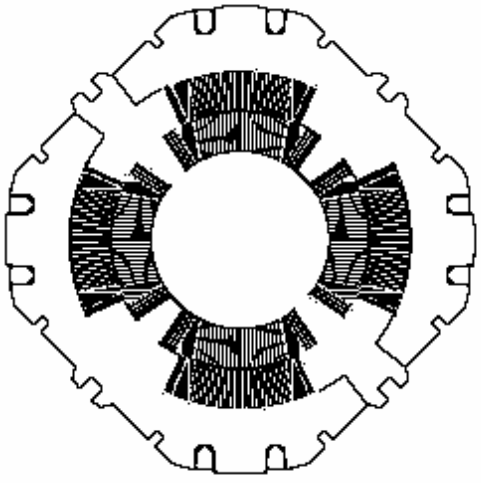

Figure 3-1: LHC Quadrupole Collared Coil.

The coil bore is 70mm, which allows for use of a beam tube with inside diameter 63mm. The reuse of the body design of the LHC quadrupole provides confidence that these magnets can work with minimal redesign, optimized for the Tevatron system. The C0 optics requires a gradient which is 20% lower than that of the LHC quadrupole. Independent of this, no changes in the coil design or body mechanical support are envisioned. Optimizations will focus on reducing the iron yoke diameter and overall cryostat size such that the height of the beam above the tunnel floor in the Tevatron can be accommodated without any new civil construction in the tunnel.

Changes that have been made include

- Reducing the iron yoke OD
- Reducing the overall magnet OD
- Modifying the quadrant splice design system
- Changing the expansion loop design
- Changing the pipes included and the interfaces of the cryostat
- Reducing the overall diameter of the cryostat

The redesign of the iron yoke results in a yoke OD of 311.15mm, and an anticipated total OD including stainless steel skin of approximately 323.85mm. Figure 3-2 illustrates a preliminary yoke redesign used in initial magnetic calculations. The harmonics were calculated and found to be acceptable.

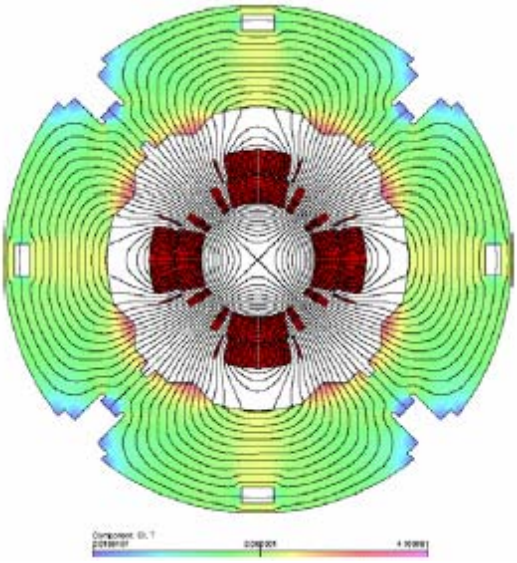

Figure 3-2: C0 IR Magnet Yoke Cross Section.

Given the smaller magnet, and the elimination of a super-fluid helium heat exchanger required in the cryostats of the LHC Inner Triplet, the C0 quadrupole cryostats are expected to be only one half of the diameter of the LHC cryostats, and allow for the beam height to be located 10" above the nominal Tevatron tunnel floor. The cold magnetic length of any of the Q1 to Q5 magnets is expected to be approximately 0.24m shorter than the warm mechanical length of the cold mass, end plate to end plate, as depicted in Figure 3-3. The length of the quadrant splice block, expansion loops, bus connections, instrumentation wires, and other components are included in the cryostat layouts, and at this stage appear consistent with the mechanical slot lengths listed in Table 3-1, as constrained by the lattice design. These lengths are still being optimized.

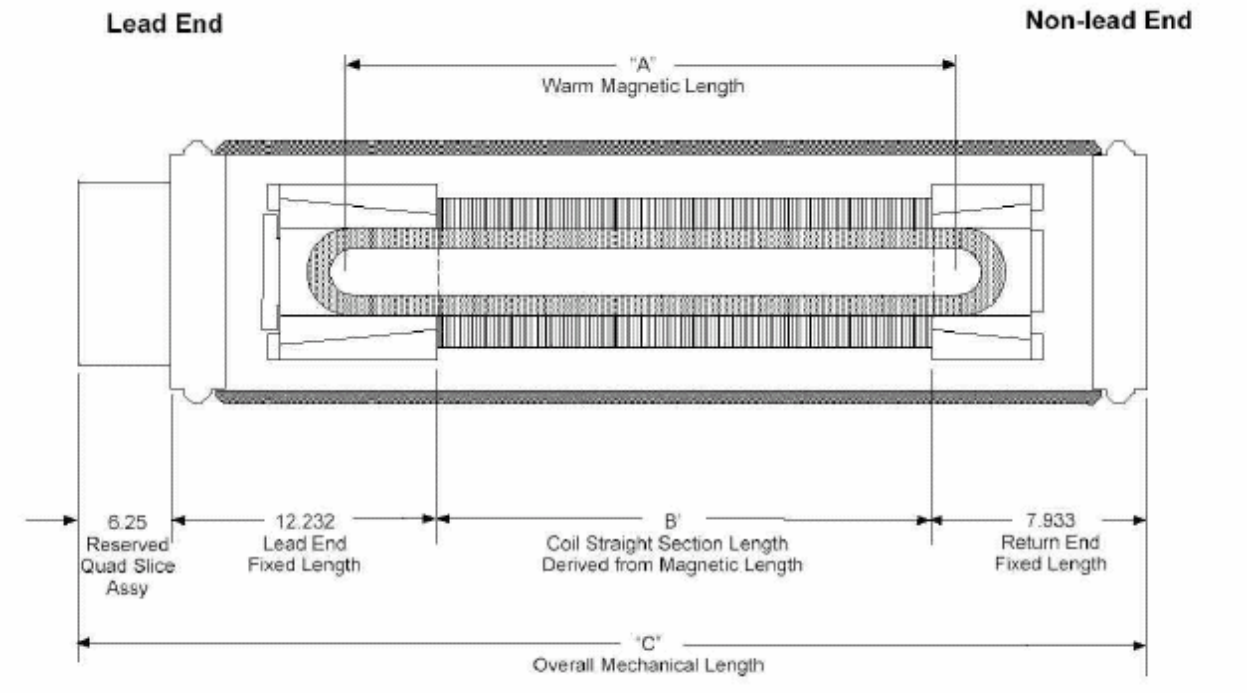

Figure 3-3: Magnetic / Mechanical Length Schematic (dimensions in inches).

The following sub-chapters document the basic quadrupole design, noting the important similarities and differences between the two designs. Necessary R&D and infrastructure is summarized in the last sub-chapter.

3.2 Magnet Coils and Mechanical Description

The collared coil of the assembly shown in Figure 3-1 consists of a two-layer coil of 70mm bore, completely supported by steel collars. The inner coil is formed from 37 strand Rutherford cable, using SSC type wire which is uncoated and unannealed. The outer cable is 46 strand Rutherford cable, again from uncoated and unannealed SSC type wire. Both cables are insulated with two wraps of Kapton insulation, with the outermost wrap including a polyimide adhesive. The end parts are of G11CR.

Table 3-2 details the strand parameters. The conductor for the inner layer has a minimum critical current of 378 A, measured at 7T and 4.22 ^{o}K. The conductor for the outer layer has a minimum critical current of 185 A, also measured at 7T and 4.22 ^{o}K. The values are determined in the

standard way, and the specifications are taken directly from SSC and the LHC IR Quadrupole program.

Table 3-2: Strand mechanical and electrical specifications

Parameter	Unit	Inner cable		Outer cable	
		Value	Tolerance	Value	Tolerance
Diameter	mm	0.808	± 0.0025	0.6505	± 0.0025
Cu/SC ratio		1.3 : 1	± 0.1	1.8 : 1	± 0.1
Surface coating		None	-	None	-
Anneal		None	-	None	-
Minimum critical current	A	378	-	185	-
Minimum RRR Residual Resistivity Ratio		70		70	
Twist direction		Left		Right	
Twist pitch	mm	13	± 1.5	13	± 1.5

Figure 3-4 shows the cable size parameters and Table 3-3 summarizes the cable mechanical and electrical specifications. Again, this specification is identical to that used in the LHC IR Quadrupole program, and there are multiple vendors capable of meeting these requirements.

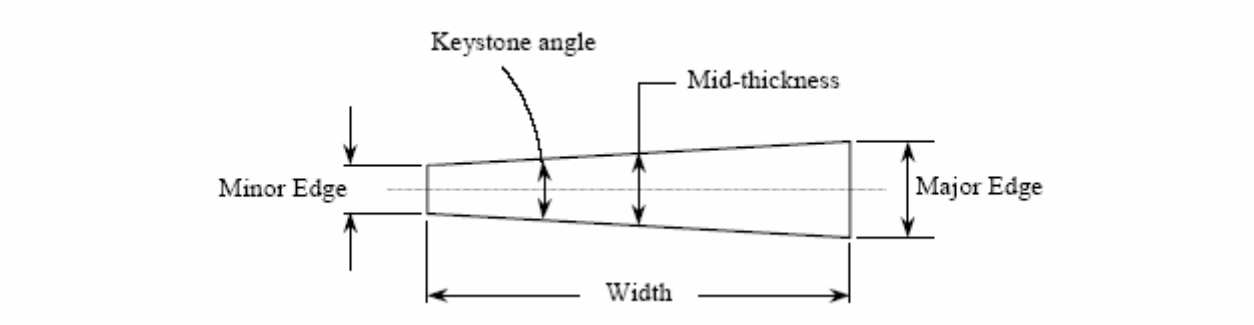

Figure 3-4: Cable size parameters.

Figures 3-5 and 3-6 show the inner and outer coils of the LHC quadrupole. For C0 the straight section lengths will be modified but the end parts will remain exactly the same.

Table 3-3: Cable mechanical and electrical specifications

Parameter	Unit	Inner Cable		Outer Cable	
		Value	Tolerance	Value	Tolerance
Number of strands		37	-	46	-
Cable width	mm	15.40	± 0.025	15.40	± 0.025
Minor edge	mm	1.320		1.051	
Cable Mid-thickness	mm	1.465	± 0.006	1.146	± 0.006
Major edge	mm	1.610		1.241	
Keystone angle	degree	1.079	± 0.05	0.707	± 0.05
Transposition length	mm	114	± 5	102	± 5
Lay direction		Right	-	Left	-
Minimum critical current	kA	14.0	-	8.5	-
Minimum unit length	m	200	-	200	-
Residual twist	degree	0 - 90		0 - 90	
Minimum bending radius	mm	7		15	

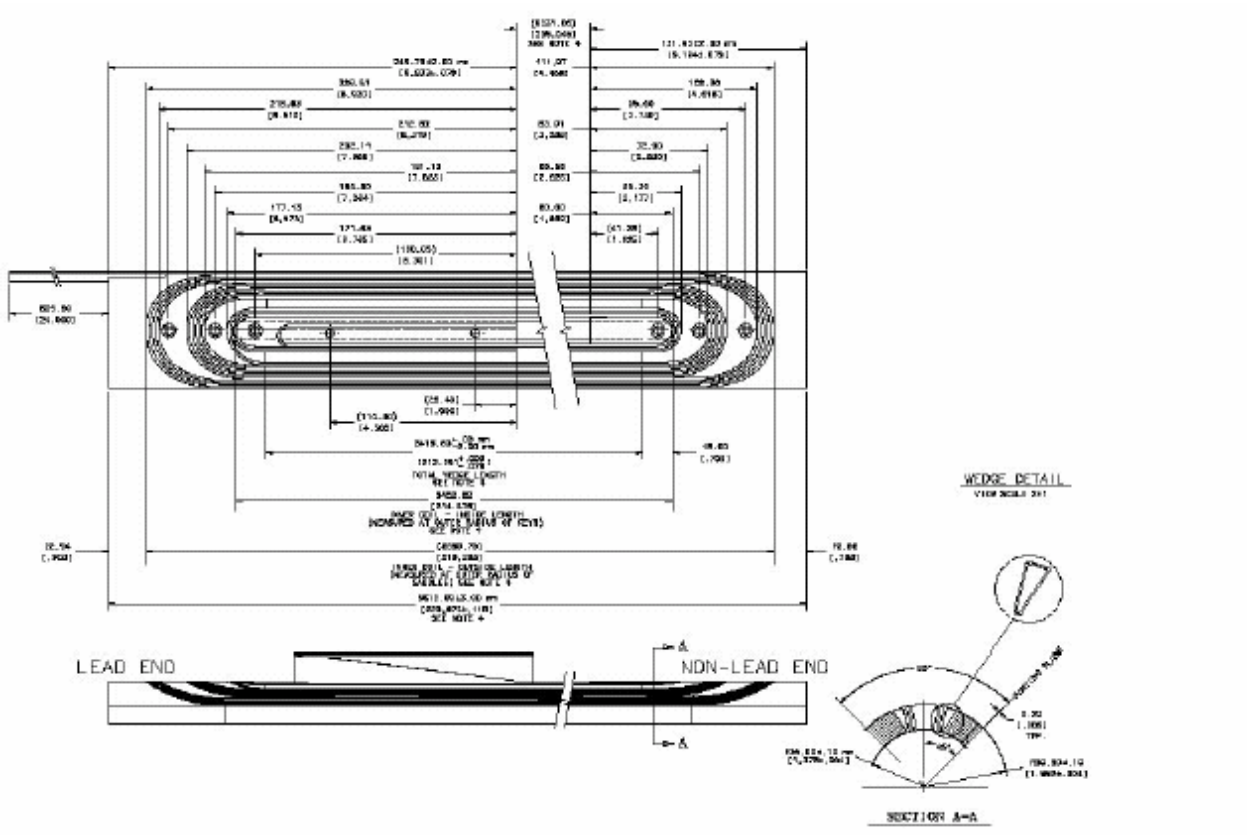

Figure 3-5: LHC Inner Coil. The straight section of the coil will be modified to accommodate the shorter magnet length.

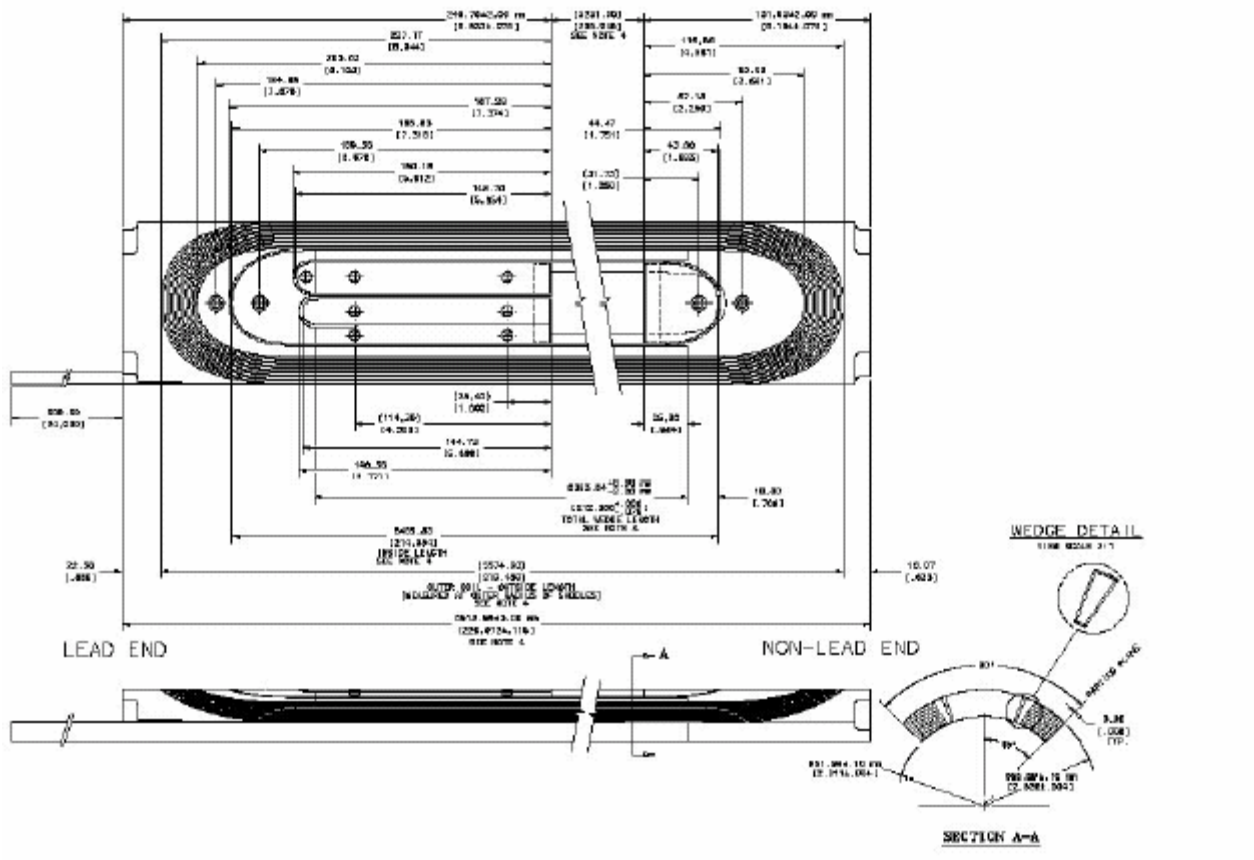

Figure 3-6: LHC Outer Coil. The straight section of the coil will be modified to accommodate the shorter magnet length.

The coils are cured in a two step cure cycle, which sets both the inter-strand resistance and the coil size properly. Mechanical support of the coils is provided by Nitronic 40 collars which are stamped, and pre-assembled into 37mm long packs and provide the required rigidity and cooling channels. The collars are keyed with 8 phosphor bronze keys, to a target warm azimuthal pre-stress of 75MPa in both the inner and outer coils. Pre-stresses in the range of 55 to 100MPa are known to produce acceptable quench performance. The LHC magnet development and production has included magnets ranging in length from 1.8m to 5.5m having acceptable quench performance. A summary of the 4 ^{o}K quench performance of the LHC model magnets and the LHC prototype magnet is shown in Figure 3-7. The magnets showed no signs of retraining. Since the C0 designs are in between these lengths, we can reasonably expect similarly good quench performance at the maximum C0 operating current of 9560A.

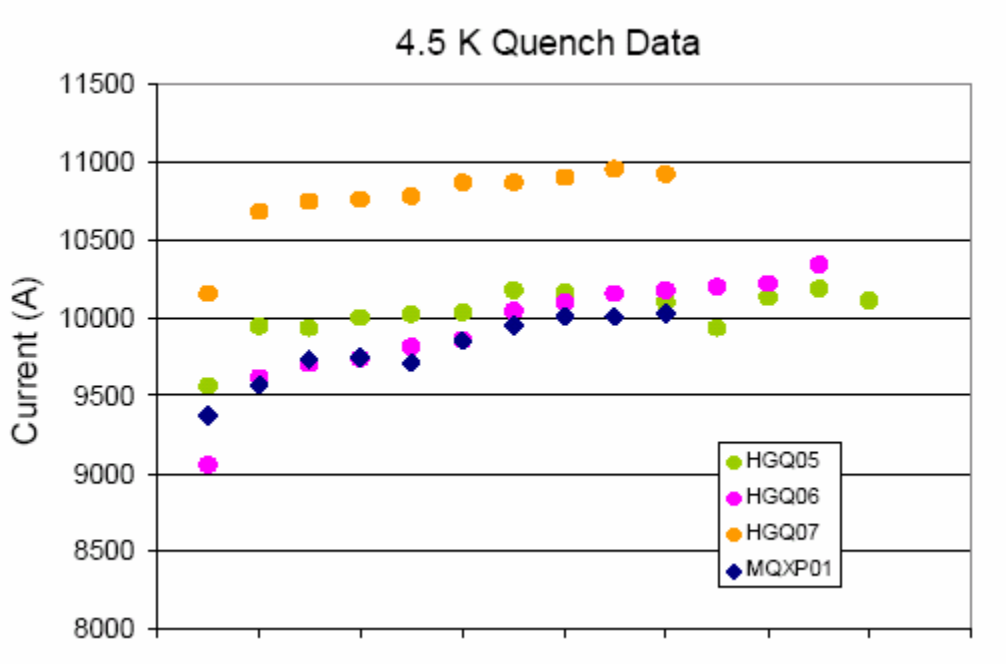

Figure 3-7: LHC Model Magnet and Prototype 4.5 ^{o}K Quench Performance.

The LHC quadrupoles were optimized for LHC operation, consequently the ramp rate dependence was not a major issue since the required current ramp rate was 10 A/s. Although the LHC quadrupoles quench current shows no change with ramp rates up to ~100A/s, one can observe a significant drop at a rate of 150-160A/s which is the dominant rate in the Tevatron ramp profile. In order to avoid premature quenching a new Tevatron ramp profile will be implemented at currents above the 8 kA range [β].

The iron yoke of the magnet provides flux return, and supports the stainless steel shell that provides helium containment. Since the C0 operating gradient is 20% lower than the LHC requirement, the iron yoke will be re-optimized and the outside diameter reduced to produce a more compact design, with acceptable harmonics. As with the LHC design, we expect to use the ICB welding press to close the skin, after it has been modified for the reduced yoke diameter.

The reduced yoke diameter of 311.15mm has no impact on the design of the mechanical support of the ends of the coils as in Figure 3-8. We will be able to use the same collet design as on the LHC quads, as well as the same mechanism for tying the collets to the magnet end plates. The quadrant splice block will need to be modified, and the coverage of some of the longitudinal restraint bolts under the quadrant splice block will need to be considered, but the mechanical support of the magnet will remain the same.

β Ramp rate dependence of the type observed here is typically ascribed to eddy current heating which is related to a low inter-strand resistance. The inter-strand resistance is determined by several parameters including the coil curing temperature and pressure and the state of strand and cable annealing. In the LHC coil fabrication, the coil curing cycle was modified to provide high pressure (forming the coil geometry) at a lower temperature, while the polyimide adhesive was set at higher temperature and lower pressure. (In the Tevatron, inter-strand resistance was controlled by coating alternate strands with ebanol or 'stabrite'; the resulting cable was dubbed 'zebra'...)

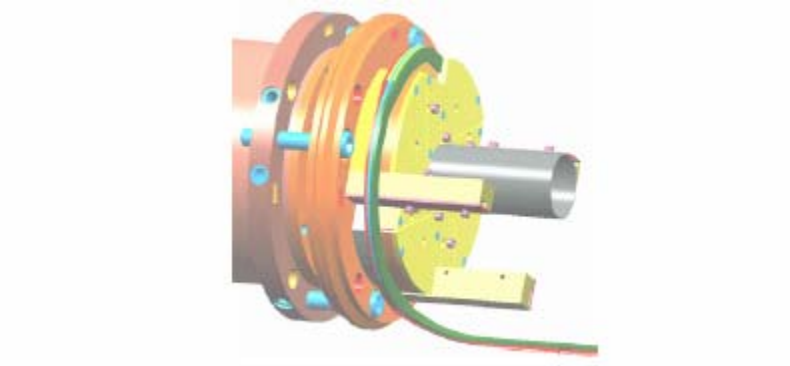

Fig. 3-8: Proposed C0 IR cold mass lead end with axial restraint system and quadrant splice assembly.

The ends of the cold mass are defined by steel end plates, which are used to anchor the collared coil longitudinally, and provide the geometry for the skin to end plate and end plate to end dome welds to be made. These welds close the cold mass. The thickness of this assembly may be optimized depending on the final weld geometry required for the skin and end dome thicknesses.

The reduced overall diameter of the magnet impacts the quadrant splice block design, which mounts to the lead end of the magnet. The LHC design has the splices in a plane perpendicular to the beam axis, but uses a diameter too large for the C0 design. We have assumed for C0 that the splices will be made parallel to the beam axis, requiring a longer splice block region, as shown in Figure 3-8.

3.3 Field Quality

The C0 IR quadrupole design is based on the LHC quadrupole [1] which was designed to operate at 1.9K in superfluid helium with the critical current and temperature margins necessary to operate in a large radiation induced heat load. The C0 IR quadrupole will utilize this proven design – particularly the collared coil assembly which determines the basic field properties – with modifications as necessary to meet C0 specifications. One such modification is to the iron yoke, originally designed for field gradients up to 230 T/m; it must be reduced in diameter to meet the beam tube height limitations imposed by the Tevatron tunnel.

3.3.1 Iron Yoke Optimization

The cross-section of the HGQ is shown in Figure 3-9. A two-layer collared coil is surrounded by a two-piece iron yoke held together by a welded skin. The iron yoke is penetrated by four large round holes required for longitudinal heat transfer by super-fluid helium from the coil to the external He II heat exchanger and four large rectangular holes reserved for the high-current bus-bars and electrical instrumentation. These holes along with the high nominal field gradient of 215 T/m resulted in the quite large iron yoke outer diameter of 400 mm.

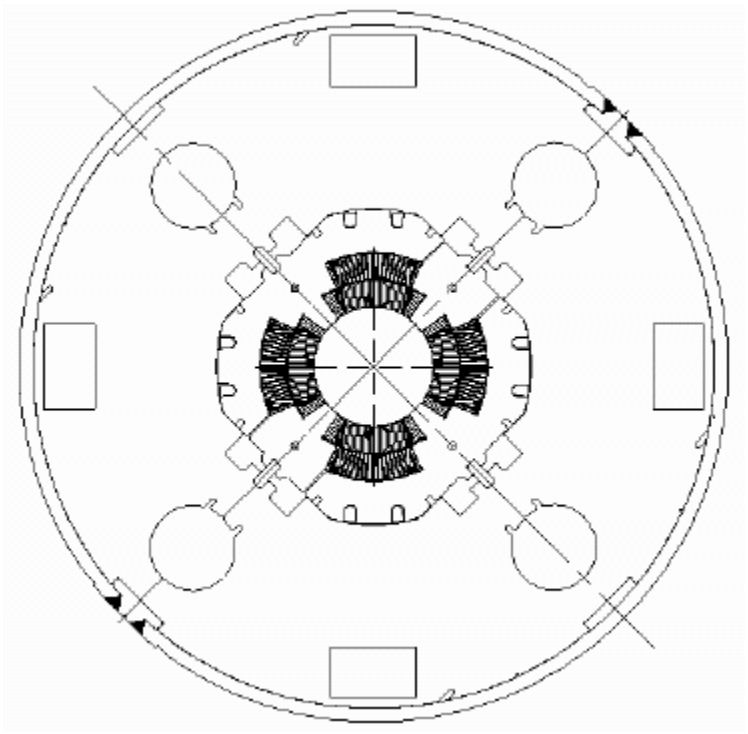

Figure 3-9: Cross-section of HGQ developed for the LHC IRs.

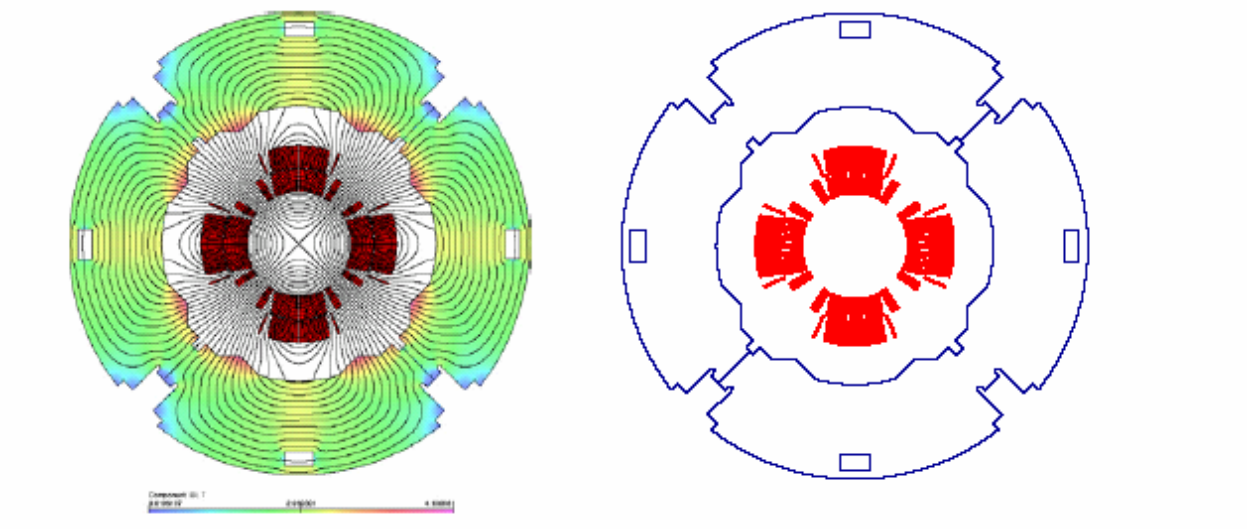

Figures 3-10a, 3-10b: C0 IR Magnet Yoke Cross-Section.

The optimization goals for the C0 IR quadrupole were reduction of the iron yoke OD from 400 mm. Initial studies used a 267 mm yoke OD, and allowed for minimal iron saturation effects while providing the channels for power and instrumentation cables as well as for helium flow. The inner shape and the size of the new iron yoke will be similar to the shape of the HGQ collared coil. The collared coil is supported and aligned inside the yoke with the help of special alignment keys. As in the HGQ, there is a small gap between the collar and yoke excluding the yoke from the coil mechanical support structure.

The initial field quality optimization was done using the OPERA2D [2] code. Iron saturation effects were kept within tolerable limits through the use of eight round holes: the position and size of the holes were optimized to restrict field quality deviations to the order of 0.15×10^{-4}.

Figures 3-10a, -10b show the flux distribution and the final optimized iron yoke geometry in the magnet cross-section with an outside diameter of 311.15 mm. Four 10.0 mm × 20.0 mm rectangular holes are used for the12-15 kA stabilized electrical bus bars. Each bus bar hole can accommodate 2 pair of stabilized bus. Not more than 2 holes are used for bus bars with the remaining holes being used for instrumentation wires. Sufficient cooling within the cold mass is provided by helium flow though the four 20 mm x 20 mm holes with a total cross-sectional area of 16 cm^2 and a 1-2 mm annular channel.

3.3.2 Magnet transfer function

Figure 3-11 shows the measured and calculated transfer function for the HGQ short models as a function of current. As can be seen in Figure 3-11, there is good correlation between measured and calculated data at all currents. The reduction of the magnet transfer function at high currents is caused by iron saturation. At an operating current of 10 kA the nominal field gradient is about 180 T/m. We are confident that the transfer function for the modified C0 quadrupole design can be calculated to high accuracy and will provide similar good agreement.

Determination of the field integral ($\int g \bullet dl$) for the C0 quadrupoles will depend on the details of the magnet ends as well as the 'as-built' coil length and thermal contraction when cold. This will be learned from tests of a prototype or model magnet and adjustments to the lengths of the production cold masses.

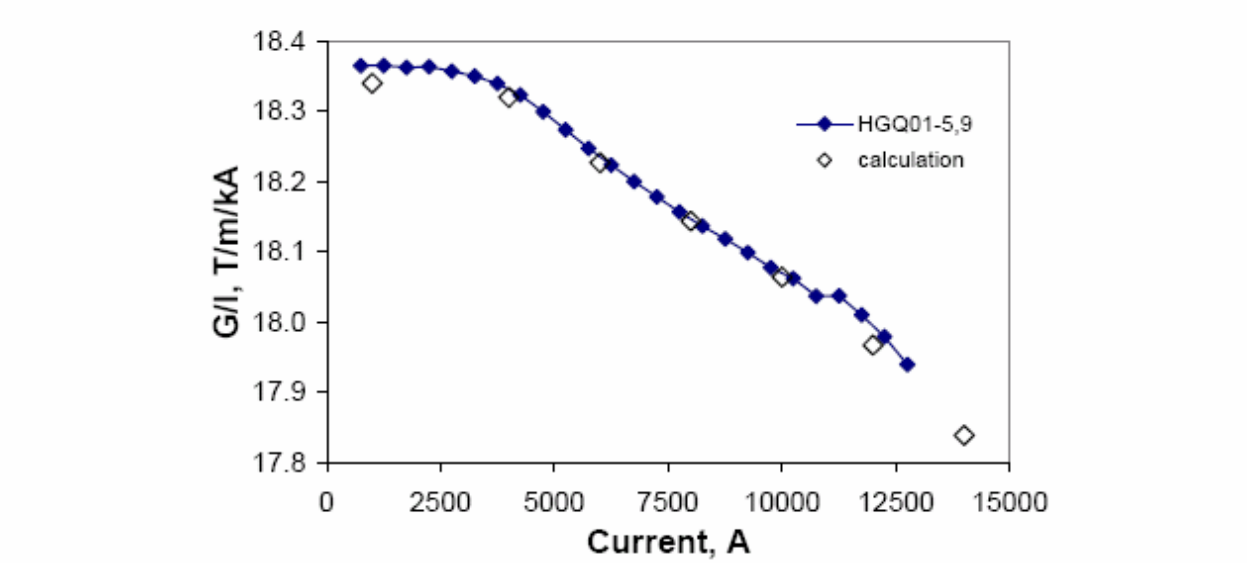

Figure 3-11: Measured and calculated magnet transfer function for HGQ Model Magnets.

3.3.3 Field Harmonics

In the magnet body, the field is represented in terms of harmonic coefficients defined by the power series expansion:

$$B_y(x,y) + iB_x(x,y) = 10^{-4} B_2 \sum_{n=1}^{\infty} (b_n + ia_n) \left(\frac{x+iy}{R_{ref}} \right)^{n-1} ,$$

where $B_x(x,y)$ and $B_y(x,y)$ are the transverse field components, B_2 is the quadrupole field strength, b_n and a_n are the "normal" and "skew" harmonic coefficients (b_2=10^4) at a reference radius R_{ref} of 17 mm.

The field quality expected in the C0 quadrupoles can be estimated from measurements of the roughly 1.5m long model magnets built and tested during the R&D portion of the LHC program and from measurements of the first few full length production magnets. Table 3-4a below shows the mean values and RMS spread at R_{ref} =17 mm of low-order field harmonics over the last five short models HGQ05-09 measured at 6 kA current, while Table 3-4b displays the same harmonics measured at 215 T/m (11922A; the LHC operating current) averaged over the first six full length cold masses.

Table 3-4a: Averages and Standard Deviations of field harmonics at 6kA for HGQ05-09.

Harmonic Coefficient	Mean	RMS
$\mathbf{b_3}$	0.49	0.26
$\mathbf{a_3}$	0.12	0.28
$\mathbf{b_4}$	-0.01	0.08
$\mathbf{a_4}$	-0.15	0.37
$\mathbf{b_5}$	-0.02	0.07
$\mathbf{a_5}$	-0.06	0.15
$\mathbf{b_6}$	-0.23	0.17
$\mathbf{a_6}$	-0.03	0.05
$\mathbf{b_7}$	0.01	0.03
$\mathbf{a_7}$	0.02	0.03
$\mathbf{b_8}$	0.00	0.01
$\mathbf{a_8}$	0.00	0.01
$\mathbf{b_9}$	0.00	0.00
$\mathbf{a_9}$	0.00	0.01
$\mathbf{b_{10}}$	0.00	0.01
$\mathbf{a_{10}}$	0.00	0.00

Table 3-4b: Averages and Standard Deviations of field harmonics at 11.9kA for First 6 Full Length Cold Masses.

Harmonic Coefficient	Mean	RMS
$\mathbf{b_3}$	0.31	0.47
$\mathbf{a_3}$	-0.57	0.65
$\mathbf{b_4}$	0.02	0.48
$\mathbf{a_4}$	0.30	0.39
$\mathbf{b_5}$	-0.03	0.13
$\mathbf{a_5}$	-0.38	0.18
$\mathbf{b_6}$	-0.02	0.45
$\mathbf{a_6}$	-0.04	0.11
$\mathbf{b_7}$	-0.01	0.03
$\mathbf{a_7}$	0.01	0.03
$\mathbf{b_8}$	0.00	0.02
$\mathbf{a_8}$	0.01	0.03
$\mathbf{b_9}$	0.03	0.01
$\mathbf{a_9}$	-0.02	0.03
$\mathbf{b_{10}}$	0.00	0.02
$\mathbf{a_{10}}$	-0.03	0.02

A detailed comparison of the field quality measurements of HGQ models with the Fermilab Low Beta Quadrupoles [4] is presented in Table 3-5. For direct comparison, the HGQ harmonics are calculated with the Tevatron reference radius of 25.4mm and a weighted end-body average is calculated for a 5.5m cold mass. The field quality of the HGQ is moderately better. The allowed harmonics are smaller, particularly b5, and the variance in normal and skew sextupole is smaller. Differences in average multipole values between the model magnets and production cold masses can be ascribed, in part, to different tooling used in making the coils

Table 3-5: A comparison of the field quality of the FNAL LBQ [5] and LHC IR quad model magnets. Harmonics are given in units (10^{-4} of the main field).

		LBQ						HGQ	
		132"		232"		54"		5.5 m	
	n	average	variance	average	variance	average	variance	<>	s
normal	*b2*	0.61	1.53	-0.55	1.95	0.62	1.03	0.90	0.73
	b3	-0.44	1.01	0.02	0.89	0.21	0.40	-0.04	0.31
	b4	-0.22	0.32	0.28	0.23	0.29	0.50	-0.11	0.61
	b5	-2.42	1.08	-2.01	0.85	-3.10	1.44	0.09	1.08
	b6	0.03	0.36	0.01	0.17	0.05	0.26	0.06	0.31
	b7	-0.04	0.18	-0.06	0.19	0.05	0.11	-0.06	0.09
	b8	-0.03	0.19	0.04	0.12	0.08	0.19	-0.03	0.12
	b9	-0.90	0.20	-0.68	0.11	-0.75	0.17	-0.36	0.28
	b10	-0.04	0.23	0.06	0.10	0.03	0.14		
	b11	0.03	0.25	-0.01	0.06	0.01	0.25		
	b12	0.14	0.25	-0.08	0.16	-0.12	0.51		
	b13	1.30	0.21	1.36	0.24	1.21	0.17	-1.81	0.21
skew	*a2*	0.30	2.59	0.12	3.17	-0.63	2.65	0.32	0.74
	a3	-0.47	0.98	-0.50	0.86	0.13	0.95	-0.43	1.53
	a4	-0.49	0.42	0.35	0.66	-0.31	0.68	-0.28	0.87
	a5	0.08	0.42	0.10	0.24	-0.03	0.59	-0.38	0.36
	a6	0.17	0.26	-0.08	0.39	0.01	0.29	0.24	0.35
	a7	0.06	0.21	-0.07	0.14	0.02	0.15	0.02	0.21
	a8	-0.04	0.20	0.08	0.11	0.05	0.13	0.03	0.14
	a9	0.16	0.20	0.14	0.20	0.17	0.10	-0.02	0.06
	a10	0.06	0.25	-0.04	0.09	-0.07	0.19		
	a11	0.07	0.19	-0.12	0.11	-0.07	0.21		
	a12	-0.04	0.21	-0.11	0.17	-0.19	0.38		
	a13	-0.58	0.26	-0.26	0.20	-0.22	0.87		

Magnetization effects are calculated to decrease b_6 by –(1.2-1.3) units at 4.5 ^{o}K at injection; its decay during the first 900 seconds is less than 0.4 units. The effect of iron saturation on b_6 and b_{10} in HGQ with the optimized iron yoke is shown in Figure 3-12.

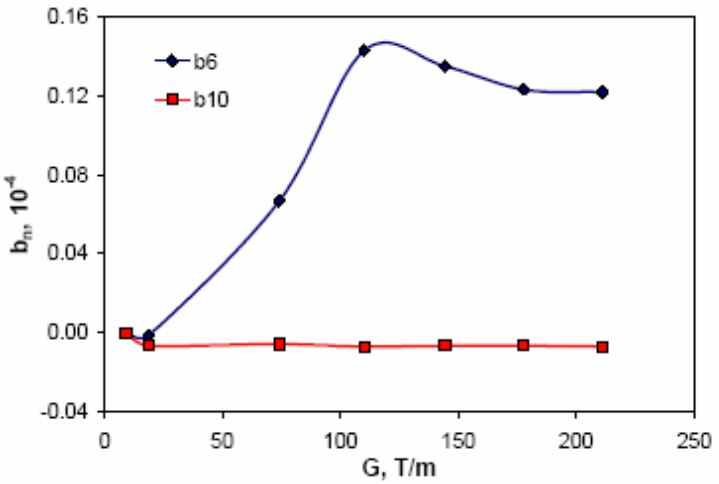

Figure 3-12: The yoke saturation effect.

3.4 Quench Protection, Electrical Specifications, and Bus

Since the design of the new quadrupole magnets for the C0 IR will be very similar to those made for the LHC, their electrical properties will be very similar as well. Quench protection of the C0 high gradient quadrupoles will closely follow the approach used with the LHC quadrupoles. The design of the high current bus will also be based on the LHC design.

3.4.1 Inductance, resistance and stored energy

The new C0 quadrupole coil configuration (number of turns, cable dimensions, end effects, etc.) will be the same as LHC quads, only the length of the coils will be different. Although the inductance depends on the yoke structure (thickness, shape and material properties of the yoke) as well, its contribution to the total inductance is small. For design purposes using LHC magnet inductance values in calculation will be adequate. The LHC magnet inductance is 3.09 mH/m (at 10kA). Based on this inductance, the expected stored energy will be 138 kJ/m (at 9450A, I/Ic=0.875, at 4.5 ^{o}K)

The inductance and Q value measured with an HP4284 LCR meter @ 1kHz for a 5.5 m long LHC quadrupole cold mass assembly is 13.4 mH and 5.2, respectively. The room temperature value of the resistance of a cold mass is 2.3 Ω. The typical RRR value is ~150.

3.4.2 Voltage taps and heaters

The LHC cold mass has voltage taps attached to each quarter coil and each cold mass has two quench heaters (covering all four quadrants) whose room temperature resistance value is 19.5 Ω. The C0 IR cold masses will be instrumented with quarter coil voltage taps. The peak heater

surface power must be kept above 55 W/cm^2. This requirement will determine the heater resistance and obviously it will be different for each different length of cold mass.

3.4.3 Quench Detection and Protection

Based on measured values from LHC cold masses, the key quench related properties are estimated as follows:

- Quench velocity: 75m/sec ± 25 m/sec (depends on the quench location; at I/Ic=0.875; 1.9K; at 4.5 ^{o}K one can expect 20 m/sec increase)
- Quench Integral limit: 21 MIITs (over 400K hot spot – estimate only)
- Quench Integral starting from the time the heater is fired: 17 MIITs (available 4 MIITs for quench detection or 40 msec at 10kA)
- Quench Detection threshold 0.3 V which is at ~10msec for I/Ic=0.875
- Quench heater operation is expected to be better or equivalent at 4.5 ^{o}K. For the LHC the quench heater firing unit parameters are the following:
  - Capacitance: 7mF
  - Voltage: 900V

It is important to keep the strip heater peak surface power the same so that we can expect similar heater behavior for the C0 IR design. The quench heater copper to stainless steel strip ratio should be adjusted to the magnet length. Peak voltage plays a bigger role than the total power, so there is no need to change the capacitance value.

3.4.4 Bus

The superconducting bus used for the LHC is suitable for conducting the current to the new magnets. The bus consists of LHC inner cable soldered to a same size cable made from pure copper. This bus was intensively tested at various current values (600A – 12000A) and it was proven that it can be protected adequately if we keep the QI within 150 MIITs (maximum temperature rise will be ~300 K - estimated). We will be well within the QI limit even if the quench detection threshold is set as high as 0.25V.

3.4.5 Shunt

In additional to the main bus, which carries 10 kA for the low beta quadrupoles, another short ~2 m long conductor is required to shunt current (up to 200A current) from the Q1 and Q3 magnets, providing additional tuning of the triplet. The bus channel provides sufficient room for this extra conductor, so it is practical to use the same conductor which is used for 10kA bus.

3.5 Cryostat Requirements

Cryostats provide the magnet closures, mechanical and electrical interfaces, mechanical support, thermal insulation, and alignment information needed for a magnet to actually be installed in an accelerator. The fundamental criteria for the new C0 quadrupoles is accommodating the Tevatron beam height off the tunnel floor, without requiring any further civil construction in the tunnel. For economy the Q1 – Q5 cryostat designs will be as similar as possible.

Figure 3-13 shows an end-on view of a preliminary cryostat for the C0 IR. With the reduced magnet diameter, it appears possible to position the magnet beam line correctly in the tunnel.

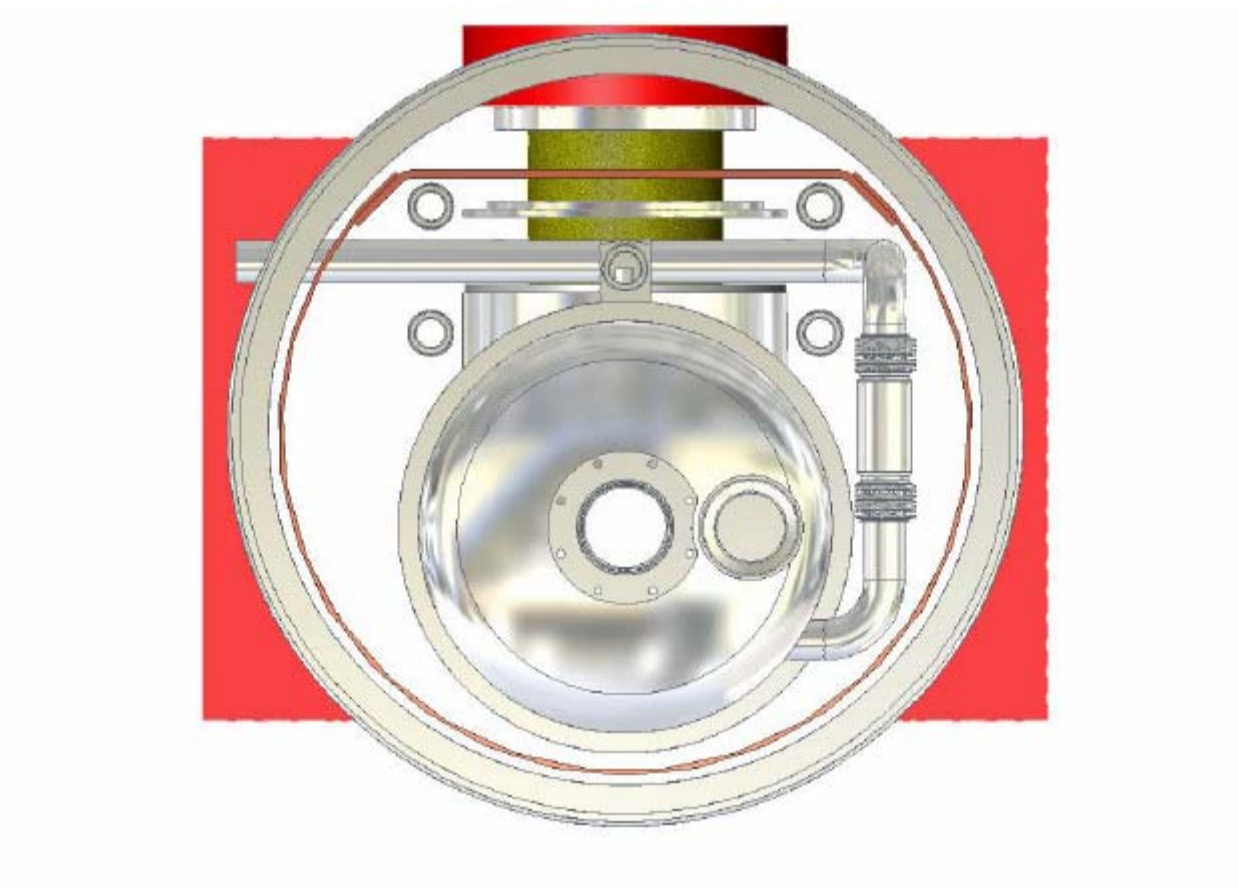

Figure 3-13: Preliminary end view of cryostat.

Schematically the Q1 to Q3, Q4, and Q5 cryostats, the main bus-work and the associated spools are shown in Figures 3-14, 3-15 and 3-16. The lead end of each magnet is denoted by the elongated end volume and the script $\mathcal{L}$. Details of the spools are discussed in Chapter 4.

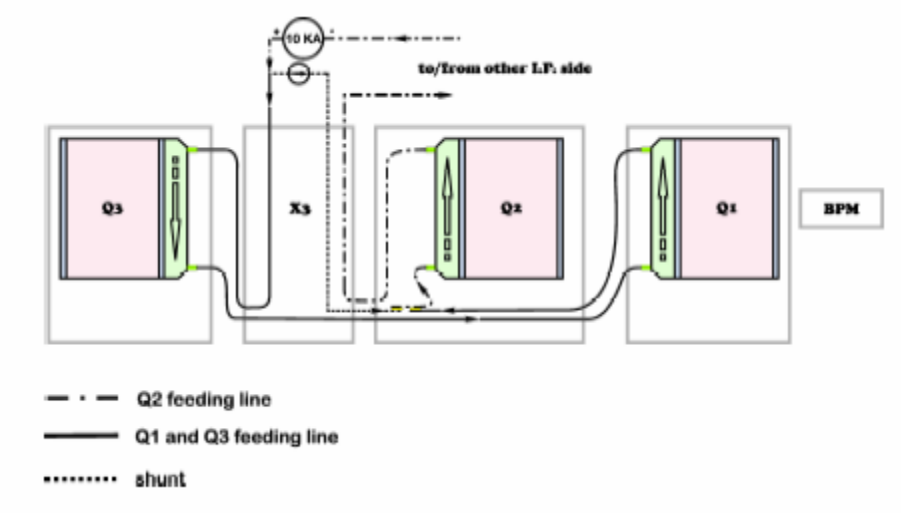

Figure 3-14: Q1 – Q3 Schematic. The IP is to the right, and the triplet mirrors about the vertical axis of the IP when moving from the B sector to the C sector.

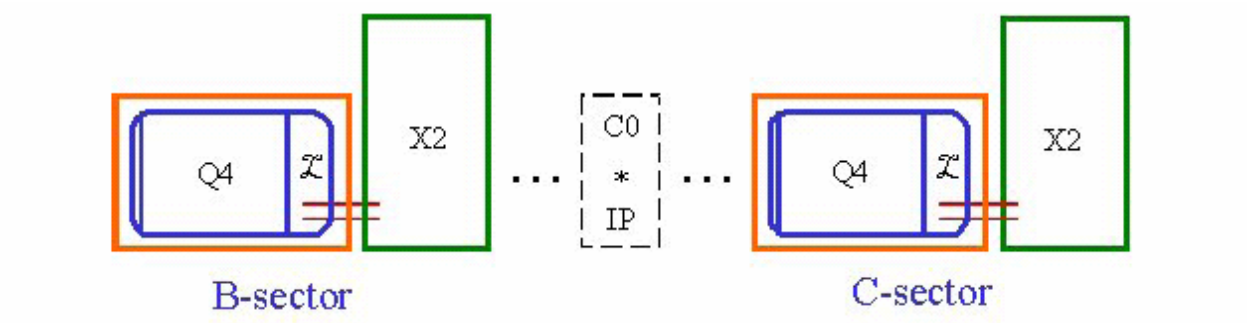

Figure 3-15: Q4 schematic. The Q4 / X2 spool combination translates when moving from the B sector to the C sector.

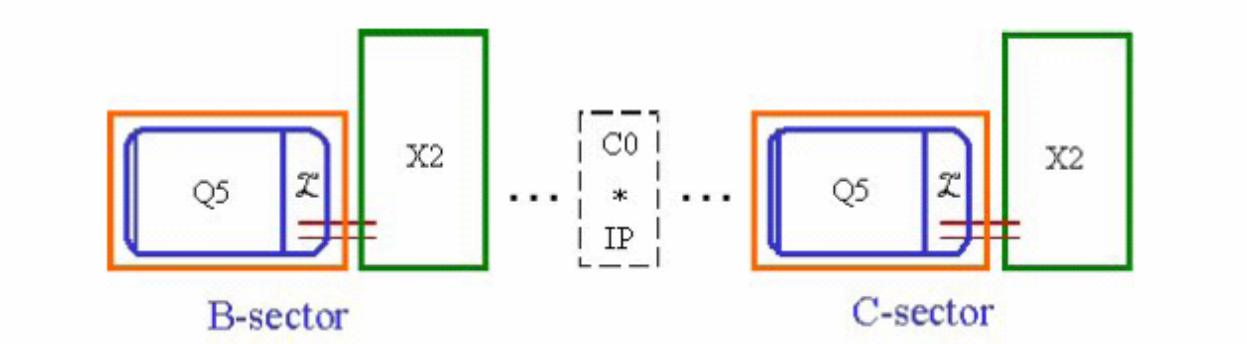

Figure 3-16: Q5 schematic. The Q5 / X2 spool combination translates when moving from the B sector to the C sector.

The Q1, Q2 and Q3 quadrupoles will be powered in series, with a shunt (not shown) across Q1 and Q3 allowing for modest variation of their gradients relative to Q2 as needed by machine operations. The orientation of lead and return ends in the triplet allow for minimal bus work to be used, and, if the bus work fix point in the Q2 can be placed at the lead end of the magnet, the expansion loops might be placed in the X3 spool. This also depends on the design of the splice block at the lead ends of the magnets, and the bus expansion loop requirements which are not known at this time.

The BPM shown at the IP end of Q1 may be mounted either internal or external to the cryostat, the choice will depend on details of the design and layout. Details of the vacuum interconnect, gate valve, and other requirements are to be determined.

A summary of the quadrupole cryostat magnetic lengths, slot lengths, and details of the interconnects is given in Table 3-6.

Table 3-6: A Summary of Quadrupole Cryostat Parameters.

BTeV Quadrupole Cryostat Parameters			
	Cold magnetic length (m)	**Interconnect configuration**	**Slot length (m)**
Q1	2.40	New interconnect using Tevatron cryogenics plus single phase, two phase, and shield returns.	3.63
Q2	4.31	New interconnect using Tevatron cryogenics plus single phase, two phase, and shield returns.	5.31
Q3	2.40	New interconnect using Tevatron cryogenics plus single phase, two phase, and shield returns.	3.45
Q4	2.01	Tevatron with small modifications to vacuum and single phase bellows and single phase flange (one end only).	2.98
Q5	1.50	Tevatron with small modifications to vacuum and single phase bellows and single phase flange (one end only).	2.47

The Q4 and Q5 magnet arrangements are shown in Figures 3-15 and 3-16, respectively. Given their pairing with a dedicated spool, the bus routing is relatively simple. However, these magnets have the constraint that the end not attached to an X2 spool must be compatible with a standard Tevatron arc interface, and the cryostat must accommodate any through piping, bus, or instrumentation required by the Tevatron string. The asymmetry of the Tevatron interconnect places a more difficult requirement on the X2 spool design, discussed in Chapter 4.

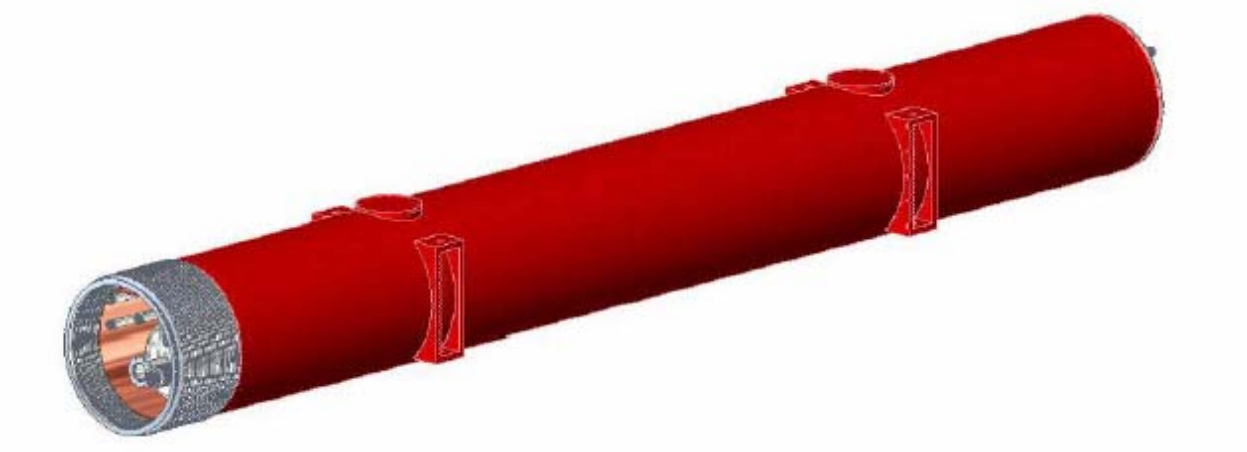

Figure 3-17: Complete Cryostat Assembly Preliminary Concept.

Figure 3-17 shows a concept of the completed cryostat assembly. Each magnet will be supported at 2 locations along the length, with the internal and external supports at the same location. Alignment fiducials are located on either side of the external reinforcing sections, and by using the single stretched wire measurement system the average cold magnetic axis can be related to these fiducials to within 200 μm. Lifting of the magnet is accomplished through the use of slings in the region near the reinforcing section.

3.6 Cryogenic Specifications

Each cryostat requires piping as shown in Table 3-7. The Q1 through Q3 cryostats are fed in a loop, and thus require return piping. The Q4 and Q5 are located in the arcs of the Tevatron, and require only through pipes. The pipes will need to be sized not only for cryogen flows, but also to accommodate any bus or instrumentation routing required, as is the case for the single phase helium. Similar to the existing Tevatron Low Beta Quadrupoles installed at B0 and D0, it is envisioned that the magnet will be cooled by a two phase heat exchanging jacket, as shown in Figure 3-18.

Table 3-7: Piping Requirements.

Magnet	1θ	2θ	Shield	1θ Return	2θ Return	Shield Return
Q1	X	X	X	X	X	X
Q2	X	X	X	X	X	X
Q3	X	X	X	X	X	X
Q4	X	X	X			
Q5	X	X	X			

Analysis of MTF data from previous LBQ tests suggest this re-cooling method is on the order of 65% effective, better than the standard arc dipole helium flow arrangement. Given that the overall size of the C0 IR quadrupole cold mass is very similar to the existing Low Beta Quadrupoles, we expect the cooling efficiency to be similar.

The heat load to 4 ^{o}K has been budgeted to be, on average, 5 watts per magnet or spool for all the new devices.

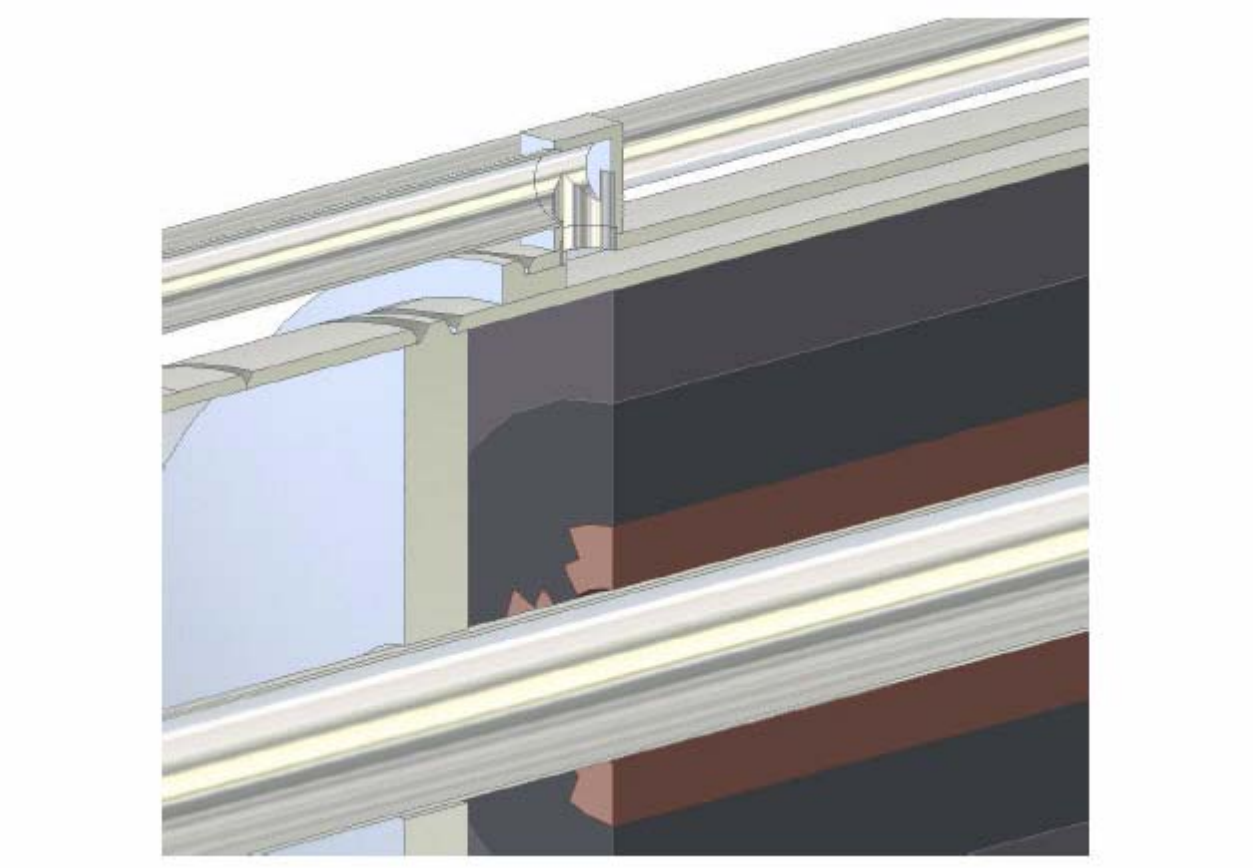

Figure 3-18: Two-phase cooling shell.

3.7 Design Changes and Infrastructure Requirements

The LHC IR Quadrupole program provides firm groundwork on which to base the C0 IR Quad design. The body mechanics and harmonics of the LHC design are well understood and repeatable; the cable is readily procured, and the production facility is in large part already completed. Many of the results, particularly at 4.5 ^{o}K, have been quoted in this chapter. However, there are details that are different and must be accounted for in the design of the C0 IR.

First, the reduced yoke diameter changes the harmonics of the magnet, and this must be thoroughly calculated. However, good agreement between electromagnetic calculations and measurements is usually seen. Finalization of the detailed yoke design should verify this.

During operation at the LHC, the IR quadrupoles ramp at only 10A/sec. For BTeV, the magnets will be ramped at up to 155A/sec if the current Tevatron acceleration ramp is used. This is a regime in which LHC models and full length magnets have shown some degradation in quench current. Initial studies will involve tests on the LHC production magnets and a review of the HGQ model magnet data.

Next, the reduced diameter changes the splice block, and the magnet to magnet splices. This is an intricate design task, and impacts the cryostat lengths. The single largest input needed is confirmation of the bus design, and the routing and fix points of the bus design.

The bus design is expected to be very similar to the LHC bus, however given the magnet diameter we may need to explore ways to make it more flexible. The use of LHC outer cable as opposed to inner cable is one possibility. Once this is fixed, details of the bus slots in the yoke, the required lengths and space for splices in the interconnects, and the required volumes for expansion loops can be determined.

As far as infrastructure, the LHC production facility in the Industrial Center Building provides the basis for the C0 production. The change in cold mass diameter and length(s) will require new mandrels for winding and curing of coils, and potentially new handling tooling if the current fixtures are simply too long for practical use. The yoke/welding press will need to be reworked to the smaller diameter of the cold mass, and qualification runs made to prove the weld quality.

In the Magnet Test Facility, magnets for the new C0 inner triplet will require a new test stand, capable of supplying 4K helium and 10kA current. (Our present 4K test stands are limited to 6kA.) The varying designs of the magnet and spool interconnects mean the test stand will require several adapters to accommodate the various interconnects. Most of the measurement equipment from LHC can be used directly for the C0 magnets. The baseline design presently includes one pair of conventional, copper current leads for 10kA.

The BTeV feed box (Figure 3-19) will have standard Tevatron test stand instrumentation (process flow thermometry, pressure taps, voltage taps on current leads, a local gauge panel, etc.) We do not plan new features for precise thermal tests except better 80K thermal shielding for lower heat loads. Thus, heat load measurements at the BTeV test stand will be of the +/-5 Watt variety typical of the Tevatron test stands. In addition to the standard instrumentation, we will include nitrogen gas flow instrumentation for spool pieces with HTS leads.

The BTeV feed box will operate in typical Tevatron magnet test modes and will have the standard MTF Tevatron test temperature range (from 4.8K down to 3.6K minimum, at the Tevatron pressure of 2.2 bar) and helium flow range (about 15 to 40 grams/sec). The new BTeV feed box will be located at the stand 6 location, taking advantage of those cryogen supply ports. Helium sub-cooling will be provided by the existing stand 6 cold pump and sub-cooler.

The C0 quadrupoles will require a dedicated turnaround box in addition to the feed box, which will be very simple with no valves and little instrumentation—basically a turnaround “cap” similar to what was used for the present Tevatron low-beta magnets.

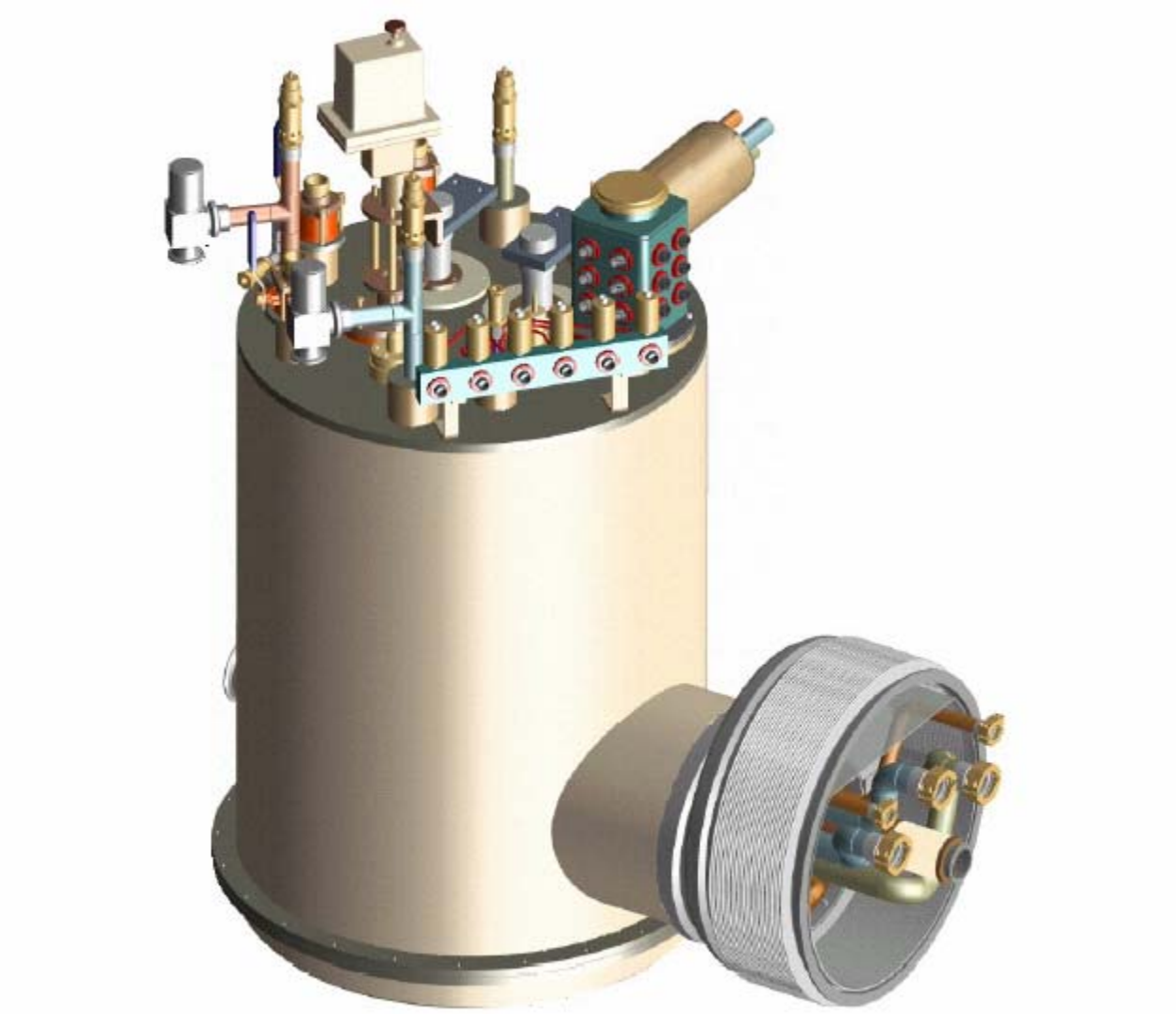

Figure 3-19: Magnet test feed box for C0 IR inner triplet quadrupoles.

References

[1] M. Andreev, et al, "Mechanical Design and Analysis of LHC Inner Triplet Quadrupole Magnets at Fermilab", (presented at MT-16 September 1999, Florida) *IEEE Transactions on Applied Superconductivity*, v.10, no.1, p.115 (March 2000).

[2] Vector Fields, Inc., Illinois, 60505, USA.

[3] P. Bauer, et al, "Busbar Studies for the LHC Interaction Region Quadrupoles" (presented at ASC September 2000, Virginia Beach, VA) *IEEE Transactions on Applied Superconductivity*, v.11, no.1, p.1613 (March 2001).

[4] P. Schlabach, private communication.

[5] Body harmonics are from model magnets hgq05-09; data for b_{13} only is from model magnets hgq01-03,05; lead end data is from models hgq06-09.

4 New Spools

4.1 Overview and Conceptual Design

Spools typically contain the magnetic correction system, power leads (HTS and/or conventional), beam position monitors (BPM's) and all necessary interfaces. The correction system includes dipole, quadrupole, and sextupole correctors combined in different packages. The different correction schemes at various locations along the interaction region (IR) dictate the total number of spool designs. Based on the current IR layout, we require three different spool designs. Table 4-1 lists the different spool designs with corresponding corrector magnets and required maximum gradients, allotted slot lengths and necessary power leads.

Table 4-1: Elements in different spool designs. Field values listed are the maximum required. "SL" designates safety leads.

Spool	Location	Slot Length, m	VD T. m	HD T. m	SQ T.m/m	Sx T.m/m^2	Q* T.m/m	BPM	HTS Leads	Other Leads
X1	packb43	1.83	0.48			450	25			3x100A+SL
X1	packb44	1.83		0.48		450	25			3x100A
X2	packb47	1.52	0.48	0.48				V&H	2x10kA	2x100A+SL
X2	packb48	1.52	0.48	0.48				V&H	2x10kA	2 x100A
X3	packc0u	1.52	0.48	0.48	7.5			V&H	2x10kA	3x100A+200A
X3	packc0d	1.52	0.48	0.48	7.5			V&H	2x10kA	3x100A+200A
X2	packc12	1.52	0.48	0.48				V&H	2x10kA	2x100A
X2	packc13	1.52	0.48	0.48				V&H	2x10kA	2x100A+SL
X1	packc16	1.83	0.48			450	25			3x100A
X1	packc17	1.83		0.48		450	25			3 x 100A+ SL

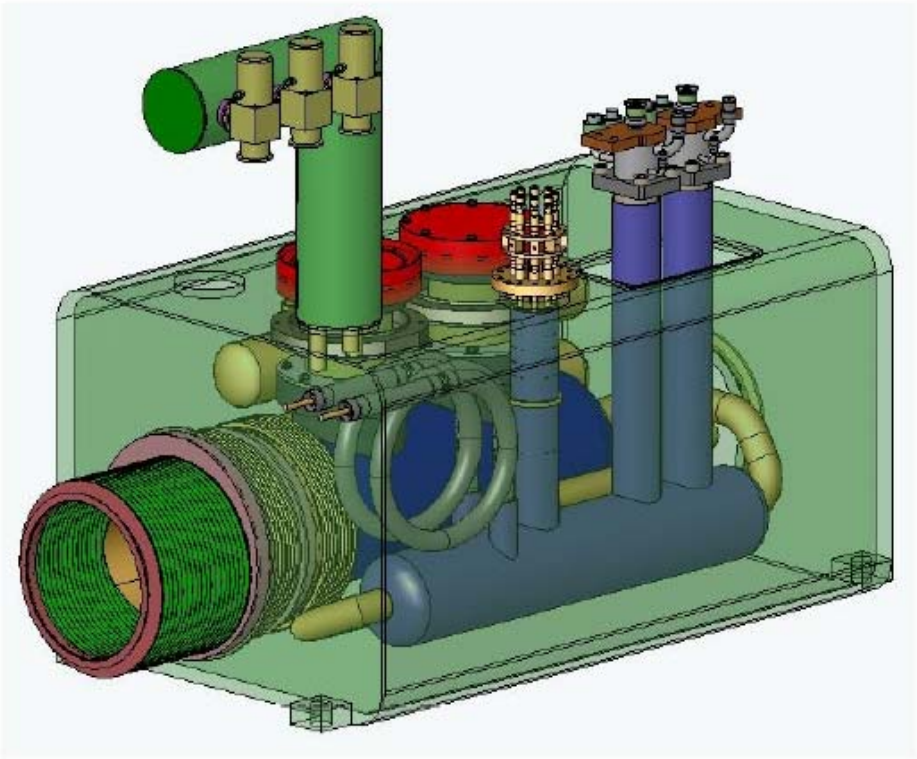

Figure 4-1: Conceptual drawing of an X2 spool layout.

The X1 spool has a slot length of 1.83 m with horizontal dipole (HD) or vertical dipole (VD) corrector depending on the location, strong quad (Q*) and sextupole (Sx) correctors. The X2 spool has a slot length of 1.52 m with horizontal and vertical dipole correctors. This spool also contains horizontal and vertical BPM's and a pair of 10 kA HTS power leads. The X3 spool which sits in the triplet region has the same allotted slot length as the X2 spool and has skew quadrupole corrector (SQ) in addition to both horizontal and vertical dipole correctors. It also has both horizontal and vertical BPM's and a pair of 10 kA HTS power leads. There will be a trim supply at this location which requires additional 200 A leads. Safety leads (SL) are also required at B43, B47, C13 and C17 locations. Figure 4-1 shows a conceptual layout of an X2 spool.

4.2 Corrector Design

A notable change in corrector requirements for the C0 interaction region is the addition of 'strong' quadrupole correctors with an integrated gradient of 25T-m/m. The other corrector strength requirements are comparable to existing Tevatron correctors. In addition, the new correctors do not contain octupole coils or skew sextupole coils, as do some of the original Tevatron correctors. Table 4-2 below summarizes the corrector strengths compared to existing Tevatron coils.

Table 4-2: Corrector maximum strength comparison.

Corrector type	Existing Correctors	C0 Requirements	units
dipole	0.460	0.480	T-m
quadrupole	7.5	7.5	T-m/m
quadrupole	none	25	T-m/m
sextupole (up)	449	450	T-m/m^2
sextupole (down)	346	none	T-m/m^2
octupole	30690	none	T-m/m^3

There are two types of corrector spools necessary for the C0 IR. The shorter X2 and X3 spools ("60in"=1420mm) have 800 mm available for containing both normal and skew dipoles in each spool type, plus an additional skew quadrupole in the X3. The longer X1 spools ("72in"=1830mm) have 1200 mm available for correction elements containing either normal or skew dipole, normal quadrupole of 25 T-m/m maximum strength and a normal sextupole of 450 T-m/m^2 maximum strength.

New correctors will be needed to meet C0 requirements. We have developed a conceptual design, employing a 'traditional' cos(nθ) design for the magnetic elements with separate correction elements for each term, which can meet the C0 requirements. We include this design for required correctors in sections (4.2.1, 4.2.2) as a "proof of principle".

However, schedule considerations and resource limitations have motivated us to seek alternatives to designing and fabricating the correction elements 'in house' at Fermilab. We have received and are in the process of evaluating proposals from Brookhaven National Laboratory (BNL, Long Island, NY) and from the Institute for High Energy Physics (IHEP, Protvino, Russia) to take on the complete task of design, fabrication, and testing of corrector magnets. We discuss the BNL and IHEP approaches in sections 4.2.3 and 4.2.4.

4.2.1 60" (1520mm) spool

In order to meet spatial constraints, some of the correction coils must be nested on top of others. The normal and skew dipoles are combined in one magnet assembly since they generate the same field strength and thus have similar magnetic lengths. All coils are based on the same ribbon cable with 10 strands of 0.3 mm diameter, slightly key-stoned for maximum efficiency. The conductor critical current density is assumed to be that of the SSC conductor. The coil cross-sections are optimized for the best field quality achievable without wedges using the ROXIE code [1]. At this stage of optimization, the magnetic permeability of the iron yoke is taken to be constant and equal to 1000. The coil inner diameter is fixed at 80 mm.

Figure 4-2 shows cross-section and the field plot in the ND/SD coils at maximum required strength in both coils and Tables 4-3 and 4-4 list the field harmonics. The peak field point is in the outer layer of the (inner) ND coil. The maximum field in the SD coil is 7% lower.

The cross-section and field plot in the skew quadrupole coil is shown in Figure 4-3 and field harmonics in Table 4-5. Peak field point in this case belongs to the pole turn of the inner layer.

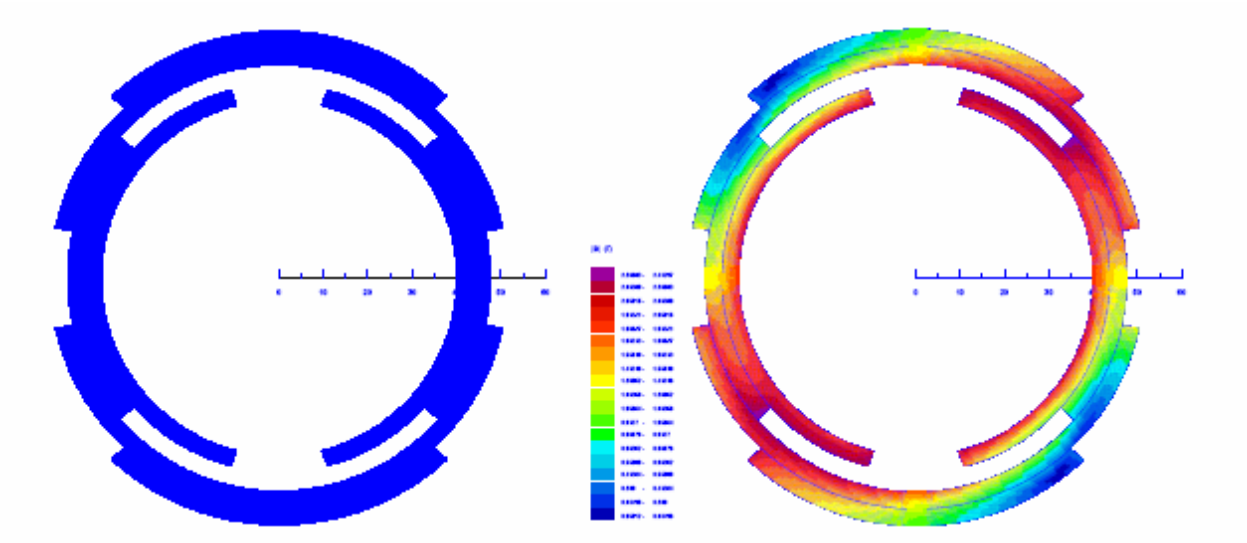

Figure 4-2: ND/SD coil cross-section (left) and field distribution (right).

Table 4-3: ND harmonics at 1” radius (SD=off), nominal current.

MAIN FIELD:	1.36986	NORMAL REL. MULTIPOLES (1.D-4):			
b 1:	10000.00000	b 2:	0.00000	b 3:	-0.63460
b 4:	0.00000	b 5:	-1.32323	b 6:	0.00000
b 7:	-12.19015	b 8:	0.00000	b 9:	-4.21001
b10:	0.00000	b11:	3.30994	b12:	0.00000
b13:	-0.82592	b14:	0.00000	b15:	0.14804
b16:	0.00000	b17:	-0.05274	b18:	0.00000
		SKEW REL. MULTIPOLES (1.D-4):			
a 1:	0.00000	a 2:	0.00000	a 3:	0.00000
a 4:	0.00000	a 5:	0.00000	a 6:	0.00000
a 7:	0.00000	a 8:	0.00000	a 9:	0.00000
a10:	0.00000	a11:	0.00000	a12:	0.00000
a13:	0.00000	a14:	0.00000	a15:	0.00000
a16:	0.00000	a17:	0.00000	a18:	0.00000

Table 4-4: SD harmonics at 1” radius (ND=off), nominal current.

MAIN FIELD:	1.36916	NORMAL REL. MULTIPOLES (1.D-4):			
b 1:	0.00000	b 2:	0.00000	b 3:	0.00000
b 4:	0.00000	b 5:	0.00000	b 6:	0.00000
b 7:	0.00000	b 8:	0.00000	b 9:	0.00000
b10:	0.00000	b11:	0.00000	b12:	0.00000
b13:	0.00000	b14:	0.00000	b15:	0.00000
b16:	0.00000	b17:	0.00000	b18:	0.00000
		SKEW REL. MULTIPOLES (1.D-4):			
a 1:	10000.00000	a 2:	0.00000	a 3:	0.41534
a 4:	0.00000	a 5:	-0.59540	a 6:	0.00000
a 7:	6.09581	a 8:	0.00000	a 9:	-0.35612
a10:	0.00000	a11:	-0.48422	a12:	0.00000
a13:	-0.09084	a14:	0.00000	a15:	-0.01239
a16:	0.00000	a17:	-0.00356	a18:	0.00000

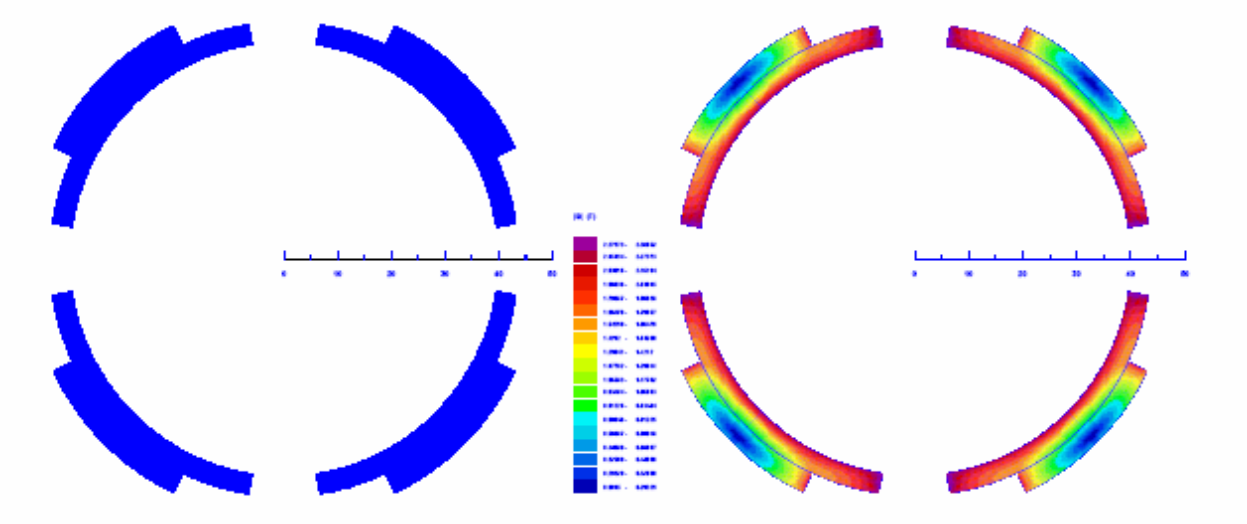

Figure 4-3: SQ coil cross-section (left) and field distribution (right).

Table 4-5: SQ harmonics at 1" radius, nominal current.

MAIN FIELD:	1.33057	NORMAL REL. MULTIPOLES (1.D-4):			
b 1:	0.00000	b 2:	0.00000	b 3:	0.00000
b 4:	0.00000	b 5:	0.00000	b 6:	0.00000
b 7:	0.00000	b 8:	0.00000	b 9:	0.00000
b10:	0.00000	b11:	0.00000	b12:	0.00000
b13:	0.00000	b14:	0.00000	b15:	0.00000
b16:	0.00000	b17:	0.00000	b18:	0.00000
		SKEW REL. MULTIPOLES (1.D-4):			
a 1:	0.00000	a 2:	10000.00000	a 3:	0.00000
a 4:	0.00000	a 5:	0.00000	a 6:	0.20147
a 7:	0.00000	a 8:	0.00000	a 9:	0.00000
a10:	-1.23434	a11:	0.00000	a12:	0.00000
a13:	0.00000	a14:	-0.30396	a15:	0.00000
a16:	0.00000	a17:	0.00000	a18:	-0.18879

The parameters of the correction elements are summarized in Table 4-6. Since they are more complicated in design, the nested ND/SD coils are provided with 55-59% quench margin while the single SQ coil has 38% margin. To provide the necessary integral field strengths, the ND/SD coils have a magnetic length of 0.35 m and the SQ coil length is 0.14 m. Given reasonable assumptions for the coil end lengths, the physical lengths of ND/SD and SQ magnets are 0.55 m and 0.25 m respectively. These lengths fill all the space available for correction elements.

Table 4-6: 60” spool corrector parameters.

Parameter	Unit	ND	SD	SQ
n		0	0	1
Coil IR	*mm*	40.0	48.0	40.0
Yoke IR	*mm*	60.0		53.0
Strands/cable		10		
Bare strand diameter	*mm*	0.300		
Cu/nonCu ratio		2.0		
J_{nonCu}(5T, 4.2K)	A/mm^2	2750		
Maximum strength required	$T \cdot m/m^n$	0.48	0.48	7.5
Current @ maximum strength	*A*	27.2	23.6	49.0
Quench margin at nominal current in all the coils	*%*	54.7	58.8	38.2
Inductance	*H/m*	15.16	25.03	6.48
Stored energy at I_{nom}	*kJ/m*	5.61	6.97	7.78
Magnetic length	*m*	0.350	0.351	0.143
Physical length	*m*	0.55		0.25

4.2.2 72” (1830mm) spool

Similar to the 60” spool, some of the coils in the 72” spool must be nested. To reduce Lorentz forces, the normal quadrupole and sextupole coils are combined in one magnet assembly. All coils are based on the same ribbon cable used in the 60” spool. Again, the coil cross-sections are optimized for the best field quality achievable without wedges using ROXIE code; the magnetic permeability of the iron yoke is taken to be constant and equal to 1000; the coil inner diameter is fixed at 80 mm.

Figure 4-4 shows the cross-section and field plot in the NQ/NS coils at the nominal current and Tables 4-7 and 4-8 list the field harmonics. The peak field point is in the inner layer of the (inner) NQ coil. The maximum field in the NS coil is 6% lower.

The cross-section and field plots for the normal dipole coil is shown in Figure 4-5 and field harmonics in Table 4-9. Peak field point in this case is in the pole turn of the inner layer.

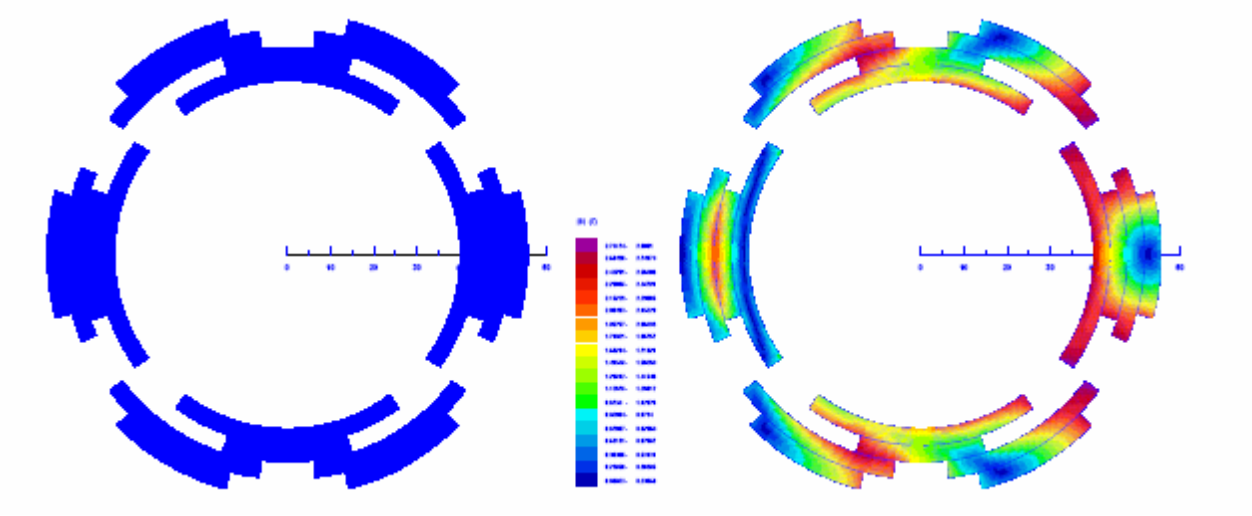

Figure 4-4: NQ/NS coil cross-section (left) and field distribution (right).

Table 4-7: NQ harmonics at 1” radius (NS=off), nominal current.

MAIN FIELD:	0.93930	NORMAL REL. MULTIPOLES (1.D-4):			
b 1:	0.00000	b 2:	10000.00000	b 3:	0.00000
b 4:	0.00000	b 5:	0.00000	b 6:	0.17997
b 7:	0.00000	b 8:	0.00000	b 9:	0.00000
b10:	0.39959	b11:	0.00000	b12:	0.00000
b13:	0.00000	b14:	0.46534	b15:	0.00000
b16:	0.00000	b17:	0.00000	b18:	-0.22728
		SKEW REL. MULTIPOLES (1.D-4):			
a 1:	0.00000	a 2:	0.00000	a 3:	0.00000
a 4:	0.00000	a 5:	0.00000	a 6:	0.00000
a 7:	0.00000	a 8:	0.00000	a 9:	0.00000
a10:	0.00000	a11:	0.00000	a12:	0.00000
a13:	0.00000	a14:	0.00000	a15:	0.00000
a16:	0.00000	a17:	0.00000	a18:	0.00000

Table 4-8: NS harmonics at 1” radius (NQ=off), nominal current.

MAIN FIELD:	0.41682	NORMAL REL. MULTIPOLES (1.D-4):			
b 1:	0.00000	b 2:	0.00000	b 3:	10000.00000
b 4:	0.00000	b 5:	0.00000	b 6:	0.00000
b 7:	0.00000	b 8:	0.00000	b 9:	-0.09100
b10:	0.00000	b11:	0.00000	b12:	0.00000
b13:	0.00000	b14:	0.00000	b15:	-0.17912
b16:	0.00000	b17:	0.00000	b18:	0.00000
		SKEW REL. MULTIPOLES (1.D-4):			
a 1:	0.00000	a 2:	0.00000	a 3:	0.00000
a 4:	0.00000	a 5:	0.00000	a 6:	0.00000
a 7:	0.00000	a 8:	0.00000	a 9:	0.00000
a10:	0.00000	a11:	0.00000	a12:	0.00000
a13:	0.00000	a14:	0.00000	a15:	0.00000
a16:	0.00000	a17:	0.00000	a18:	0.00000

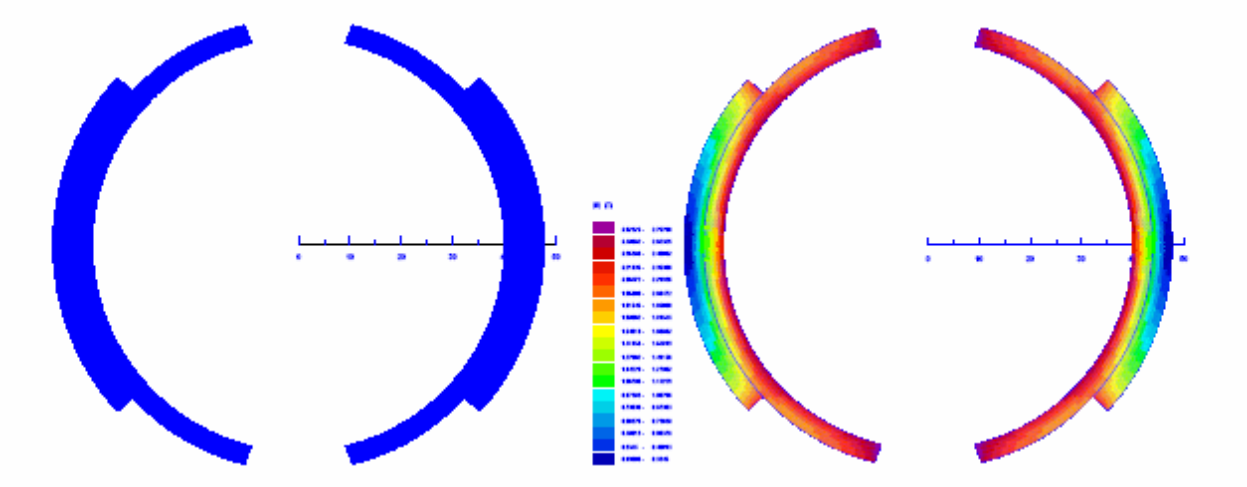

Figure 4-5: ND coil cross-section (left) and field distribution (right).

Table 4-9: ND harmonics at 1" radius, nominal current.

MAIN FIELD:	-2.39854	NORMAL REL. MULTIPOLES (1.D-4):			
b 1:	10000.00000	b 2:	0.00000	b 3:	0.03621
b 4:	0.00000	b 5:	-5.69697	b 6:	0.00000
b 7:	-13.22185	b 8:	0.00000	b 9:	-2.67747
b10:	0.00000	b11:	2.89949	b12:	0.00000
b13:	-0.79648	b14:	0.00000	b15:	0.14924
b16:	0.00000	b17:	-0.05175	b18:	0.00000
		SKEW REL. MULTIPOLES (1.D-4):			
a 1:	0.00000	a 2:	0.00000	a 3:	0.00000
a 4:	0.00000	a 5:	0.00000	a 6:	0.00000
a 7:	0.00000	a 8:	0.00000	a 9:	0.00000
a10:	0.00000	a11:	0.00000	a12:	0.00000
a13:	0.00000	a14:	0.00000	a15:	0.00000
a16:	0.00000	a17:	0.00000	a18:	0.00000

Parameters of the correction elements are summarized in Table 4-10. The nested NQ/NS coils have 41-43% quench margin while the single ND coil has 39% margin. To provide the necessary integral field strengths, the NQ/NS coils will have magnetic lengths of 0.68 to 0.70 m and the ND coil of 0.20 m. Given reasonable assumptions on the coil end lengths, the physical lengths of NQ/NS and ND magnets are 0.8 m and 0.4 m respectively. This utilizes all the space available for correction elements.

Table 4-10: 72" spool corrector parameters.

Parameter	Unit	NQ	NS	ND
n		1	2	0
Coil IR	*mm*	40.0	48.0	40.0
Yoke IR	*mm*	60.0		53.0
Strands/cable		10		
Bare strand diameter	*mm*	0.300		
Cu/nonCu ratio		2.0		
J_{nonCu}(5T, 4.2K)	A/mm^2	2750		
Maximum required strength	$T \cdot m/m^n$	25	450	0.48
Current @ maximum strength	*A*	40.0	36.6	43.0
Quench margin at nominal current in all the coils	*%*	40.6	42.9	39.2
Inductance	*H/m*	5.42	6.24	17.01
Stored energy at I_{nom}	*kJ/m*	4.34	4.18	15.73
Magnetic length	*m*	0.676	0.696	0.200
Physical length	*m*	0.8		0.4

4.2.3 Brookhaven Corrector Approach

BNL has been using a 'direct wind' technique in which individual wires are deposited on the surface of a cylinder in precise winding patterns through the use of computer-controlled machine tools. BNL has employed this technique in building correctors for the RHIC, HERA, and Beijing accelerator facilities. Preliminary studies indicate that BNL can meet the magnetic strength requirements within the 100A current limit negotiated with the FNAL Accelerator Division. The field quality obtained with this technique can meet the relatively modest corrector requirements without adding significant complexity to the design or the winding procedure. (In the case of stringent limits, it is possible to measure each layer and determine corrections to be included in subsequent layers to reduce any non-uniformities to the desired level.) Figure 4.6 show the BNL direct wind process in action.

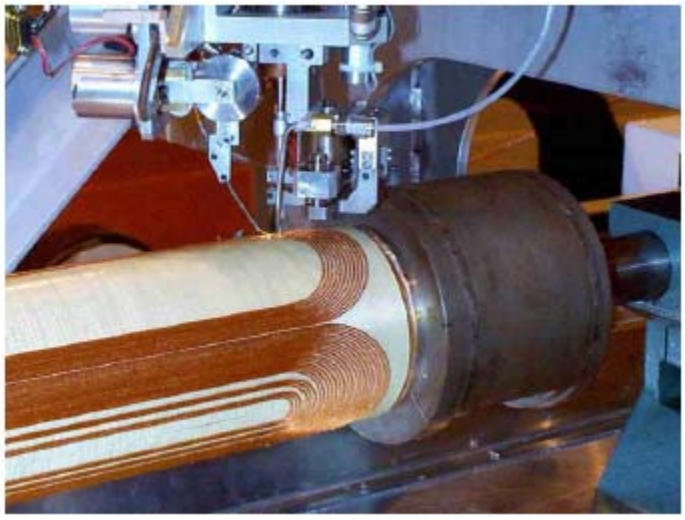

Figure 4-6: Photograph of BNL Direct Wind corrector fabrication in process.

4.2.4 IHEP Corrector Approach

The magnet design group at IHEP, Protvino has proposed a 'conventional' cos(nθ) design similar to that presented in 4.2.1 and 4.2.2 above. The IHEP approach would use ribbon cable similar to that in the CERN correctors and in the Fermilab conceptual design described above. They have designed and built similar correctors for the UNK project at IHEP and have recently designed, built, and delivered superconducting solenoid plus correction elements magnet assemblies to Fermilab for use in the current Run II beam-beam tune shift compensation project[α].

4.2.5 Corrector Summary

At this juncture, we have decided to pursue a source outside of Fermilab to provide the correctors. The proposals from BNL and IHEP, Protvino are being evaluated in terms of cost, schedule, and ability to meet requirements.

4.3 Dimensional Specifications

The length of the corrector packages described in the previous section is designed such that the overall length of the spool matches that of the allotted slot length. Figure 4-7 shows the dimensional specifications for X2 spool. The helium vessel is supported inside the vacuum vessel using two suspension posts identical to the ones used in the cryostat to support quadrupole cold mass. The corrector magnet will be supported inside the helium vessel with two stainless steel rings. Once the corrector is aligned inside the helium vessel, the rings will be welded to the

---

[α] Tevatron Electron Lens (TEL-1 in 1999, TEL-2 in 2003), each consists of a 6.5T superconducting solenoid and 6 superconducting dipole corrector coils in the same cryostat, 2 copper solenoids for 0.4T with 8 weak corrector coils in them, plus support frame. The superconducting magnet includes 7 coils in one package, in a limited space with very high tolerances on magnetic field quality (V. Shiltsev, private communication)

inside of the helium vessel to lock it in place. The corrector support rings will be coincident with the suspension posts. Note that unlike in X2 and X3 spools, there are no HTS power leads in X1 spools. Hence the outer vacuum vessel houses only the helium vessel that contains corrector package and the necessary interfaces.

The beam tube has an inner diameter of 63 mm and an outer diameter of 66.7 mm. It will be insulated with Kapton which raises the outer diameter to about 67.1 mm. Note that the bore diameter for corrector magnets ≥70 mm and for quadrupole magnets the diameter is 70 mm.

BPM's will be embedded in the spool between flanges and the corrector magnet. The allotted slot length for BPM's is 10 inches. The BPM design will be similar to those already installed in the Tevatron.

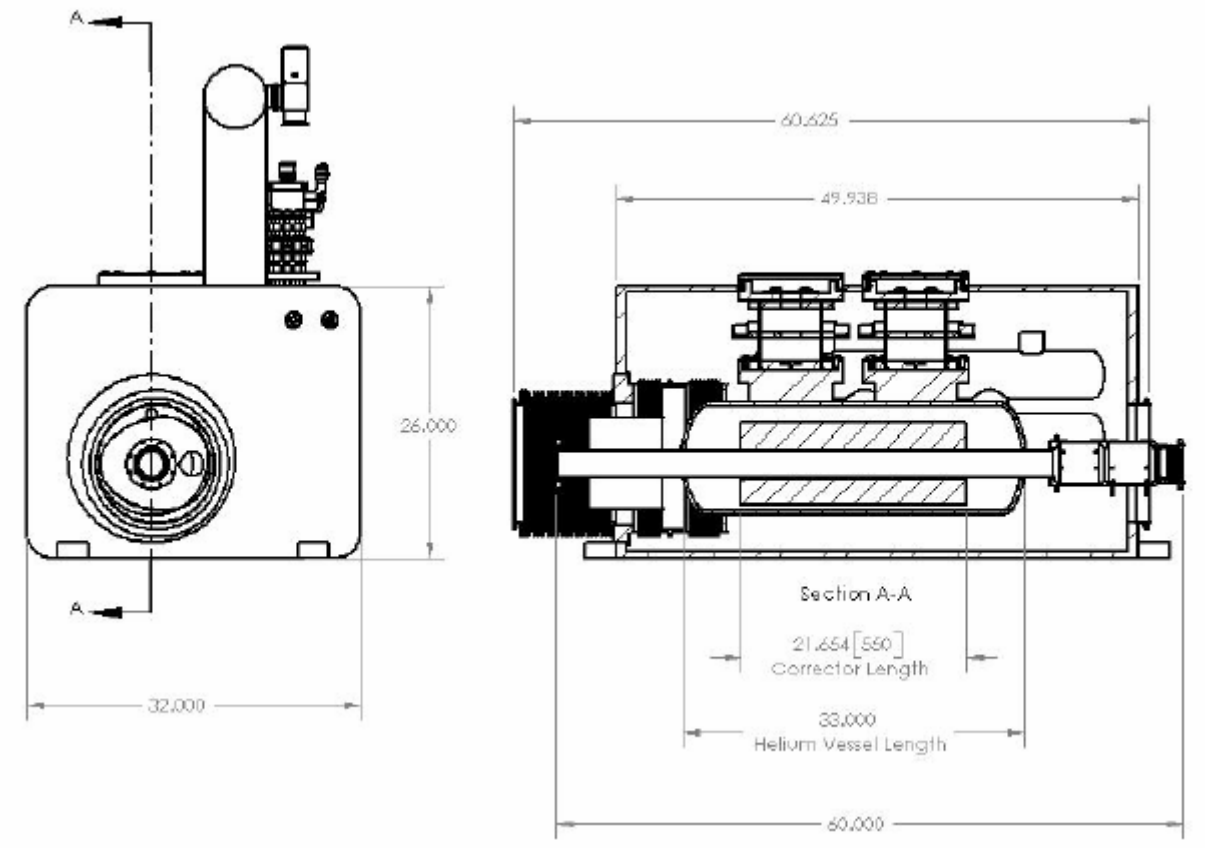

Figure 4-7: Dimensional specifications for X2 spool.

4.4 Cryogenic Specifications

Table 4-11 gives the expected heat loads for various components in the spool pieces. The design goal for the heat load to 4 ^{o}K in a given spool piece is ≤10W. (This is a conservative number based on measurements of existing spool heat loads and is consistent with allocated refrigeration budget. The design heat load is 5 watts per spool.)

Item	Heat to 4 ^{o}K (W)	Helium consumption (l/hr)	Nitrogen consumption (l/hr)	Design goal
Each HTS lead		0.7	3.6	
Each AMI lead		12.0		
Each corrector pkg		1.0		
Spool piece	10			5

Table 4-11: Expected heat loads.

The 2-phase flow is designed such that it will flow in and out at the top (see Fig 4-9). Liquid drops and fills the 2-phase volume up to the exit port. Each spool will require 3 Kautzky valves: for single-phase, 2-phase, and nitrogen. Furthermore, X1 and X2 spools need to have insulation vacuum breaks. Note that while X1 and X2 spools have piping for only inlet, X3 spools will have both inlet and return feed-throughs.

4.5 Quench Protection

Preliminary calculations indicate that the new corrector magnets (using the skew dipole parameters from Table 4-6 above) can be adequately protected with an external dump resistor of 7.5 Ω. The quench protection threshold should be 1V or less. During a quench, some fraction of the magnet coil becomes resistive which helps to absorb the stored energy. Even if we neglect this extra resistance, the magnet peak temperature will be well under 300 ^{o}K. Also, the peak voltage to ground is estimated to be less than 370V, the maximum voltage across the dump resistor. Although the magnet operating current is roughly 40% of the critical current value, we still expect relatively fast (larger than 1-2 m/s) quench propagation velocity since the coils are epoxy impregnated which reduces the coil cooling drastically. Detailed calculations will be done for the complete set of correctors.

4.6 Connections and Interfacing

Table 4-12 summarizes the interfaces required for each spool. Both X1 and X2 spools at all locations interact with Tevatron interfaces at least on one side. This requires that the cryostat for the quadrupole magnets at these locations also have standard Tevatron interfaces.

Table 4-12: Upstream (US) and downstream (DS) interfaces for various spools.

Location	*Designation*	*US comp.*	*US interface*	*US bus*	*DS comp.*	*DS interface*	*DS bus*
packb43	X1V	Quad	Tev	Tev	Dipole	Tev	Tev
packb44	X1H	Quad	Tev	Tev	Dipole	Tev	Tev
packb47	X2	Q5	Modified Tev?	Tev, LHC	Dipole	Tev	Tev
packb48	X2	Cold bypass	Tev	Tev	Q4	Tev	Tev, LHC
packc0u	X3	Q3	New	LHC	Q2	New	LHC
packc0d	X3	Q2	New	LHC	Q3	New	LHC
packc12	X2	Dipole	Tev	Tev	Q4	Tev	Tev, LHC
packc13	X2	Q5	Modified Tev?	Tev, LHC	Dipole	Tev	Tev
packc16	X1V	Quad	Tev	Tev	Dipole	Tev	Tev
packc17	X1H	Quad	Tev	Tev	Dipole	Tev	Tev

The X3 spool is within the triplet region and is connected to Q2 and Q3 quadrupoles. This allows the X3 spool to have interfaces that are different from standard Tevatron interfaces. These interfaces are currently being finalized. In addition, the X1 and X2 spools have a Tevatron through bus, whereas the X3 spool has LHC type bus.

Both the X2 and X3 spools will have a pair of 10 kA HTS power leads. The HTS leads are discussed in section 4.7.1.

Apart from the 10 kA HTS power leads, the spools also have leads for the corrector magnets. For the baseline design, the corrector leads will carry currents less than 100A. In addition, the X3 spool will have 200 A power lead for a trim shunt across the Q1/Q3 LHC style quads.

4.7 Measurements and R&D to Date

4.7.1 HTS Leads

The 10kA current leads for the high gradient quadrupoles in the C0 IR will be made from high temperature superconductor (HTS) to avoid additional loading of the 4.5 ^{o}K He system. In the present Tevatron configuration, four spool pieces have been modified to incorporate 5kA HTS leads, and one of these has been installed and operated in the ring for several years. One of these modified spool pieces is shown in Figure 4-8 below. The HTS lead assembly and the LN2 reservoir are clearly visible in the foreground and right side of the picture, respectively.

Figure 4-8: modified H-spool with HTS lead package on the floor at MTF.

Based on R&D tests performed during the 5kA lead program, it appeared that it could be possible to operate the leads at higher currents by increasing the coolant flow.
Preliminary tests of an existing HTS spool at the Magnet Test Facility verified this hypothesis: it ran in a stable mode at the nominal operating current. More detailed tests of a second pair of HTS leads have been recently carried out in a dewar facility which allowed greater control over cryogenic pressure, temperature, and flow. These tests were very successful. Both the upper conventional copper section which is cooled with liquid nitrogen vapor and the lower HTS section cooled with liquid helium vapor exhibited stable operation up to 10 kA and up to 200 A/s current ramp rate.

A summary plot of the current and the Cu and HTS section voltages for the recent test is displayed in Figure 4-9. The leads were stable for more than 5 hours at the nominal operating current of 9560A followed by 'saw tooth' ramping from 0 to 9650A at a ramp rate (dI/dt) of 200 A/sec. These tests were followed by a brief (~30 min) period of operation at 10000A (on the far right hand side of the plot); again, the leads exhibited stable behavior.

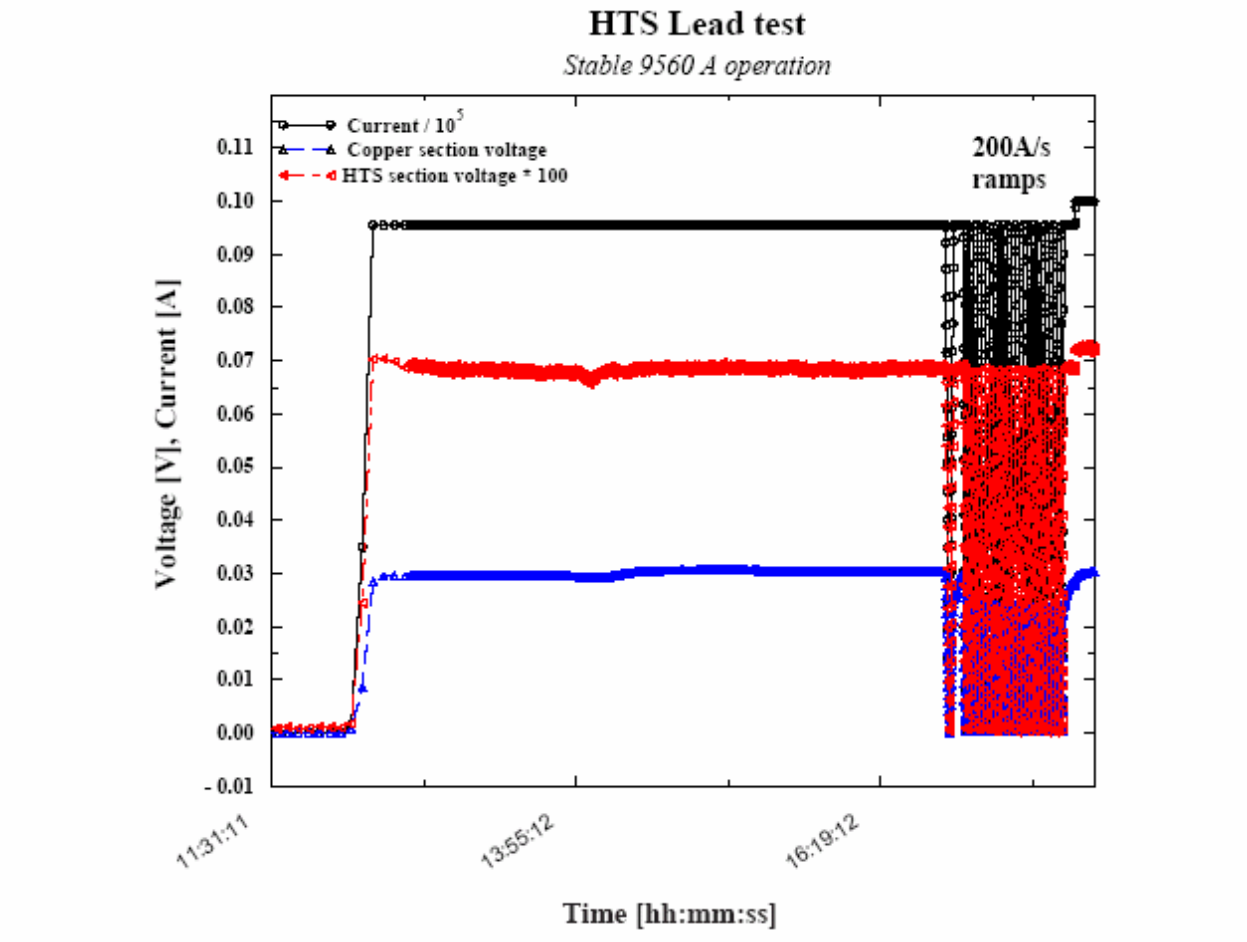

Figure 4-9: HTS lead test: 5 hours of stable DC operation at 9560A, followed by roughly one hour of ramping 0 - 9560 - 0 at 200 A/sec.

We are now confident that a single pair of leads of the existing design will be sufficient for operation at 10kA and the spool design reflects this.

References

[1] S. Russenchuck, "A Computer Program for the Design of Superconducting Accelerator Magnets", CERN AT/95-39, LHC Note 354, Geneva, Switzerland, (September, 1995)

5 Power Supplies

5.1 High Current Power Supply Layout

The low beta quadrupole power supplies for the C0 interaction region will be located in the B4, C0, and C1 service buildings. A listing of these supplies is given in Table 5-1 below.

Table 5-1: High current power supply layout.

B4-Service Building

Circuit	Magnet	Power	Volt	Current
C:QB45	B45-"old-Q1"	50 KW	10 V	5,000 A
C:QB46	B46-"old-Q1"	50 KW	10 V	5,000 A

C0-Service Building

Circuit	Magnet	Power	Volt	Current
C:C0Q5	B47-Q5, C13-Q5	300 KW	30 V	10,000 A
C:C0Q4	B48-Q4, C12-Q4	300 KW	30 V	10,000 A
C:C0Q123	B49-Q1, Q2, Q3 C11-Q1, Q2, Q3	300 KW	30 V	10,000 A
C:C0QSU	B49-Q1, B49-Q3		10 V	200 A
C:C0QSD	C11-Q1, C11-Q3		10 V	200 A

C1-Service Building

Circuit	Magnet	Power	Volt	Current
C:QC14	C14-"old-Q1"	50 KW	30 V	5,000 A
C:QC15	C15-"old-Q1"	50 KW	30 V	5,000 A

These high current supplies will be 12 pulse SCR phase controlled power supplies. They will be purchased from industry in a similar fashion as the Main Injector P1/P2 Quadrupole supplies. A detailed specification will be written for the cabinet, high power conversion equipment (input circuits, bridge and filter). Fermilab will supply the voltage regulation chassis that will be integrated in the supply cabinet and then tested by the vendor.

Each current regulation system will be a 10ppm system based on the exacting regulation of the existing B0/D0 low beta supplies.

The Q1/Q3 shunt will be similar to the existing C0 shunt that tunes the Main Injector magnets, installed in the C0 straight section to replace the TeV Abort Lambertson magnets. This installation took place in the fall of 2003. The required changes will be a peak current on the order of 2X the present system and additional circuitry to protect the shunt from quench-induced voltages.

5.2 Bus-work

Bus-work to and from the magnet loads will be the main resistive loss in the system and will drive the power supply voltage requirements. The correct amount of copper to use in the bus work is such that the installation cost is equal to the power bill for running the system for a set period of time (like three years). As with the Main Injector, this works out to be on the order of 4 square inches of copper bus per 5,000 A RMS of current. For the 10,000 A runs the plan is to install two 4 square inch runs in parallel for supply and return. Bus lengths for the various circuits are given in the Table under Electrical Specifications.

The bus-work in C0 will come from the service building through an outdoor bus duct ~50 ft upstream of the existing large penetrations. The outdoor portion of the bus duct will have heaters installed to avoid freezing in winter conditions. All high current bus in the tunnel will be routed on the ceiling. To connect upstream and downstream loads, the bus will be routed through the tunnel bypass.

In the B4 and C1 service buildings the existing Main Ring bus (~0.85 square inches) will be removed and replaced with new 4 square inch bus. This bus is mounted to the ceiling of the service building stair well.

5.3 Electrical Specifications

Table 5-2 lists the main electrical parameters for each high current circuits. In the table, dI/dT is the maximum ramp rate, which occurs during the acceleration cycle in all cases.

Table 5-2: Electrical parameters for high current circuits.

B4-Service Building

Circuit	Ind [H]	dI/dT [A/sec]	L*dI/dT [Volts]	Bus L [feet]	R*I [Volts]	PS V [Volts]
C:QB45	0.01075	70	0.8	100	3.3	4.1
C:QB46	0.01075	70	0.8	218	6.0	6.8

C0-Service Building

Circuit	Ind [H]	dI/dT [A/sec]	L*dI/dT [Volts]	Bus L [feet]	R*I [Volts]	PS V [Volts]
C:C0Q5	0.0093	155	1.4	780	18.9	20.4
C:C0Q4	0.0124	155	1.9	642	15.8	17.7
C:C0Q123	0.0561	155	8.7	370	9.5	18.2

C1-Service Building

Circuit	Ind [H]	dI/dT [A/sec]	L*dI/dT [Volts]	Bus L [feet]	R*I [Volts]	PS V [Volts]
C:QC14	0.01075	70	0.8	218	6.0	6.8
C:QC15	0.01075	70	0.8	100	3.3	4.1

Notes:
1. Bus l is the one way bus length
2. I*R includes the DC resistance of the filter chokes -- 0.2 mΩ for 5,000 A supplies; 0.1 mΩ for 10,000 A supplies
3. 5,000 A magnet bus has a resistance of 2.3 μΩ/ft

5.4 AC Power and LCW Requirements

AC power for the high current supplies will be derived from Tevatron Feeder #23. At B4 and C1 a 500 KVA pulsed power transformer (13.8 KV to 480 V) will be installed that will feed a 1,200 A panel board to be used for the two high current loads driven from each building. At C0 a 1.5MVA pulsed power transformer (13.8 KV to 480 V) will be installed that will feed a 2,000 Amp panel board to be used for the three high current loads to be driven from C0.

LCW requirements for the bus work will be quite modest and in general will be used to stabilize the electrical resistance. The 2-5/8 in OD by 1-3/8 in ID bus has a resistance of 2.3μ ohms per foot at 40˚C. At 5,000 amps RMS the power dissipated is ~57.5 watts per foot. The bus-work will represent a very modest heat load to the LCW system.

For the power supplies the passive filter choke is the largest heat load It is estimated that the 10,000 amp supplies will need about 55 gpm each and the 5,000 amp supplies will need about 35 gpm each. See section 11.2.2 for additional LCW specification.

5.5 Controls Specifications

The control of a magnet/power system for Collider operation will require a very stable and proven interface to the existing operation system. With this in mind we will use an updated version of the existing designs for the TeV Low Beta's, Main Injector and NuMI power systems.

The current reference for each magnet loop will use an FNAL C468 ramp generator card connected to the FNAL ultra stable current regulation system. This system includes a current regulator chassis and a commercial DCCT current monitor as well as the FNAL voltage regulator installed in the power supply. The C468 card will provide a 16 bit reference to the DAC in a temperature controlled module in the current regulator. In the temperature regulated module the measured current from a DCCT and the analog output from the reference DAC are subtracted and the difference is sent to the power supply as the correction for the supply. The power supply acts as a closed loop voltage source, using the FNAL voltage regulator, that operates inside the current loop of the current regulator chassis. The voltage and current monitor signals will be provided to ACNET (Accelerator Controls Network) through the controls MADC system for use in operation.

The on/off control and status will be provided using the same C468 card that has up to 32 bits of digital status. The power supplies will be specified to include all the necessary connection to the control system and the Quench Protection Monitor (QPM) that monitors and protects the magnets from quenches.

In addition to the QPM connection, a fast bypass failure detector will be installed that will trip the power supply through an independent hardware connection if the supply is told to be off but the output voltage does not go to zero.

Electrical Safety System (ESS) connections are built into the power supplies as part of the specification. The connection uses relay hardware to trip the main 480 Vac breaker and will provide the first level of protection for personnel safety. A KIRK lock system will be used to ensure that access to the power supply equipment will not expose personnel to any hazards.

For diagnostic purposes, a transient recorder will be installed at each power supply or in each building to monitor and collect data for analysis of any trip that may occur. These devices are similar in operation and use to the circular buffers that are an integral part of the QPM system and are used to provide detailed information during trips.

5.6 Corrector Power Supply Configuration

The independent corrector power supplies required for the C0 IR are detailed in Table 5-3 and 5-4. For B4 and C1 sectors, the count of independent channels goes from 19 for Run II to 34 for the C0 IR. The B4 and C1 service building corrector power supply installations will be maintained for the 50 Amp corrector elements in the P spools and other existing elements driven from B4 and C1 but outside of the IR region. The B4 existing 50 Amp unit count will decrease from the existing 9 to 4 and the C1 existing 50 Amp unit count will decrease from 10 to 4. The 11 channels removed will be added to the TeV spares.

The new X1, X2 and X3 spools will need 100 Amp corrector power supplies. We will install 4 packages to satisfy these needs, one each at B4 and C1 and two at C0. Each installation will consist of a new bulk supply and individual switch mode, four-quadrant power supplies providing the regulation off of the bulk supply. The proposed supplies are a very mature design and are a virtual copy of the Main Injector system which is barely 5 years old. An external quench protection system will be designed and installed for these correction elements.

X2 and X3 spools need both horizontal and vertical correctors installed. This will be accomplished by a single 4 coil magnet delivering the sum and difference to the diagonal corrector coils.

Table 5-3: Correctors in B4 and C1 for Run II.

Name	Type	Location	Spool Elements	PS Name	PS Current	PS House
packb43	D spool	B43-1a	T:VDB43, (T:QDD1), (T:SD), (C:S1B3A), (T:OD)	T:VDB43	50 Amps	B4
packb44	C spool	B44-1a	T:HDB44, (T:QFA4), (T:SF)	T:HDB44	50 Amps	B4
packb45	B spool	B45-1a	T:VDB45, (T:QDD1), (T:SD)	T:VDB45	50 Amps	B4
packb46	C spool	B46-1a	T:HDB46, (T:QFA4), (T:SF), (T:SQ)	T:HDB46	50 Amps	B4
packb47	DR spool	B47-1a	T:VDB47, (T:QDD1), (T:SD), (C:S2B4A)	T:VDB47	50 Amps	B4
packb48	A spool	B48-1a	T:HDB48	T:HDB48	50 Amps	B4
packb49	H spool	B49-1a	T:HDB49, T:VDB49	T:HDB49, T:VDB49	50 Amps	B4
packc11	H spool	C11-1a	T:HDC11, T:VDC11	T:HDC11, T:VDC11	50 Amps	C1
packc12	F spool	C12-1a	T:VDC12, (T:O2)	T:VDC12	50 Amps	C1
packc13	C spool	C13-1a	T:HDC13, (T:QFA4), (T:SF), (T:SQ)	T:HDC13	50 Amps	C1
packc14	F spool	C14-1a	T:VDC14, (T:QDD1), (T:SD)	T:VDC14	50 Amps	C1
packc15	A spool	C15-1a	T:HDC15 ,(T:QFA4), (T:SF)	T:HDC15	50 Amps	C1
packc16	F spool	C16-1a	T:VDC16, (T:QDD1), (T:SD)	T:VDC16	50 Amps	C1
packc17	C spool	C17-1a	T:HDC17, (T:QFA4), (T:SQ), (T:SF), (T:O1)	T:HDC17	50 Amps	C1
other PS at B4				T:HDB42	50 Amps	B4
other PS at C1				T:VDC18, T:HDC19	50 Amps	C1
			Total=	**19**		

Note: Spool elements in parentheses are driven from PS's in a house other than B4 or C1.

Table 5-4: Correctors in B4, C0 and C1 for the C0 IR.

Name	Type	Location	Spool Elements	PS Name	PS Current	PS House
packb43	X1 spool	B43-1a	T:VDB43,T:QB43, T:SDB44	T:VDB43,T:QB43, T:SDB44	100 Amps	B4
packb44	X1 spool	B44-1a	T:HDB44, T:QB44, T:SFB44	T:HDB44, T:QB44, T:SFB44	100 Amps	B4
packb45	P spool	B45-1a	T:VDB45, (T:SQ)	T:VDB45	50 Amps	B4
packb46	P spool	B46-1a	T:HDB46, (T:SQ)	T:HDB46	50 Amps	B4
packb47	X2 spool	B47-1a	T:VDB47, T:HDB47	T:VDB47, T:HDB47	100 Amps	C0
packb48	X2 spool	B48-1a	T:HDB48, T:VDB48	T:HDB48, T:VDB48	100 Amps	C0
Packc0u	X3 spool	B49-3a	T:HDB49,T:VDB49, T:SQB4	T:HDB49,T:VDB49, T:SQB4	100 Amps	C0
Packc0d	X3 spool	C10-2a	T:HDC11,T:VDC11, T:SQC1	T:HDC11,T:VDC11, T:SQC1	100 Amps	C0
packc12	X2 spool	C11-5a	T:VDC12, T:HDC12	T:VDC12, T:HDC12	100 Amps	C0
packc13	X2 spool	C13-1a	T:HDC13, T:VDC13	T:HDC13, T:VDC13	100 Amps	C0
packc14	P spool	C14-1a	T:VDC14, (T:SQ)	T:VDC14	50 Amps	C1
packc15	P spool	C15-1a	T:HDC15, (T:SQ)	T:HDC15	50 Amps	C1
packc16	X1 spool	C16-1a	T:VDC16, T:QC16, T:SDC16	T:VDC16, T:QC16, T:SDC16	100 Amps	C1
packc17	X1 spool	C17-1a	T:HDC17,T:QC17, T:SFC17	T:HDC17,T:QC17, T:SFC17	100 Amps	C1
other PS at B4				T:HDB42, TQB42	50 Amps	B4
other PS at C1				T:VDC18, T:HDC19	50 Amps	C1
			Total=	**34**		

Note: Spool elements in parentheses are driven from PS's in a house other than B4, C0 or C1.

5.7 B4 and C1 QPM Modifications

The only modification necessary to the quench protection modules (QPMs) at B4 and C1 will be the addition of one HFU at each location and two lead voltages at each house for the high temperature leads in the feed can at B49-2 and the feed can at C10-3A.

5.8 Electrostatic Separator Power Supplies

Six electrostatic separators are needed with the new C0 low beta system. The separators will be located at B49 and C11. B49 has one vertical and two horizontal separators. The two horizontal separators will be driven in parallel. At C11 there are two vertical and one horizontal separators and again the two vertical units will be driven in parallel.

The power supplies and controls will be identical to the systems currently used in the Tevatron. The separator controls consists of a chassis of low level electronics modules that interface the high voltage supplies to the Fermi control system, count sparks, and provide local/remote switching. The power system consists of two high voltage (180KV) power supplies. These supplies put out a positive and negative voltage applied on the plates of the separator in the

tunnel. Each system also has a high voltage reversing switch to reverse the polarity on the electrostatic plates of the separator. Connected in parallel with the load is a discharge resistor.

6 Cryogenic Systems

The C0 low beta cryogenic components are cooled by a hybrid cryogenic system that consists of the C1 and B4 satellite refrigerators, and the Central Helium Liquefier (CHL). The heat load of the magnets, static and dynamic, is removed by the single-phase, and then is absorbed by the latent heat of vaporization of the two-phase helium. The single-phase helium is also used to cool correction, safety, power and crossover leads. To lower the operating temperature of the magnets, a single stage cold compressor is used in each house. The total load on the cryogenic system is comprised of magnet strings static and dynamic heat load, lead flows, and cold compressor heat of compression.

6.1 Heat Load

Table 6-1 represents the heat load estimate for B4 and C1 cryogenic components. The total heat load is comprised of a refrigeration and liquefaction portion. The refrigeration part of the heat load is used to cover conduction and radiation static heat leak as well as dynamic losses of the cryogenic components. Liquefaction is used to reduce the heat leak associated with leads. The values of existing component heat loads are estimated based on MTF test results, Tevatron operational experience, and engineering calculations. For the C0 quadrupoles, spools, and power lead cans, design parameters for heat leak are used. All of the heat loads are referenced to the 4.5K temperature level. The increase in component heat leak at the normal lower temperature of Tevatron operation is ignored. It should be noted that the additional load associated with the production of the lower temperature refrigeration is not negligible.

Table 6-1: C0 IR Cryogenic Component Heat Load.

Component Type	Heat Load		B4	C1
	Refrigeration	Liquefaction		
	[W @4.5K]	[g/sec]	[each]	[each]
Double Turnaround Box	5	0.018	1	1
Warm Iron Quadrupole	8	0	3	5
Low Beta Quadrupole	8	0	2	2
BTeV Q1,Q3,Q4,Q5	7	0	4	4
BTeV Quadrupole Q2	12	0	1	1
Dipole	8	0	31	34
TSC Spool	9	0.046	1	0
TSB Spool	8	0.037	0	1
TSE Spool	7	0.046	0	1
TSF Spool	9	0.060	0	1
TSP Spool	14	0.881	2	2
TSX1 Spool	10	0.060	2	2
TSX2,X3 10 kA Spool	10	0.049	3	3
Cold Spacer	2	0	1	1
Feed Can	10	0	1	1
Cryogenic Bypass	4	0	2	2
Turnaround Can	12	0.049	1	1
Valve Box	10	0	1	1
Total Refrigeration Load, [W]			**462**	**517**
Total Liquefaction Load, [g/sec]			**2.140**	**2.237**

6.2 Cryogenic Capacity Limitation

The total cryogenic system refrigeration and liquefaction requirements are provided by the satellite refrigerators and the CHL. The total usable cryogenic system capacity is reduced by the amount necessary to compensate for the heat of compression of the cold compressor for operation below 4.5 K. Heat of compression is determined by the mass flow rate and pressure ratio of the cold compressor.

Mass flow rate depends on the heat leak of the tunnel cryogenic components. Pressure ratio across the cold compressor is determined by the maximum allowable superconductor operating temperature. For a given component, the superconductor temperature depends on the effectiveness of the heat transfer between single-phase and two-phase, as well as dynamic coil losses. Components with ineffective heat transfer are required to be operated at lower temperature and thus lower two-phase pressure and higher cold compressor pressure ratio.

Heat of compression is linear with cold compressor mass flow rate, but is exponential with pressure ratio. Therefore, it is important to not only minimize the heat leak of a component, but also to design the components in such a way as to efficiently transfer the heat to the two-phase in order to minimize the peak single-phase temperature.

A previously developed thermal model of the Tevatron magnet strings was used to identify the temperature profile in the C0 IR downstream (B4) magnet string. The detailed discussion of the model used is presented at [1]. The downstream string was analyzed to identify the impact of the new C0 components on the temperature profile. The results of simulation are presented in Figure 6-1.

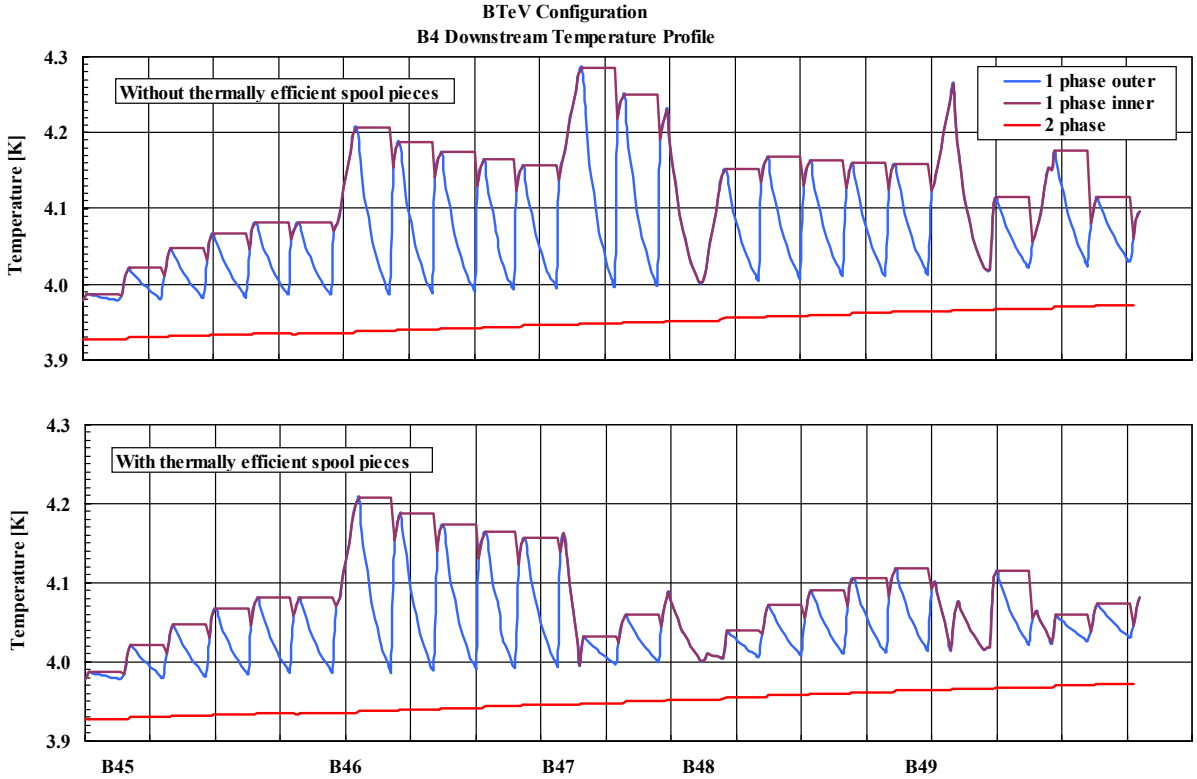

Figure 6-1: Temperature profile comparison.

The abscissa represents Tevatron station points, with B45 being the satellite refrigerator feed point. The triplet quadrupole magnets located to the right of the B49 station point. Both of the temperature profiles are generated using identical heat leak values for cryogenic components. The major difference is that the spool heat leak on the upper graph directly deposited to the single phase, where the lower trace assumes that spool's heat leak is removed by the two-phase. Since the B46 spool is an existing style, heat leak at this location goes directly to the single-phase in either case. The thermally efficient spools allowed for considerably flatter temperature profile from B47 downstream, which leaves larger quench margin for magnets in those locations.

The addition of an interaction region to the Tevatron adds both a refrigeration and liquefaction load to the system. Refrigeration loads are jointly satisfied by the satellite refrigerator and CHL. Liquefier loads, such as power lead flows, are satisfied entirely by CHL. The addition of a C0 interaction region to B0 and D0 puts a large burden on CHL to support the liquefier load required by the large number of conventional 2,000 amp and 5,000 amp power lead flows. A design constraint for the C0 IR was to leave the existing B0 and D0 IRs in place and powered.

Table 6-2 : CHL Production Usage

	Collider Run II		BTeV			
	980 GeV Conventional		980 GeV Conventional		980 GeV HTS	
Power Leads	36.6 g/s	21%	48.4 g/s	28%	40.8 g/s	24%
Summer Operation						
Refrigeration	128 g/s	75%	130 g/s	76%	130 g/s	76%
Sub Total	165 g/s	96%	178 g/s	104%	170 g/s	99%
CHL Capacity	171 g/s	100%	171 g/s	100%	171 g/s	100%
Reserve	6 g/s	4%	-7 g/s	-4%	1 g/s	1%
Winter Operation						
Refrigeration	108 g/s	57%	109 g/s	57%	109 g/s	57%
Sub Total	145 g/s	76%	158 g/s	82%	150 g/s	78%
CHL Capacity	192 g/s	100%	192 g/s	100%	192 g/s	100%
Reserve	47 g/s	24%	34 g/s	18%	41 g/s	22%

Summary of the Fermilab's CHL liquid helium production and usage is presented in the Table 6-2. The capacity given is at maximum CHL operating pressure utilizing a three stage and four stage compressor as well as ring return flow. The summer/winter production capacity is based on the average July/January temperature in Illinois, not the maximum/minimum temperature.

The table compares the current Collider Run II operations with the further BTeV operation utilizing conventional and high temperature superconductor (HTS) power leads. For the 980GeV Run II operation, CHL capacity reserve is 4% and 24% for summer and winter seasons respectively.

Adding conventional leads flow for the BTeV configuration results in the negative 4% margin in the summer time. Using HTS where possible in the BTeV IR allows for a positive 1% reserve in the summertime.

An increase in required CHL capacity over predicted for BTeV IR would be compensated by adding third compressor. The use of the third compressor reduces redundancy and efficiency of the CHL. Thus should be considered as a fall back operation condition only. It should be noted that three compressor operation mode could be considered to be use for short periods of time during hottest days of the summer. Such three compressor operation is inefficient with respect to operating costs.

In order to not overload CHL with the C0 IR power lead requirements, HTS lead designs are being applied in as many circuits as practical. This is particularly important since the design calls for several 10,000 amp circuits. It is assumed that the components added for the C0 low beta system have sufficient margin and thermally efficiency to not require operating B4 and C1 at a temperature colder than during Run II.

6.3 Layout

Layout of cryogenic components for the C0 IR are presented in drawings 1650-MC-257471 and 1650-MC-257471 for the upstream (B4) and downstream (C1) systems, respectively. Similar to the existing B0 and D0 I.R.s, the turnaround box is located before the triplet. This requires both a

supply and return circuit for the single-phase, two-phase and nitrogen within the triplet. Quench relieving of the triplet is accomplished on the single-phase supply and return in the turnaround can as well as on each end of the single-phase supply for Q2.

The Tevatron bus power leads are located in the turnaround can. This will require superconductor in the separator bypass.

The requirement to mirror the full triplet necessitates the need for a single-phase, two-phase and nitrogen interface transition on the C1 side. This transition is accomplished within the C1 separator bypass. Like B0 and D0, this results in the separator bypasses being unique on the B4 and C1 sides. The B4 and C1 turnaround cans will be identical and will require only a single spare.

6.4 Cryogenic Controls Modifications

Cryogenic controls software modifications are minimal. The ramp permit will be updated to include low beta power leads and spools temperature. Cool-down, Quench Recovery, Kautzky and Lead Controls Finite State Machines will be modified as well.

Additional platinum thermometers and flow control is required for each of the conventional power leads. Each 5 kA and 10 kA HTS lead has four platinum resistors, two for helium and two for nitrogen, and flow controls. Similar to the Tevatron leads, flow control is accomplished with sets of fixed size orifices and solenoid valves. A considerable amount of lead flow tubing and controls cable runs will have to be made to the B4 and C1 refrigerator and C0 compressor buildings.

It is known that there is a long term drift in calibration of Allen-Bradley carbon resistor thermometers. Any new cryogenic components, like spools, that require thermometry should have a pair of the standard 18 Ω calibrated Allen-Bradley carbon resistors and a single calibrated Cernox^{TM} thermometer. Unlike 18 Ω carbon resistors that can be driven by the pulsed current of the Tevatron thermometry crate, the Cernox^{TM} sensors require a variable current source to maintain the constant voltage signal across the resistor. To drive a Cernox^{TM} thermometer, Lake Shore Cryotronics temperature transmitter model 234 can be used. The transmitter output can be read into ACNET via an ADC channel of the Tevatron satellite I/O crate.

It is desired to try out a new controls scheme to protect Kautzky valves that are located in hard-to-access locations due to the proximity of detector related shielding. The scheme prevents valve chattering which can significantly reduce the valve lifetime. It relies on forcing the relief valve to stay open until the single phase pressure has stabilized below its set point. This scheme is planned to be implemented at B0 and D0 during 2004 Tevatron shutdown.

References

[1] Theilacker, J. C., Klebaner, A. L. "Thermal Modeling Of The Tevatron Magnet System," in *Advances in Cryogenic Engineering* 47A, AIP Conf Proc 613, (90) 2002.

7 Vacuum Systems

7.1 Layout

Table 7-1: Vacuum devices between B43 and C17.

location	vacuum device
B43-1a	2 piranis, cold cathode, ion gauge
B44-1a	2 piranis, 2 cold cathodes, ion pump
B45-1a	2 piranis, 2 cold cathodes
B46-1a	pirani, cold cathode, ion pump
B47-1a	4 piranis, 2 cold cathodes, 2 ion pumps, ion gauge, 2 gate valves
B48-1	2 piranis, cold cathode, 2 ion pumps
B48-6	2 piranis, cold cathode, 2 ion pumps
B49-2	2 gate valves, 6 convectrons, 3 ion gauges, 3 ion pumps
B49-3a	2 piranis, cold cathode, 2 ion pumps
C-0 u.s.	gate valve
C-0 d.s.	gate valve
C10-2a	2 piranis, cold cathode, 5 ion pumps, 2 gate valves, 6 convectrons, 3 ion gauges
C11-5a	2 piranis, cold cathode, 2 ion pumps
C13-1a	2 piranis, cold cathode, ion pump, ion gauge
C14-1a	2 piranis, 2 cold cathodes, ion pump
C15-1a	2 piranis, 2 cold cathodes
C16-1a	pirani, cold cathode, ion pump
C17-1a	pirani, ion gauge
C17-2	2 gate valves, 8 convectrons, 4 ion gauges, 4 ion pumps

7.2 Requirements for Cryogenic Vacuum

The Tevatron beam pipe is at 4.5 ^{o}K, therefore cryo-pumping is very effective in maintaining good vacuum. Keeping the Tevatron at cryogenic temperatures requires an insulating vacuum for thermal isolation. The operational requirement for the insulating vacuum is $1x10^{-4}$ Torr warm and $1x10^{-8}$ Torr cold.

7.3 Requirements for Warm Vacuum

Even though 95% of the Tevatron total length is cryogenic, poor vacuum in warm sections of the Tevatron is currently the major source of beam halo background in the collider detectors at B0 and D0 [1]. Generally the vacuum requirement for the Tevatron warm straight sections is an absolute pressure of $1x10^{-9}$ Torr. This should be used as an operational goal for warm vacuum sections which do not contain electrostatic separators. Individual components should be designed for better than that, perhaps $3\text{-}5x10^{-10}$ Torr, if this can be achieved by reasonable means such as hydrogen degassing, electro-polishing and baking. Hydrogen degassing of stainless steel parts is

considered particularly important, as this process has historically achieved the most satisfactory results and improvements over the untreated product. The only warm straight section without electrostatic separators and within the scope of this project is the 2.6 meter section near B47-4 which will be used for collimators. Previous experience (14 previous collimator installations in the Tevatron for Run II) has shown that, with proper vacuum techniques, a vacuum of $1x10^{-9}$ Torr can be maintained in these devices.

The vacuum requirement for warm sections which contain electrostatic separators is more stringent. Electrostatic separators run at voltages as high as 125 kV per plate and exceedingly good vacuum is required in order to avoid excessive sparking. A separator spark will generally cause a loss of luminosity and sometimes will even cause the beam to abort. The operational goal is $5x10^{-11}$ Torr. Long term experience with electrostatic separators in the Tevatron has shown that this is achievable. The 8.7 meter B49 and C11 warm sections will each contain 3 electrostatic separators.

The vacuum in the BTeV detector itself may be poorer, with pressures on the order of $1x10^{-8}$ Torr being discussed as an operational goal. Gas load migrating from this region into the Tevatron regions will be mitigated by 50 l/sec ion pumps located on either side of the I.R.

References

[1] A Drozhdin, et al, "Beam Loss and Backgrounds in the CDF and D0 Detectors due to Nuclear Elastic Beam Gas Scattering", PAC 2003, Portland OR, 2003

8 Controls

8.1 Integration with Current Tevatron Systems

One additional abort input module will be required at B4,C0, and C1 service buildings to accommodate inputs from the low beta power supplies and QPMs. Modifications will be made to the abort application to include these new inputs. No changes are necessary to the Tevatron permit system itself. One additional Camac crate will be installed at the B4 service building which presently has only two Camac crates.

No changes to MDAT itself are required, however, a new Tevatron state will be defined to distinguish between running with collisions at C0 and B0/D0.

The additional separators at C0 will require power supply controls and vacuum monitoring hardware. Additional collimators will require a standard motion control VME crate and motor power supply. Processor boards and controller cards can be moved from other unused collimator locations. All of these will be using standard controls hardware designs, the same as used for existing separators and collimators.

Sufficient Ethernet bandwidth is available in the service buildings for controls requirements.

8.2 Low Beta QPM System

There will be three new quench protection monitor VME crates, one each at B4, C0, and C1 service buildings. These QPMs will be functionally identical to those existing at B0 and D0 but will have fewer circuits in each. The detection algorithms will be the same. There will be no dumps or quench bypass switches, and heaters will be fired to provide quench protection. Each QPM will have uninterruptible power for up to 30 minutes, a 6 second circular memory buffer for quench analysis, and a suite of applications programs for control and data display. The QPMs will communicate via Ethernet to the ACNET control system in the standard fashion. Standard low beta QPM voltage to frequency converters and Tevatron heater firing units will be used.

The crate at C0 will monitor the Q1,2,3 triplet, Q4 and Q5 circuits. The major difference from B0/D0 in these circuits is the maximum current and the allowed number of MIITs. Quench detection thresholds will be adjusted if necessary.

The B4 and C1 QPMs will service the Q6 and Q7 circuits which are single magnet circuits using the 54” low beta quadrupole magnets (“old-Q1’s”) no longer used at B0 and D0. The major difference for these circuits will be the number of voltage taps available and therefore the number of magnet cells used in the quench detection algorithm. The fewer number of voltage taps effectively increases the quench detection voltage from 0.33 volts to 0.5 volts. The quench limits will be lowered to compensate for the fewer taps to keep the effective quench detection threshold at the same .33 volts.

Connections to the refrigerators at B4 and C1, the abort and Tevatron clock will be done in the same fashion as for B0 and D0. The existing B0/D0 low beta QPMs have no MDAT connections and these are also not required for the C0 IR.

8.3 Controls Modifications

Tables 8-1 through 8-3 list controls software and hardware modifications required to commission the C0 IR. No major new controls software is required, but minor modifications to a large suite of programs, and some duplication of existing software will be necessary. A significant number of database entries will also need to be made for new power supplies, separators, vacuum devices, etc. Software specific to Tevatron instrumentation is discussed in Section 9.3.

If conventional nested coil correctors are used in the new spools, then the standard corrector power supply controls will be used. The only software modification will be to add the new correctors to the existing applications programs and database entries for the new devices.

Table 8-1: Application programs and CLIB routines requiring modification for commissioning the C0 IR.

Program Name	Index Page	Changes Needed
UL_CBSAUX	CLIB routine	Add c200 modules at B4,C0&C1
Low Beta Quench Protection	java	Add houses for B4,C0 & C1 QPMs
Tevatron LCW	T12	Add new devices; modify graphics
Tevatron Power Supply status	T21	Add PSs for C0 IR
Tevatron Orbit	C50	Add BPMs
Tevatron Vacuum	T18	Add/modify vacuum devices
Tevatron Abort Status	T67	Add c200 at C0,B4 & C1
Ramp Generator for Collider	C49	Add C0 IR PSs & correctors; new squeeze
Tevatron Sequencer	C48	Add C0 IR squeeze
Tevatron Separators	C13, C15	Add new separators
Scraping Program for Collider	C10	Add new collimators
ADC compare	C23	Add new devices
HOPS	I15	Add new power supplies
Tev Magnet Database	T126	Add new magnets

Table 8-2: Front-end code modifications required for commissioning the C0 IR.

Front-end	Modifications needed
QPM	New QPM code for B4, C0, and C1 QPMs
Vacuum	add CIA crates for new separators
Collimator	New collimator motion control front end at B4
TLLRF	change in Tevatron orbit length
Refrigerator	added instrumentation
TEVCOL (OAC)	addition of new collimator
GLFRIG (OAC)	addition of new calculation of CC control at B4/C1
CBSHOT(OAC)	addition of SDA data for C0
MCRVCR(OAC)	addition of Video recording of C0 data for SDA
VLOGGR (OAC)	addition of new Tevatron State transition

Table 8-3: Controls hardware modifications/additions required for the C0 IR.

System	Item	Description	Number
vacuum	CIA crate & PS	Required by separators	1
	Interface board	Acnet interface to front end	1
Power Supplies	c460	Control cards for correctors	16
	C468	Control cards for power supplies	9
Camac	Crate	One additional crate at B4	1
	C290	Multiplexed Analog to Digital converter	1
Quench Protection	QPM	VME Crate w PS and I/0 boards	3
	c184 or Enet	For remote rebooting of QPMs	3
Abort	C200	Abort	3
Separators		c185	6
		c465	3
		c052	3
Collimators	VME crate	Five slot crate with power supply	1
	Power supply	Motor power supply for 8 motors	1

9 Beam Instrumentation

9.1 Synchrotron Light Monitor

The synchrotron light monitor [1] is located in a unique warm straight section in the Tevatron at C11. It is located directly between 2 dipoles, one half-length and one full-length, so that it can monitor both proton and antiproton off-axis synchrotron light, generated at the magnetic transition at the far end of the dipoles [2]. This monitor is the only non-destructive technique currently available in the Tevatron for monitoring beam profiles during a collider store. When the C0 area of the Tevatron is converted to a "normal" straight section, this unique warm straight section at C11 will be lost.

We propose replacing this synchrotron light monitor with monitors at two distinct locations in the Tevatron ring. The pbar synchrotron light monitor will be located at the downstream end of the D48 warm straight section and will pick off light from the downstream end of the D48-3 dipole. The two transverse damper pickups currently in this location will be moved slightly to accommodate the synchrotron light monitor. The QD37 66" quad will be modified to accommodate the proton synchrotron light monitor. The BPM currently installed in this quad will be moved a few inches upstream to make space for the proton synchrotron light pickoff mirror as sketched in Figure 9-1. This mirror will be in a cryogenic section of the Tevatron. The sketch shows the pickoff mirror as being movable in and out of the aperture, but it is not yet clear if this facility is required. These two locations have a favorable β_x/D_x ratio so that the transverse emittance of the beam can be more easily separated from the momentum spread.

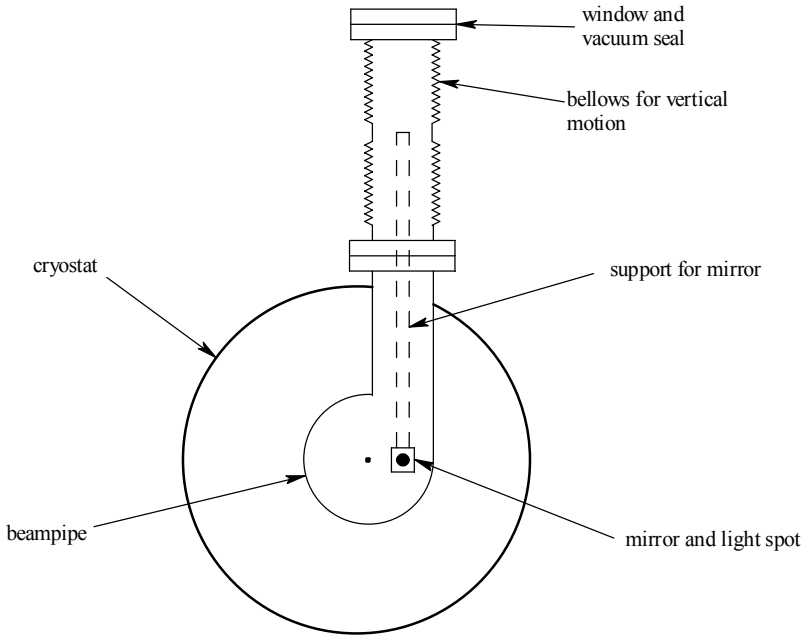

Figure 9-1: Sketch of proton synchrotron light monitor pickoff mirror location.

The light boxes housing the synchrotron light monitor optics and light transducers will only require minor modifications to fit in the new locations. All signal processing hardware in the service buildings will remain the same as it is now.

9.2 Instrumentation between B4 and C1

There are currently 12 Beam Loss Monitors (BLM) located in each of the B4 and C1 houses. This is more than the usual number per house because additional BLMs were required in this area for the C0 abort. This number is adequate for the C0 IR. They will be repositioned in the tunnel for optimum utility.

There are currently 19 Beam Position Monitors (BPM) located in the B4 and C1 houses. For the C0 IR this number will be increased to 30. The new BPM pickups will be identical to either of two designs already present in the Tevatron [5]. The Tevatron BPM upgrade will provide a BPM relative position accuracy of <20μm [6].

Tilt-meters similar to what currently exist on the B0 and D0 low beta quadrupoles will be installed on the C0 low beta quadrupoles [7]. This is an essential piece of instrumentation because the Tevatron orbit and coupling are very sensitive to motion of these quadrupoles due to the large β functions. Unlike on the B0 and D0 low beta quads, robust mounting and alignment of these tilt-meters will be designed into the cryostat housing of the C0 low beta quads.

9.3 Instrumentation Software Modifications

Listed below is the Tevatron instrumentation which will require minor modification to associated software – either application programs, front-end code, or Open Access Clients (OAC). These instruments are generally dependent on the global Tevatron lattice, Tevatron state, and/or synchronizing clock events (TCLK): Flying Wires, Synchrotron Light Monitor, Mountain Range Display, Ion Profile Monitor (new device), 1.7 GHz Schottky Monitor, Beam Position Monitors, and Sampled Bunch Display.

References

[1] A. Hahn, P. Hurh, "Results from a Prototype Beam Monitor in the Tevatron Using Synchrotron Light", 1991 PAC, p1177, (1991)

[2] R. Coisson, "Angular-spectral Distribution and Polarization of Synchrotron Radiation from a "Short" Magnet", *Phs. Rev. A*, 20, #2, p524, (1979)

[3] Two bypasses of this type were initially installed to accommodate "Roman Pot" detectors.

[4] J. Johnstone, "Tevatron Optics with Magnet Moves for Roman Pots at CDF", Fermilab-TM-2157 (2001)

[5] Tevatron Low Beta Quadrupoles – Requirements and Specifications, (the "Pink Book"), Fermilab, (1990)

[6] J. Steimel, et. al, “Tevatron Beam Position Upgrade Requirements”, Fermilab Beams-doc-554, (2003)

[7] Applied Geomechanics model 711. A 2-axis tilt-meter with 100 nanoradian resolution.

10 Commissioning

10.1 Operational Scenarios

The procedure for operating the Tevatron collider is to load all waveforms (power supply ramps, etc) and timer channels into the control cards in the field prior to beginning the collider fill process. The sequencer (control room application program) then coordinates the sequence of events that initiate beam transfers, state changes, and changes in operating conditions. Since the low beta squeeze process will be different for C0 operation and B0/D0 operation, modifications will be necessary in order to switch between the two modes. Beam transfers into the Tevatron and the acceleration to 1 TeV will be identical for the two operating modes.

There are two possible simple methods of integrating C0 operation into collider operation without completely redefining the current control process. One method is to use the identical set of clock events for C0 operation as for B0/D0 operation to control the optics changes for each mode. In this case the waveforms for the power supplies would be reloaded at the beginning of each collider fill, depending on which mode is desired. The second method is to load both sets of waveforms to the power supply controllers, and determine which set plays by triggering different clock events.

Option 1 (using the same events and reloading waveforms):

This method has the advantage that fewer application programs need to be modified. A second operational file will be defined in the power supply waveform generator page (C49), and the proper file will be activated between stores. A file for dipole correction elements will need to be loaded from the orbit correction program after the C49 file is activated. This process currently takes about ½ hour. It is not particularly prone to errors, however the chance for a mistake by the operator will increase with the number of files that need to be loaded.

Option 2 (using separate clock events and having both sets of waveforms loaded):

This method has the advantage that a single file of ramp waveforms can be used for both modes of operation, and file activation will not be required between stores. More changes will need to be made to C49 to recognize the different sequences. The orbit correction program will need to know about the second set of waveforms as well. The waveform generators, and the design of the sequencer in general, was originally set up to handle this type of mode switching. Figures 10-1 and 10-2 show how some of the waveform ramp cards will be set up in this option. In these examples, XX and YY represent the new clock events for low beta squeeze and un-squeeze of C0 operation.

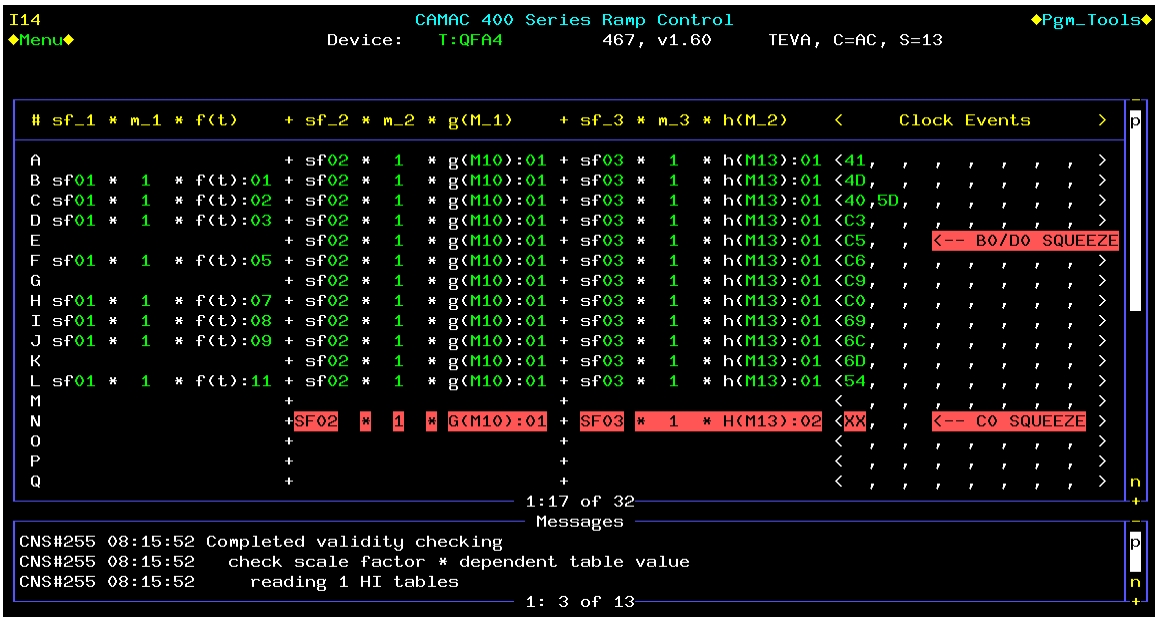

Figure 10-1: Example of the configuration of a tune quad circuit.

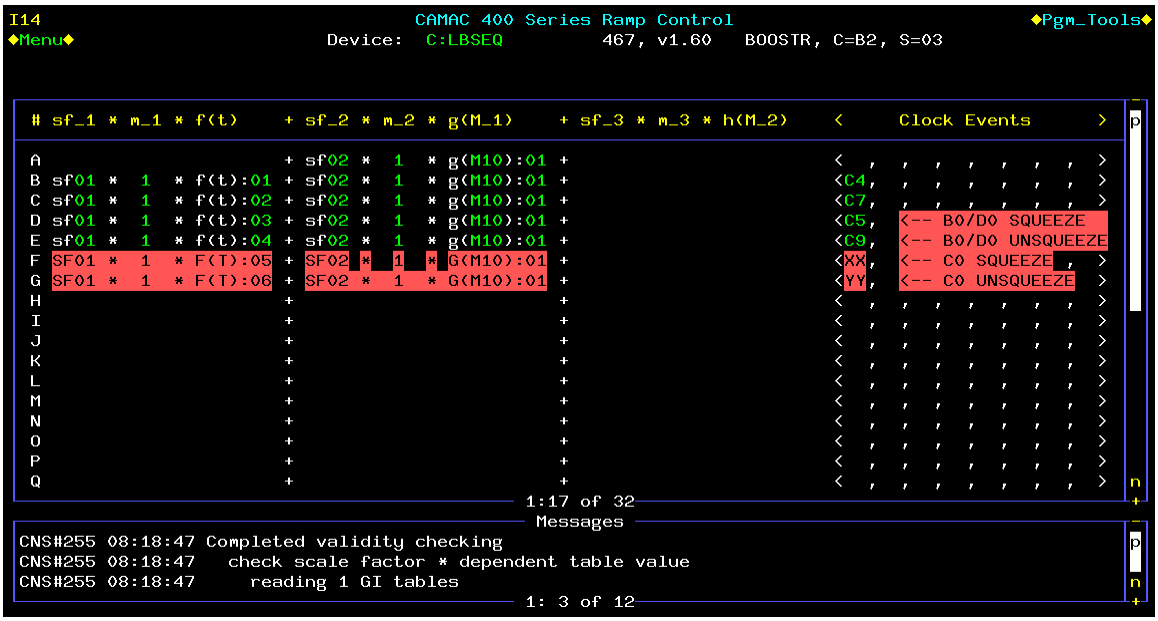

Figure 10-2: Example of the configuration of the low beta controller card.

10.2 Commissioning Plan

Responsibility for development of the full capability of the Tevatron with the new C0 IR lies with the Tevatron Group in the Accelerator Division. Commissioning of the C0 IR project will consist only of commissioning the newly installed hardware and will not require beam studies. The major steps required for hardware commissioning include the following.

1) Verify correct B48 collimator motion.

2) Test the abort loop and new accelerator clock events.

3) Test the new QPM system.

4) Load all acceleration ramps into ramp modules (465 cards), and train all magnets up to 1010 GeV, starting with 900 GeV. This includes the new separators.

5) Load all low beta squeeze ramps into ramp modules and run both operational sequences: accelerate and perform B0/D0 low beta squeeze; accelerate and perform C0 low beta squeeze. This includes the new separators.

6) Test that all new correctors can run at maximum current.

7) Hold the Tevatron at 980 GeV for at least one hour and adjust all lead flows for stable temperature and voltage.

11 Conversion of C0 to a Normal Straight Section

11.1 Overview

During an early shutdown (currently scheduled for late summer of 2005), the remnants of the Fixed Target abort system at C0 will be removed and replaced with a standard long straight section to allow installation of BTeV experiment components.

11.1.1 Motivation

Currently, the Tevatron straight section at C0 includes the collision hall for BTeV and the remnants of the decommissioned Tevatron abort extraction system for Fixed Target operations. Even before the installation of the low-β* insertion at C0 (currently scheduled for 2009), BTeV plans a phased installation of components into the collision hall during annual accelerator shutdowns for maintenance and upgrades starting in 2006. There are two main reasons for this.

First, there are some prototype components such as the pixel vertex detector that would benefit from early operation in the Tevatron. This operation could be passive -- observing the environment of the circulating proton and antiproton beams and their electromagnetic pulse and the radiation background fields. It could also be active -- inserting a thin transmission target or turning the electrostatic separators off to provide low luminosity collisions at C0 at the end of collider stores. These studies could be used for testing prototype detectors or commissioning the final detector elements and systems. Similarly, the impact of the BTeV components on the Tevatron operations, such as impedances, vacuum, 3-bump dipole spectrometer, and apertures, could be studied early.

Second, the assembly hall at C0, outside of the shielding door, was consciously made too small to stage the entire BTeV experiment before installation. The idea was that each component of the experiment would be fabricated somewhere else, final-assembled and tested in the assembly hall, and, when ready, installed during the next scheduled Tevatron shutdown. The physical size of the SM3 analysis magnet and space needed for assembly requires that it be installed in the collision hall as soon as testing is completed.

In order to make space for the installation of BTeV experiment components, starting with the SM3 analysis magnet, compensating dipoles, and muon toroid in 2006, the remnant components of the Fixed Target abort system must be removed from the C0 collision hall and replaced by a simple beam pipe. This will also require the replacement of two half-length Tevatron dipoles with full-length Tevatron dipoles in the B4 and C1 cryogenic sectors. At this time the ventilation systems of the collision hall and the Tevatron tunnel will be isolated, allowing the collision hall to become ODH Class 0 to facilitate activities by experimenters and contractors.

The BTeV installation, including the low-β insertion, could, in principle, be accomplished without the intermediate step of a standard straight section. However, this more direct approach would preclude much early testing and, subsequently, lengthen the experiment installation and commissioning period, which would then begin only after CDF and D0 are completed.

11.1.2 Scope of Change

The Tevatron C0 straight section had previously been the site of the abort channel for Fixed Target operations with specific abort elements located between the B48 and C12 stations [1]. Since there is no plan for further Tevatron Fixed Target operations, this abort is no longer needed and the C0 area has been assigned to the collider experiment BTeV. The Fixed Target abort consisted of a set of five kicker magnets (at the B48 straight section), two half-length Tevatron dipoles (at B48-3 and C11-3), two C-magnets, and three Lambertson magnets. In January 2003, in order to increase the vertical aperture in the Tevatron collider, the three Lambertson magnets were replaced with four Main Injector dipoles (three 240" long, and one 160" long – slot lengths are 16" longer). The five kicker magnets were also removed and replaced with beam pipe at that time. In the C0 collision hall, the Main Injector dipoles sit on a wall of shielding blocks and the C-magnets sit on a steel I-beam catwalk [2]. Both of these magnet systems interfere with the installation of experimental components for BTeV.

The total bend of the two half-length Tevatron dipoles plus the two C-magnets plus the four Main Injector dipoles (with active trim shunting of the current in the Main Injector dipoles) exactly matches the total bend of two full-length Tevatron dipoles. The basic plan is to remove the two half-length Tevatron dipoles, the four Main Injector dipoles, and the two C-magnets, and replace them with two full-length Tevatron dipoles (to be purchased from inventory, reducing the number of spares available) plus additional vacuum pipe (see Figure 11-1). The full-length dipoles will be placed approximately at the position of the half-length dipoles. Since the effective magnetic bend points will change, all the elements between these half-dipoles must be repositioned transversely inward (toward the center of the Tevatron ring) with the maximum move of 4.2 inches at the 99" quadrupoles near B49 and C11. This will reconstitute a normal long straight section [3] [4].

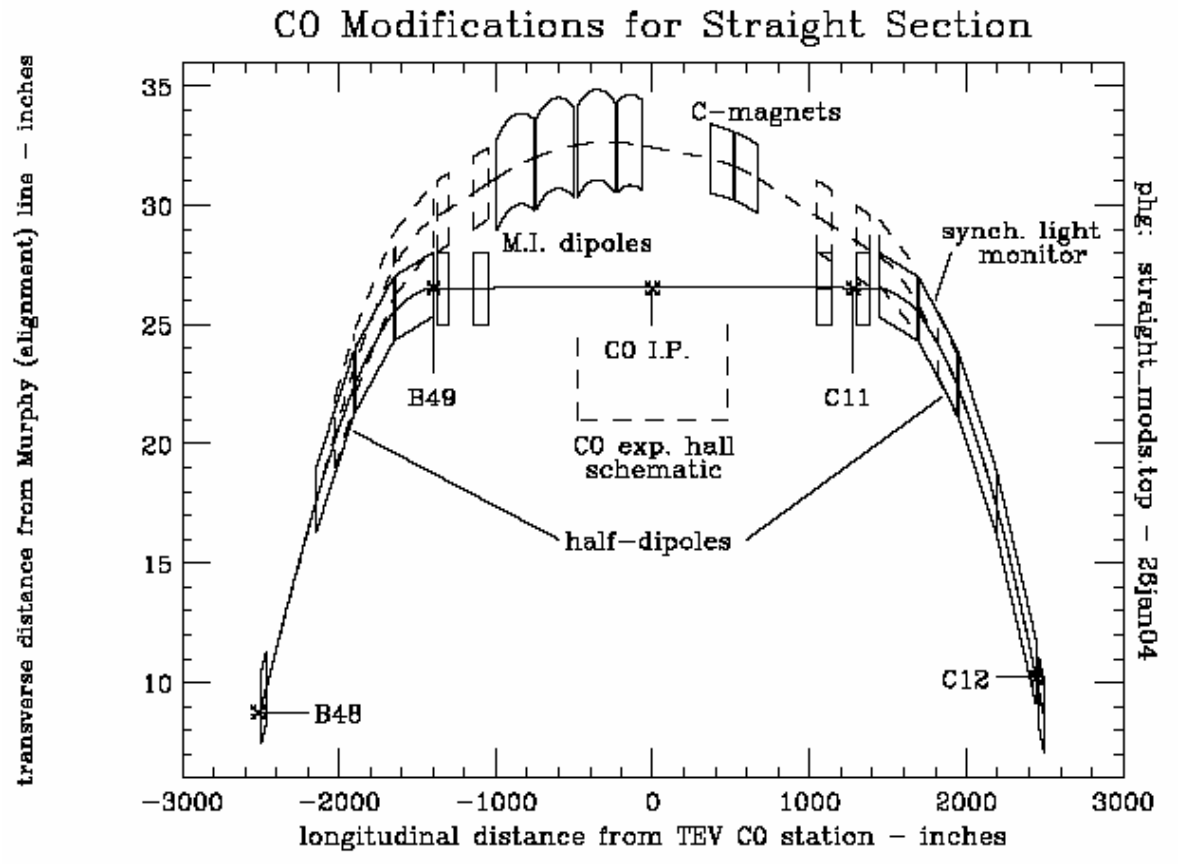

Figure 11-1: The existing C0 abort (dashed) and future straight section (solid) trajectories.

Since the removal of the Main Ring accelerator, there remains an excess capacity in the Low Conductivity Water (LCW) system in the Tevatron tunnel. This system will be slightly reconfigured to cool the BTeV SM3 analysis magnet, the compensating dipoles, toroid, water-cooled power bus, and power supplies (in the C0 collision hall), both for the final installation and for component testing in the assembly hall.

The removed four Main Injector Dipoles and two C-magnets will be replaced with (~107 feet total length) of 4 inch diameter, electro-polished, hydrogen-degassed, stainless steel vacuum pipe which will be baked out. The vacuum goal for this section of beam pipe is $1x10^{-9}$ Torr. The existing ion pumps and controls in this region will provide adequate vacuum pumping. A series of simple stands (existing design) will support the vacuum pipe at beam heights of 10.4 inches, 40 inches, and 100 inches above the existing floors.

Two additional horizontal and vertical readout Beam Position Monitors (BPM) will be installed on the C0 side of the last Collins straight section quadrupoles QUADC0U (near B49) and QUADC0D (near C11). These will provide additional diagnostics in understanding the local 3-bump made by the SM3 analysis magnet and compensating dipoles. Signal analysis and readout hardware for these BPMs can be easily accommodated in the existing B4 and C1 BPM controls system.

Although not needed for the configuration change to the straight section, eventually, for the installation of the low-β* insertion, the warm Tevatron power bus must be relocated to the outer wall or ceiling of the flare tunnel and massive amounts of new water cooled bus must be installed for the LHC quadrupoles and relocated Q1 quadrupoles from CDF/D0. In order to minimize time impact during the shutdown for the installation of the low-β* insertion, these bus relocation and additions should be done starting during the early shutdown for straight section reconfiguration and continuing through the shutdowns in between.

11.1.3 Tevatron Beam Optics Considerations

The reconfiguration to a normal straight section changes the longitudinal positions of two bend points, while maintaining the longitudinal positions and strengths of all quadrupole magnets. Therefore, the Tevatron tune is (to very high order) **not** changed, and the lattice functions around the ring are negligibly perturbed. The moving of the bend points does mean that the components in between will move slightly in the transverse horizontal plane, radially inward. The circumference of the Tevatron orbit will thus be decreased by 1.6 mm, in the direction which will reduce the present 39 mm mis-match between the Tevatron and Main Injector rings.

With the B2 compensating dipoles installed in the C0 collision hall, the physical aperture at C0 will be a minimum at the injection energy with beam on the helix. Figures 11.2 and 11.3 show the physical aperture in the C0 straight section in units of transverse beam σ's for 20π-mm-mrad (95% normalized emittance) and $\sigma_p/p = 5x10^{-4}$, which are typical injected proton beam parameters in Run II operation. The size of the beam pipe in a B2 magnet is 2.0" horizontally and 4.0" vertically. We have assumed a minimum beam pipe ID of 2.0" between the B2's for these plots. Under these conditions the minimum aperture is 10.8σ and is located at the outboard end of the downstream B2 compensating dipole in the horizontal plane. For comparison, in the present Tevatron configuration, the minimum injection energy aperture is at the F0 injection Lambertson and is nominally ~5σ [5]. The nominal injection energy apertures at B0 and D0 low beta quads are ~10σ [6]. The C0 Lambertson magnets mentioned earlier in this section were removed in 2003 because their vertical aperture was ~3σ. The beam trajectories, beam sizes, and apertures must be considered when installing BTeV experiment equipment and beam pipes in the region between the B2's (± 27' from I.P.). The present configuration of horizontal and vertical correctors near C0 allow for independent horizontal and vertical beam position and angle control at C0 in the range of ±9mm and ±0.100mrad at 1 TeV, which is more than adequate steering capability.

The present warm gap next to the half-dipole at C11 is unique in the Tevatron. It provides a location between two cryogenic dipoles for a single synchrotron light monitor to view off-axis synchrotron light from both proton and anti-proton beams. With the replacement of the half-dipole with a full dipole, this location will be lost, and alternatives for the synchrotron light monitor must be considered (see section 9.1).

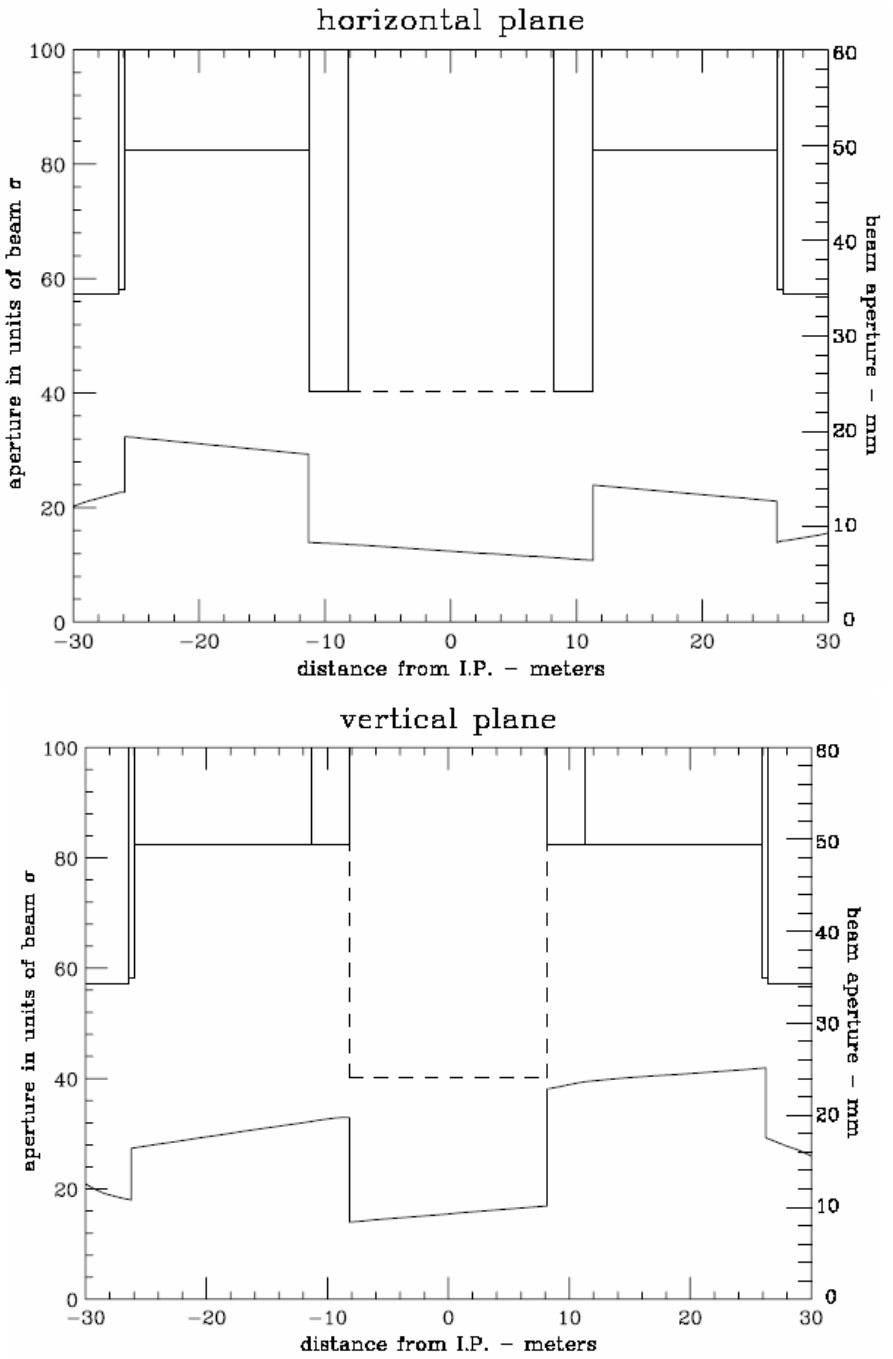

Figures 11-2 and 11-3: Horizontal and vertical aperture and beam pipe radius vs. distance from C0. Bottom trace in each plot is the aperture. Beam is @ 150 GeV and on the injection helix.

11.2 Installation Plan

The early shutdown for the installation of the normal straight section is anticipated to be 8 weeks in duration. Not only is the straight section reconfiguration planned for this shutdown, but also considerable utility outfitting in the collision hall (see C0 Outfitting Project CDR). Based on the

effort that was required for the replacement of the C0 Lambertson magnets with MI dipoles in January, 2003, it is anticipated that the rigging work to remove the four Main Injector dipoles and the concrete shielding block base can be accomplished within the first week of the shutdown. In the collision hall, this would leave the middle 5 weeks of the shutdown exclusively for utility outfitting, with the final 2 weeks for vacuum pipe installation, leak checking, and bake-out, along with finishing the utility outfitting work.

Certain activities can be accomplished before the early shutdown begins. These include design and procurement of beam tubes, vacuum components, magnet and beam tube stands, LCW components, simple cryogenic piping extenders, jumpers between power bus and cryo lead boxes, and pre-fabrication of isolation doors between tunnel and collision hall.

The following is a listing of the "work crews" required to complete the conversion to a straight section denoted by the tasks they are to accomplish. This planning is in a preliminary stage. There will likely be some consolidation of crews designation to optimize manpower. The jobs are listed in approximate order of activities.

Once the early shutdown begins, the following tasks must be accomplished in this approximate order for the Tevatron to begin operation again. We are then committed to completion of all items–operation of the Tevatron with any of these items only partially complete is not possible.

1) Warm-up cryogenic houses B4 and C1 (cryo technicians)

2) Unhook water, bus jumpers, vacuum, instrumentation (technicians and electricians):

- Remove water hoses and power cables from 6 warm magnets & 2 cryo lead boxes

- Let up to atmosphere warm vacuum and remove components

- Remove guard rails from shield block wall, isolation gratings, LCW piping, cable trays, and supports in region of FMI dipoles and C-magnets

3) Open shield door (PPD/FESS + riggers or technicians)

4) Remove FMI dipoles & 61 concrete blocks and catwalk for C-magnets (Rigging crew with heavy fork lift)

5) Tunnel magnet moves (technician or rigging crew):

- Remove: 2 half dipoles, 2 C-magnets, two warm bypasses, and remnant (vertical) MR B2 magnet at B48-4 location

- Reposition transversely: 3 full length, 4 quadrupoles, 6 cryo boxes: which include 55.6" bypass, 43" spool, 125.9" spool, 50" spool, and two turn-around boxes

- Install: 2 full dipoles, one warm bypass (existing standard 48-section bypass)

6) As-found, rough component placement, and final alignment of components and vacuum pipe (alignment crews)

7) Cryo device moves: undo 17 cryo interfaces, move remaining components and install new cryo components, make up 16 cryo interfaces (one interface will be eliminated in this reconfiguration), leak check all cryo components (cryo/vacuum technicians)

8) Bus modifications: possibly start on bus modifications for low-β quads (continues thru 2009) (electricians)

9) LCW modifications: extend LCW into collision hall and assembly bldg – interface w/construction (pipefitters)

10) Extensions for cryo relief, suction, and gas piping (cryo/pipefitter)

11) Rehook-up lead boxes to Tevatron power bus (electricians)

12) Install warm beam pipe in place of MI and C-magnets, install beam tube supports, warm vacuum beam line diagnostic components, beam tubes, vacuum pumps, vacuum monitoring components, leak check, and bake out (vacuum technicians)

13) Install two new BPMs (Instrumentation technicians + electricians)

14) Install two walls at tunnel-collision hall interface (mechanical technicians)

15) Close shield door after completion of collision hall outfitting (PPD/FESS + technicians)

16) Cool-down cryogenic houses B4 and C1 (cryo technicians)

11.2.1 Tunnel modifications

The required modifications to the existing Tevatron tunnel are minimal for this straight section phase. The two junctions of the tunnel with the collision hall will be sealed with solid doors, separating the ventilation systems for the tunnel and the collision hall, providing Oxygen Deficiency Hazard isolation, and maintaining independent search and secure zones for the tunnel and collision hall. The beam pipe and LCW supply and return pipes will penetrate these doors. These doors will have to be able to be opened or removed to allow optical survey and alignment tasks into, and through, the collision hall, as needed.

11.2.2 LCW modifications

The entire C0 Interaction Region will ultimately require approximately 700 gpm of Low Conductivity Water (LCW). The purpose of the LCW at C0 is to provide sufficient heat rejection for magnets, magnet power supplies, and copper bus work. The LCW will be supplied from the Tevatron LCW system. The existing centrifugal pumps at B3, B4, and C1 will provide the flow needed for BTeV. Individually, they are each capable of providing 400 gpm with a pressure head of 140 psi (355 TDH). The Tevatron supply and return header pressures are nominally 160 psig and 20 psig respectively. The typical supply temperature is 90 F. All heat will be rejected to the ponds at B3, B4 and C1 via the heat exchangers located at those service buildings. There will not need to be any significant LCW controls or instrumentation upgrades. The current ACNET read backs of temperature, flow, and pressure shall suffice. However, local instrumentation will be installed in the C0 assembly hall and C0 service building to aid in troubleshooting the system.

The C0 Assembly and Collision Halls will need approximately 250 gpm. The existing 4" Aluminum LCW header will be extended into the C0 Collision Hall to provide magnet cooling and also into the Assembly Hall to cool the power supplies. The new header must provide adequate flow to the vertex magnet when it is located in its experimental and assembly (testing) positions. The table below outlines the LCW requirements for each of the primary components. The flow requirements are clearly dominated by the Vertex Magnet. The maximum temperature rise should be approximately 23º F. The flow to the water-cooled bus will be restricted to about 5 gpm per bus pair.

.

Table 11-1: LCW requirements for C0 collision hall and assembly hall.

System	Qty	Current	Power	Flow Requirement	Temperature Rise	Diff. Pressure Req'd
		A	*kW*	*GPM*	*F* [*C*]	*psi*
Vertex Magnet	1	4200	440	151	23 [13]	120
Vertex Power Supply*	2	-	35	11	-	100
Vertex Bus	1	4200	<5	5	<10 [6]	<100
Toroid Magnet*	2	1500	35	22.6	8 [4]	120
Toroid Power Supplies	1	-	2	5.5	-	100
B2 Magnet*	2	2300	36	23.4	10 [6]	110
B2 Power Supply	1	-	6	5.5	-	100
B2 Bus*	2	2300	<5	11	<10 [6]	<100
		Total	**564**	**235**		

*- power and flow are for both units combined

Additional LCW flow will be required for the low beta installation in the area surrounding C0. A new 3" header will be run from the tunnel to the C0 service building to cool the (3) 300 kW power supplies and the load resistors associated with the electrostatic separators. The B4 and C1 service buildings will each house (2) 150 kW power supplies. Additional taps will be installed to provide the proper flow to these supplies. The flow required to cool the 2 5/8" O.D. round bus used to power the low beta quads will be supplied from the tunnel. As in the rest of the Tevatron, LCW will be used to warm the new cryogenic leads associated with the C0 interaction region. The table below summarizes the flow requirements.

The BTeV/C0 leg of piping will be filled from the Tevatron. This can be accommodated by the Tevatron LCW system since it has a reservoir capacity of well over 3,000 gallons and the additional volume of the new BTeV/C0 area will only be on the order of 1000 gallons.

During the conversion of the C0 region to "normal" straight section, LCW hoses feeding the MI dipoles will be removed. Also, existing 2" LCW copper piping on the B4 and C1 side of C0 will be removed to ease magnet removal.

Table 11-2: LCW requirements for C0 IR low beta installation.

Element	Circuit #	Current	Total Flow Req'd	Diff. Pressure Req'd
		Amps	*GPM*	*psi*
C0 300 kW Power Supplies	1,2,3	10000	165	100
C0 2 5/8" Bus	1,2,3	10000	45	<100
B4 150 kW Power Supplies	4,5	5000	70	100
B4 2 5/8" Bus	4,5	5000	18	<100
C1 150 kW Power Supplies	10,11	5000	70	100
C1 2 5/8" Bus	10,11	5000	18	<100
C0 E.S. Separators (Load Resistors)	-	-	20	100
Cryogenic Leads**	-	-	50	<100
		Total	**456**	

**Pair of 5 kA leads at: B45, B46, C14, and C15; Pair of 10 kA leads: B47, B48, B49, C10, C12, C13.

11.2.3 Controls, PS, and QPM modifications

The inductance value of one quench detection unit at B4 and C1 will increase by half of a magnet's inductance. Otherwise, no modifications are necessary to the Tevatron QPMs. The shunt circuit on the MI dipoles will be eventually removed from the service building to make room for future PS installations. There will be a need for the installation of two new horizontal and vertical BPMs inboard of the last Collins straight section quadrupole, along with the associated cables and readout electronics. The present set of Beam Loss Monitors (BLM) in the C0 area will be moved to new locations on the beam pipe.

11.3 Recommissioning Plan

In the 2/03 shutdown the C0 Lambertson magnets were replaced with MI dipoles, so the Tevatron Department already has experience in recommissioning the C0 straight section after modifications. Since the lattice change is negligible, we expect recommissioning to be straightforward. Aside from the normal recommissioning tasks required after a shutdown, the following steps will be required after C0 has been converted to a normal straight section.

1) Recommission the QPM system: New database constants (inductance and resistance) for the changed magnet strings require verification while ramping magnets. Beam is not required for this step.

2) Train new magnets to 1010 GeV: The newly installed full length Tevatron dipoles need to be ramped to 1010 GeV to verify that there is adequate quench margin for 980 GeV operation. Beam is not required for this step.

3) Change Tevatron injection frequency: This is required because the central orbit length changes. The RF frequency (53.1 MHz) must change by 13.3 Hz. No change is required in MI operation because it phase locks to the Tevatron frequency during beam transfer.

4) Local orbit correction: It is expected that the local orbit will need to be corrected at all energies and at all steps of the low beta squeeze. This step includes local aperture scans to verify that the aperture is adequate. Since the beam pipe in C0 will initially be 4"dia, we expect the aperture to be large. This step requires beam.

5) BPM and BLM checkout: The 4 new BPMs and the repositioned BLMs require testing with beam.

6) Synchrotron light monitor: This device will require extensive parasitic studies before it can be considered operational. See section 9.1 for a more detailed discussion.

References

[1] M. Harrison, "The Tevatron Abort System", Fermilab UPC-153, 1981

[2] Fermilab Drawing #1780.003-ME-140999 (7 sheets)

[3] S. Ohnuma, "Geometry of the Superconducting Ring", Fermilab UPC-163, 1982

[4] C.T. Murphy, "The Brass Plug Monument System for Doubler Alignment", Fermilab TM-1067, 1981

[5] P. Ivanov, "InjectNote", Fermilab Beams-doc-990, 2004

[6] M. Church, "Summary of B0 and D0 Aperture Scans, Alignment Studies, and Quad Tickling Measurements Done Between 9/01 and 10/01", Fermilab Beams-doc-900, 2003

12 Installation, Integration, Schedule, and Cost

12.1 Tunnel installation

Tunnel drawings for the shutdown work will be created. For reference, the present magnet and vacuum configuration appears on drawings ME-140999, ME-140070 and ME-140071. A 3 dimensional model, with input from the lattice design program MAD, civil construction drawings, and shell models of tunnel elements, is being developed to help understand interference and integration issues.

Installation work will be assigned as follows:

Warm Vacuum – AD Mech. Support Dept. technicians, with augmentation by other FNAL technicians

Shield door moves, concrete block removal, catwalk removal, shield wall assembly, guard rails and interlock gates removal and installation – subcontracted T&M ironworkers, with FNAL task manager

Cryo beamline components – AD Mech. Support Dept. technicians, with augmentation by AD Cryo. Dept. technicians

Cryo piping – AD Cryo. Dept. technicians and possible subcontracted T&M pipefitters

LCW – subcontracted T&M pipefitters, with FNAL task manager

Water Cooled Bus – subcontracted T&M electricians, with FNAL task manager

Interlock gates wiring and switches – T&M electricians, with FNAL task manager

Alignment – FNAL Alignment and Metrology Group

Cable pulls - T&M electricians, with FNAL task manager

The Alignment and Metrology Group has created a new system of positioning which replaces the Murphy line system. This will be used to align the beam line components of the Tevatron.

12.1.1 Magnetic Element Installation

Tevatron cryogenic sectors B4 and C1 will be warmed to room temperature to perform the installation. All Tevatron dipoles between B45 and C15 (31 magnets) will be moved longitudinally and/or transversely to accommodate the new lattice arrangement and the shortened Tevatron arc length. All other magnetic elements currently installed between B43 and C17, with the exception of the 4 66” quads at B43, B44, C16, and C17, will be removed (26 magnets). Table 12-1 lists the magnetic elements which will be installed in the Tevatron between B43 and C17.

Table 12-1: Newly installed magnetic elements between B43 and C17.

Device	Locations
4 Tevatron Q1's (from A4, B1, and storage)	B45,B46,C14,C15
2 LHC-style 54" Q5's	B47,C13
2 LHC-style 79" Q4's	B48,C12
2 LHC-style 96" Q3's	B49,C11
2 LHC-style 173" Q2's	B49,C11
2 LHC style 96" Q1's	B49,C11
4 new X1 spools	B43,B44,C16,C17
4 Tevatron P spools (from A4,B1, and storage)	B45,B46,C14,C15
4 new X2 spools	B47,B48,C12,C13
2 new X3 spools	B49,C11
1 Tevatron H spool (from storage)	B49
total = 29	

12.1.2 Electrostatic Separators

Six new separators, identical to previously built separators, are required. There will be 2 horizontal and 1 vertical separator at B49 and 2 vertical and 1 horizontal separator at C11. These separators are delicate, and special handling equipment and false floors must be provided to install them. The separators are located above a 2'6" deep channel in the tunnel floor on either side of the collision hall (see Figure 12-1), so that holes do not have to be cored in the tunnel floor to accommodate them. An air spring transporting cart exists for the separators, which is towed behind a golf cart, then pushed into place manually.

Alternatively, these separators could be mounted on girder modules similar to those which were used at D0. Installation equipment exists which was used for the separator girders at D0. The installation of these girders through the D0 drop hatch requires opening up the hatch to its largest configuration and careful handling of the girders, for which a procedure was written at the time of the D0 installation in 1992.

The practical advantage of placing the separators on a common girder is that the separators could be evacuated in the clean shop, backfilled with a nitrogen purge, transported to the tunnel and installed, then evacuated, and never opened to air in the tunnel.

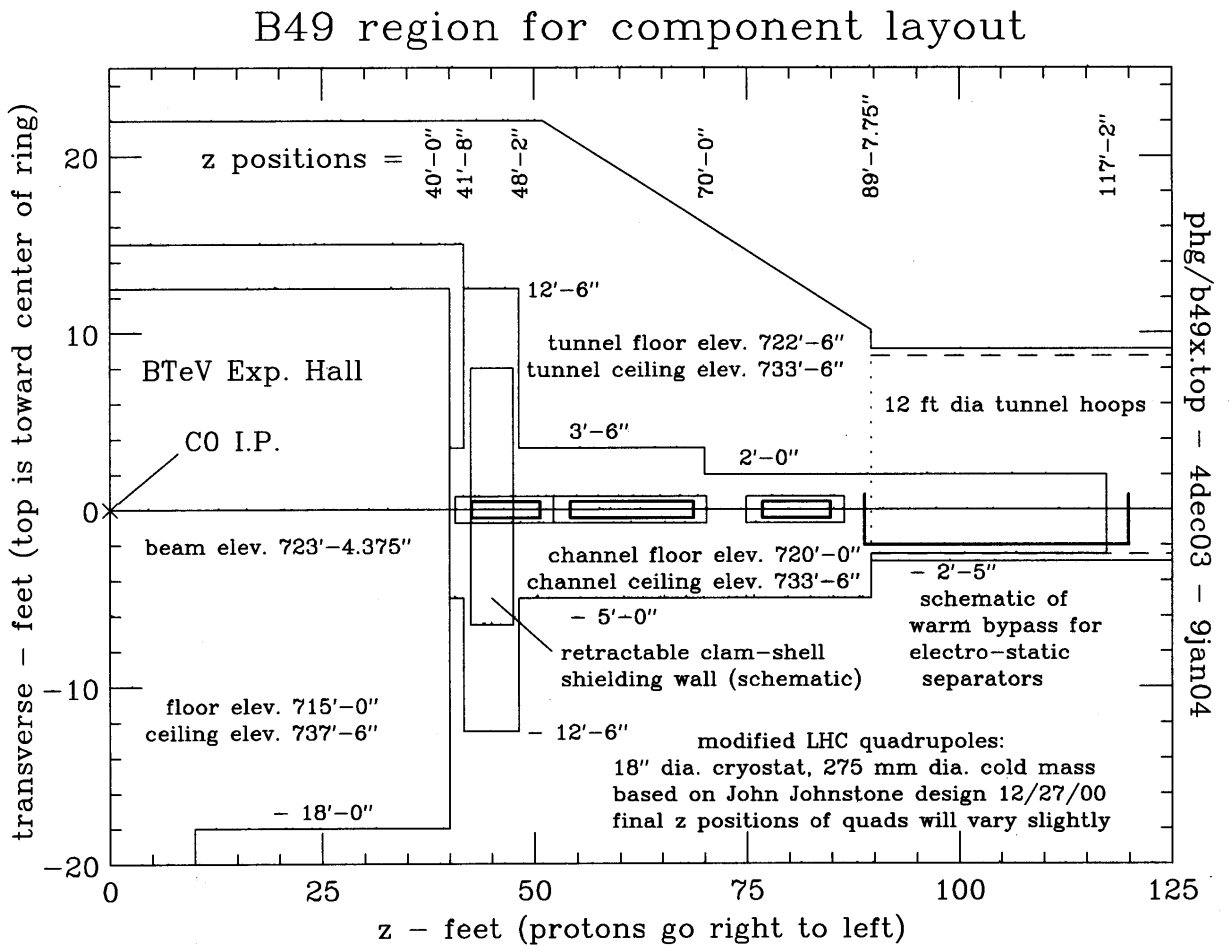

Figure 12-1: Tevatron tunnel plan view on the B side of the collision hall. The C side is the mirror image.

12.1.3 Q1 and P Spool Removal from A4/B1

The Tevatron Q1's and the P spools currently installed at A49 and B11 will be removed from those locations and reinstalled at B45 and C15. In the current Tevatron configuration the Q1's are not powered (they have been removed from C49 and D11 to provide space for the D0 Forward Proton Detector), however the present functionality of these 2 devices at A49 and B11 must be replaced.

At A49 the Q1 and P spool are adjacent and the P spool is inboard of the Q1. A dipole is just upstream of the Q1, and the start of the bypass for the separators is just downstream of the P spool. There is main TeV bus through these devices, but it is not connected in these 2 devices. The circuits used in the P spool are HDA49, VDA49, and SQA4 which are all essential for Tevatron Run II operation. HBPMA49 and VBPMA49 are also in the P spool and are essential for Run II operation. The Q1 slot length is 72.827" and the P spool slot length is 56.149".

A plan to replace the present functionality of these devices at A49 is as follows. Replace the Q1 and P spool with two devices: a (new) cold spool containing a horizontal BPM and an H spool. The H spool has VD, HD, and SQ coils and a VBPM. The slot length of an H spool is 49.910".

The slot length of the new HBPM spool will need to be 79.066". The H spool should be inboard of the cold BPM spool in order to maximize the effectiveness of VDA49 in making IR position bumps.

At the B11 location the Q1 and P spool are adjacent and the P spool is inboard of the Q1. The end of the separator bypass is just upstream of the P spool, and an R spool is just downstream of the Q1. A dipole is downstream of the R spool. There is main TeV bus through these devices, but it is not connected in the Q1 or P spool. The circuits used in the P spool are HDB11, VDB11, and SQB1 which are all essential for Run II operation. HBPMB11 and VBPMB11 are also in the P spool and are essential for operation. The R spool has no internal coils and is used only to provide an (external) turnaround for the main TeV bus. It has reversed cryogen pipes. It has a slot length of 40.729".

A plan to replace the present functionality of these devices at B11 is as follows. Replace the Q1, P spool, and R spool with two devices: a (new) cold spool containing a horizontal BPM and an H spool. The H spool has VD, HD, and SQ coils, a VBPM, and will provide an external turnaround for the main TeV bus. The slot length of the new HBPM spool will need to be 119.795". The H spool should be inboard of the cold BPM spool so that the cryogen pipes can be reversed in the BPM spool. This will require TeV through bus in the BPM spool.

12.1.4 Beam Collimators and Shielding

Concrete shielding walls at the upstream and downstream ends of the C0 collision hall will be of a clamshell design and on rollers, so they can be easily moved when changing a magnet in the area. Figure 12.1 shows the approximate location of the shielding wall on the B side of the collision hall. They will surround the Q1 low beta quad cryostat and could have dimensions up to 6' thick, 12' high, and 12' wide. Gaps around the quadrupole cryostat and cryostat stand will be filled with easily removable sandbags. The gaps will be large enough to provide for sighting for alignment needs.

Two new collimators, of standard design, will be installed in a a 2.6 meter warm straight section near B47-4. Collimator stands, motors, lvdt's, etc. will be taken from the currently unused collimators at E0(2) and F17(1).

12.2 Interfacing with civil construction project

All work performed by any building trades will be the responsibility of FESS, with the exception of ironworkers and electricians removing or installing accelerator components and their related supports, which will be the responsibility of the Accelerator Division. The civil construction subproject of the BTeV project (WBS3.0) will provide AC power distribution to the B4, C1, and C0 service buildings, and modifications to the C0 service building to accommodate new power supplies. WBS3.0 will also provide the housing and environmental protection for the external bus-work between the C0 service building and the penetration entering the Tevatron tunnel.

12.3 Interfacing with Detector Installation

After C0 is converted to a normal straight section in 2005, the warm vacuum beam pipe in the collision hall is not included within the scope of this project. The C0 IR project will provide vacuum gate valves on the inboard ends of the Q1 quads. All work between these gate valves is

the responsibility of the Detector Group. However, the B2 compensating dipoles inside the toroids on both sides of the I.P. must have provision for being changed in the event of a failure. We envision this to involve some sort of handling mechanism and equipment in the accelerator tunnel. A cooperative design effort for this magnet changing process between the Accelerator Division and the Detector Group must be carried through.

12.4 Schedule and Cost

The current schedule and cost estimates can be found in the latest Open Plan WBS2_0 file which is BTeV Document #3145.

13 Appendices

13.1 Table of beam line elements between B43 and C17

type	location	start z coordinate	slot length	high power leads	internal BPM	Power Supplies
66" quad	B43-1	0.0000	2.31140		vbpmb43	T:IB=4350A
X1 spool	B43-1a	2.3114	1.82880			T:VDB43,T:QB43, T:SDB43; 100A max
TB	B43-2	4.1402	6.40080			T:IB=4350A
TB	B43-3	10.5410	6.40080			T:IB=4350A
TC	B43-4	16.9418	6.40080			T:IB=4350A
TC	B43-5	23.3426	6.40080			T:IB=4350A
66" quad	B44-1	29.7434	2.31140		hbpmb44	T:IB=4350A
X1 spool	B44-1a	32.0548	1.82880			T:HDB44, T:QB44, T:SFB44; 100A max
TC	B44-2	33.8836	6.40080			T:IB=4350A
TC	B44-3	40.2844	6.40080			T:IB=4350A
TB	B44-4	46.6852	6.40080			T:IB=4350A
TB	B44-5	53.0860	6.40080			T:IB=4350A
cold spool	B44-6	59.4868	0.12764			
old-Q1 (Q7)	B45-1	59.6144	1.84980			C:QB45=5KA max
P spool	B45-1a	61.4642	1.42618	5KA for old-Q1	hbpmb45, vbpmb45	T:VDB45, T:SQ; 50A max
feedcan	B45-1b	62.8904	0.73660			
TB	B45-2	63.6270	6.40080			T:IB=4350A
TB	B45-3	70.0278	6.40080			T:IB=4350A
TC	B45-4	76.4286	6.40080			T:IB=4350A
TC	B45-5	82.8294	6.40080			T:IB=4350A
TC	B45-6	89.2302	6.40080			T:IB=4350A
old-Q1 (Q6)	B46-1	95.6310	1.84980			C:QB46=5KA max
P spool	B46-1a	97.4808	1.42618	5KA for old-Q1	hbpmb46, vbpmb46	T:HDB46, T:SQ; 50A max
TC	B46-2	98.9070	6.40080			T:IB=4350A
TC	B46-3	105.3078	6.40080			T:IB=4350A
TB	B46-4	111.7086	6.40080			T:IB=4350A
TB	B46-5	118.1094	6.40080			T:IB=4350A

type	location	start z coordinate	slot length	high power leads	internal BPM	Power Supplies
59" LHC quad (Q5)	B47-1	124.5102	2.47075			C:C0Q5=10KA max
X2 spool	B47-1a	126.9810	1.52400	10 KA	hbpmb47, vbpmb47	T:VDB47, T:HDB47; 100A max
TB	B47-2	128.5050	6.40080			T:IB=4350A
TB	B47-3	134.9058	6.40080			T:IB=4350A
79" LHC quad (Q4)	B48-1	141.3066	2.97875			C:C0Q4=10KA max
X2 spool	B48-1a	144.2853	1.52400	10KA	hbpmb48, vbpmb48	T:HDB48, T:VDB48; 100A max
cold bypass	B48-1b	145.8093	0.43815			
warm straight		146.2475	3.72614			
cold bypass		149.9736	0.31115			
TC	B48-2	150.2847	6.40080			T:IB=4350A
TC	B48-3	156.6855	6.40080			T:IB=4350A
TB	B48-4	163.0863	6.40080			T:IB=4350A
TB	B48-5	169.4871	6.40080			T:IB=4350A
cold bypass	B49-1	175.8879	0.43815			
separator		176.3261	3.03270			
separator		179.3588	3.03270			
separator		182.3915	3.03270			
cold bypass		185.4242	0.31115			
cryo turnaround	B49-2	185.7353	0.73660	5KA for main bus		
94" LHC quad (Q3)	B49-3	186.4719	3.45122			C:C0Q123, 10KA max; C:C0QSU, 200A max
X3 spool	B49-3a	189.9232	1.52400	10kA, 200A	hbpmb49, vbpmv49	T:HDB49,T:VDB49, T:SQB4; 100A max
170" LHC quad (Q2)	B49-4	191.4472	5.31178			C:C0Q123, 10KA max
94" LHC quad (Q1)	B49-5	196.7589	3.63220		hbpmc0u, vbpmcou	C:C0Q123, 10KA max; C:C0QSU, 200A max
warm straight	C-0	200.3911	12.19512			
C0 IP	C-0	212.5863	0.00000			
warm straight	C-0	212.5863	12.19512			

type	location	start z coordinate	slot length	high power leads	internal BPM	Power Supplies
94" LHC quad (Q1)	C10-1	224.7814	3.63220		hbpmc0d, vbpmc0d	C:C0Q123, 10KA max; C:C0QSD, 200A max
170" LHC quad (Q2)	C10-2	228.4136	5.31178			C:C0Q123, 10KA max
X3 spool	C10-2a	233.7254	1.52400	10kA, 200A	hbpmc11, vbpmc11	T:HDC11,T:VDC11, T:SQC1; 100A max
94" LHC quad (Q3)	C10-3	235.2494	3.45122			C:C0Q123, 10KA max; C:C0QSD, 200A max
cryo turnaround	C10-3a	238.7006	0.73660	5KA for main bus		
cold bypass	C10-4	239.4372	0.43815			
separator		239.8754	2.90414			
separator		242.7795	2.90414			
separator		245.6836	2.90414			
cold bypass		248.5878	0.31115			
TC	C11-2	248.8989	6.40080			T:IB=4350A
TC	C11-3	255.2997	6.40080			T:IB=4350A
TB	C11-4	261.7005	6.40080			T:IB=4350A
TB	C11-5	268.1013	6.40080			T:IB=4350A
TB	C11-6	274.5021	6.40080			T:IB=4350A
79" LHC quad (Q4)	C12-1	280.9029	2.97875			C:C0Q4=10KA max
X2 spool	C12-1a	283.8817	1.52400	10KA	hbpmc12, vbpmc12	T:VDC12, T:HDC12; 100A max
TB	C12-2	285.4057	6.40080			T:IB=4350A
TC	C12-3	291.8065	6.40080			T:IB=4350A
59" LHC quad (Q5)	C13-1	298.2073	2.47075			C:C0Q5=10KA max
X2 spool	C13-1a	300.6780	1.52400	10KA	hbpmc13, vbpmc13	T:HDC13, T:VDC13; 100A max
TC	C13-2	302.2020	6.40080			T:IB=4350A
TC	C13-3	308.6028	6.40080			T:IB=4350A
TB	C13-4	315.0036	6.40080			T:IB=4350A
TB	C13-5	321.4044	6.40080			T:IB=4350A
old-Q1 (Q6)	C14-1	327.8052	1.84980			C:QC14=5KA max
P spool	C14-1a	329.6550	1.42618	5KA for old-Q1	hbpmc14, vbpmc14	T:VDC14, T:SQ; 50A max

type	location	start z coordinate	slot length	high power leads	internal BPM	Power Supplies
TB	C14-2	331.0812	6.40080			T:IB=4350A
TB	C14-3	337.4820	6.40080			T:IB=4350A
TC	C14-4	343.8828	6.40080			T:IB=4350A
TC	C14-5	350.2836	6.40080			T:IB=4350A
TC	C14-6	356.6844	6.40080			T:IB=4350A
cold spool	C14-6a	363.0852	0.12761			
old-Q1 (Q7)	C15-1	363.2128	1.84980			C:QC15=5KA max
P spool	C15-1a	365.0626	1.42618	5KA for old-Q1	hbpmc15, vbpmc15	T:HDC15, T:SQ; 50A max
feedcan	C15-1b	366.4888	0.73660			
TC	C15-2	367.2254	6.40080			T:IB=4350A
TC	C15-3	373.6262	6.40080			T:IB=4350A
TB	C15-4	380.0270	6.40080			T:IB=4350A
TB	C15-5	386.4278	6.40080			T:IB=4350A
66" quad	C16-1	392.8286	2.31140		vbpmc16	T:IB=4350A
X1 spool	C16-1a	395.1400	1.82880			T:VDC16, T:QC16, T:SDB43; 100A max
TB	C16-2	396.9688	6.40080			T:IB=4350A
TB	C16-3	403.3696	6.40080			T:IB=4350A
TC	C16-4	409.7704	6.40080			T:IB=4350A
TC	C16-5	416.1712	6.40080			T:IB=4350A
66" quad	C17-1	422.5720	2.31140		hbpmc17	T:IB=4350A
X1 spool	C17-1a	424.8834	1.82880			T:HDC17,T:QC17, T:SFC17; 100A max
cold bypass	C17-2	426.7122	0.30163			
open space		427.0138	0.00515			
separator		427.0190	2.91048			
separator		429.9295	2.91048			
separator		432.8399	2.91048			
separator		435.7504	2.91048			
open space		438.6609	0.00515			
cold bypass		438.6660	0.42862			
TB	C17-3	439.0947	6.40080			T:IB=4350A
TB	C17-4	445.4955	6.40080			T:IB=4350A